Politecnico di Torino

Master's Degree in Environmental Engineering
Natural Hazards and Civil Protection

THE 'MISSISSIPPI RIVER DELTA TRANSITION INITIATIVE'

AN ECO-HYDROLOGICAL MODEL TO ASSESS THE IMPACTS OF EXTREME DROUGHTS AND SALTWATER INTRUSION IN THE MISSISSIPPI RIVER DELTA REGION

Supervisor:
Prof. Pierluigi Claps

Candidate:
Carlotta Tranchini

Co-supervisors:
Prof.ssa Annalisa Molini,
Dr. Giulia Evangelista

Academic Year 2024/2025

”Allenati mentre gli altri dormono,
Studia mentre gli altri escono,
Resisti mentre gli altri mollano,
Alla fine vivrai quello che gli altri
Sognano.”

Contents

List of Figures

Abstract

The Mississippi River Delta (MRD) is a complex and dynamic eco-region that plays a key role in supporting biodiversity and protecting the coast. However, the MRD is becoming increasingly vulnerable to climate change, saltwater intrusion, and severe droughts, all of which pose a significant threat to its ecological stability.

This study developed and applied an eco-hydrological model to analyze the combined effects of these stressors on wetland vegetation. Specifically, it focused on the increase in salinity during the 2022 drought and its negative impact on plant productivity. A Soil-Plant-Atmosphere Continuum (SPAC) model, Photo3 [22] was modified to account for the effects of salinity on plant transpiration.

Meteorological and micrometeorological data to calibrate and validate the model were obtained from the United States Geological Survey (USGS) Eddy Covariance stations located in the Barataria basin in Louisiana. Information on salinity, water level, and plant types was sourced from the Louisiana's Coastwide Reference Monitoring System (CRMS). This setup enabled realistic simulations of the environmental conditions and physiological responses of vegetation. The study focused on two species: *Spartina Patens*, which dominates coastal brackish marshes, and *Sagittaria Lancifolia*, which is prevalent in freshwater areas not affected by salt stress.

The results highlighted the crucial role of salinity as a limiting factor during the drought in 2022. In saline areas, salinity levels largely exceeded the tolerance thresholds of *Spartina Patens*, resulting in extended stress and a substantial decrease in transpiration and the carbon assimilation rate. Still, our modeling approach presents some limitations, including the

oversimplification of salinity effects and the exclusion of dynamic processes such as water redistribution, submergence, and variations in groundwater.

Future research should incorporate stochastic climatic drivers, interactions between soil, water, and salinity, and a water balance that considers groundwater dynamics. This study offers new insights into wetland resilience and serves as a foundation for sustainable management strategies in deltaic ecosystems that are increasingly threatened by global change.

1. Overview of the Area of Interest and Its Associated Impacts

1.1 Mississippi river delta Geographical framing

The Mississippi River, the largest river system in North America, has had a significant impact on the geological history of the northern Gulf of Mexico since the Late Jurassic period. Currently, the river discharges an average of 15,360 cubic meters of water per second and transports approximately 621 billion kilograms of sediment annually, mainly consisting of fine-grained clays and silts[29]. The Mississippi River Delta (MRD), known as the seventh-largest delta globally, covers approximately 11,000 square kilometers of coastal wetlands, representing 37% of all estuarine marshes in the United States [58].

A critical aspect to consider is the construction system of the delta, characterized by cycles of deposition and abandonment, commonly referred to as ”delta switching.” This phenomenon involves the river periodically altering its course, thereby generating new delta lobes and continuously reshaping the landscape [25]. Louisiana’s coastal wetlands began forming thousands of years ago, primarily as a result of sediment deposition from the Mississippi River. This process was further facilitated by periodic flooding, which left nutrient-rich soils that supported the expansion of extensive deltaic wetlands.

The MRD complex consists of six distinct sub-deltas: Mariggouin, Teche, St. Bernard, La Fourche, Plaquemine-Balize, and Atchafalaya/Wax Lake Outlet[44](See Figure 1.1).

Figure 1.1: The rapresentation of the six subdeltas [56]

The focus of this thesis will primarily be on the southern section of the Balize sub-delta, known as the ”Birdfoot,” a unique feature of the modern Mississippi River Delta. Its name derives from its distinctive shape, resembling the outstretched toes of a bird’s foot, formed by a series of narrow distributary channels extending into the Gulf of Mexico. As illustrated by the following figure, it has been possible to outline, for the sub-delta, four complexes different such as West Bay (A), Cubit’s Gap (B), Baptiste, Collette (C), and Garden Island Bay (D).

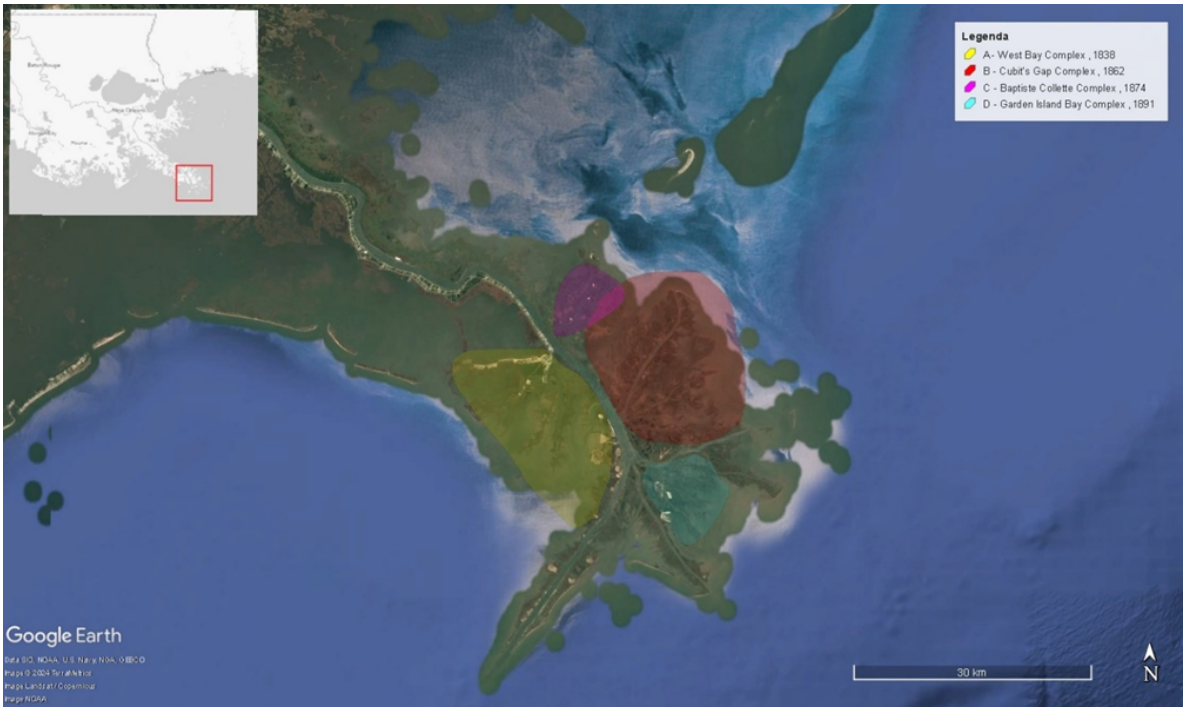

Figure 1.2: Index map showing the different complexes of the modern Mississippi River Delta (MRD) in southeastern Louisiana. Dates indicate the year of crevasse opening

During the progradation phase, the growth of sub-deltas initiates with the formation of crevasses, although the rate of growth is not constant. Due to the uneven distribution of coarse sediments, which primarily settle near the initial breach, finer sediments are transported further into the bay, creating a platform that encourages subsequent progradation and channel development. After approximately 10-15 years, the main channels are established, and a well-organized bifurcation system emerges. Only after the establishment of a well-structured channel system (see Figure 1.3) that facilitates sediment transport does subaerial growth accelerate, leading to the proliferation of marsh vegetation, which provides a protective layer over the underlying deposits[62].

Figure 1.3: Channel system [6]

Despite the loss of emergent land, the total sediment volume within each complex has increased due to subsidence. With an average subsidence rate of 1.5 cm per year and an estimated sub-delta lifespan of 150 years, subsidence may reach around 2.25 meters over the life of the sub-delta. Consequently, while sedimentation does not fully offset subsidence, it continues to fill the sub-delta basins, which would otherwise revert to open water areas. Eventually, when the marsh surface can no longer sustain its growth rate relative to degradation processes, the marsh vegetation becomes submerged, resulting in the formation of small lakes and bays. [62].

However, human intervention has drastically altered these natural processes. The construction of levees and dams has diminished the volume of sediment reaching the delta, undermining its ability to regenerate and maintain its size. These changes have led to a significant loss of territory. The wetlands, which are essential for biodiversity and coastal

protection, have experienced erosion and degradation. It is estimated that Louisiana has lost over 4,833 square kilometers [10] of wetlands in recent decades, representing approximately 80% of the total wetland loss in the United States. This erosion not only poses a threat to the ecosystem but also has direct repercussions on the local economy and the quality of life for the communities that inhabit the region [25].

The analysis conducted by [49] indicates that, without any restoration efforts, an additional 2,254 square kilometers of land could be lost over the next 50 years under the moderate environmental scenario. This represents a striking 36% of the total coastal area.

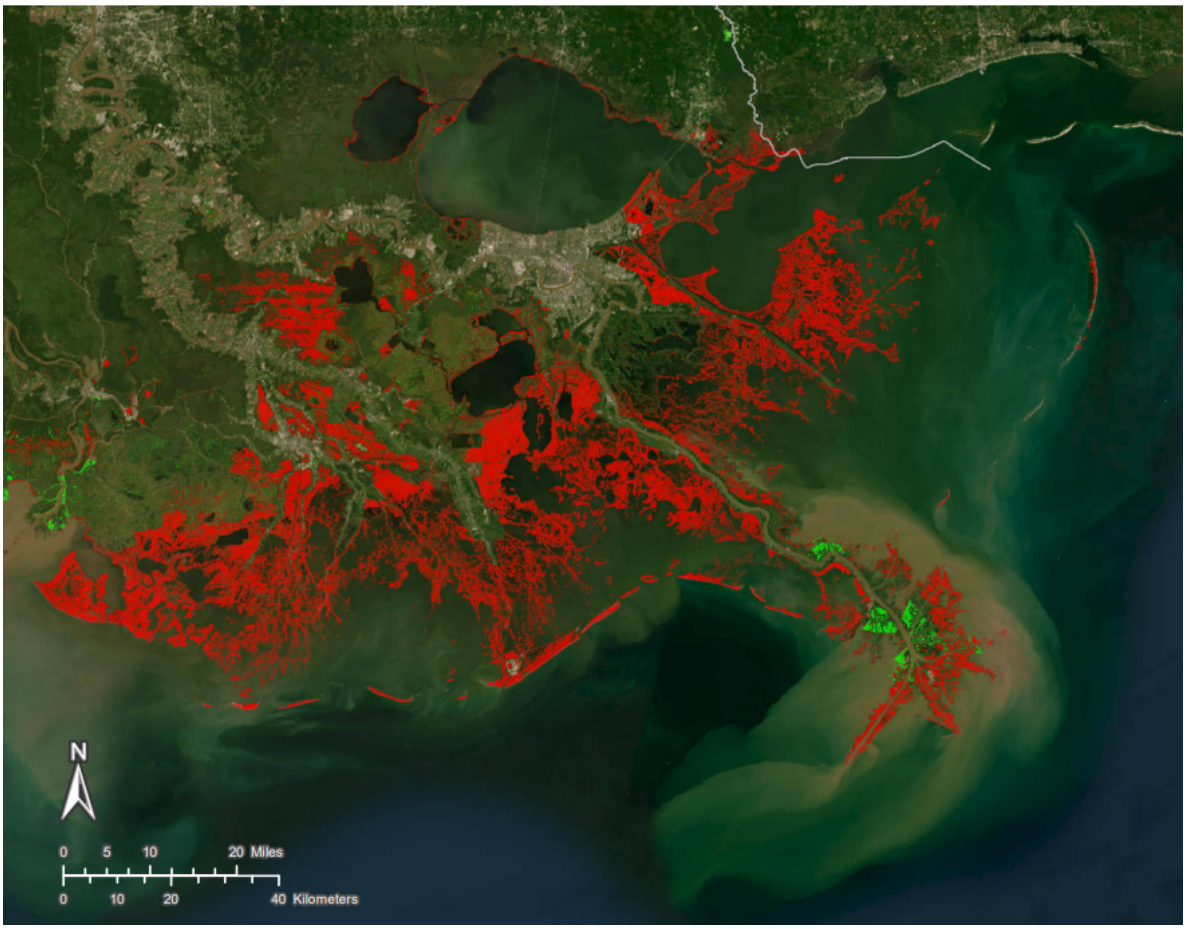

Figure 1.4: Land change: land gain (green), land loss (red)[49].

1.2 Coastal Wetland

Wetlands are unique ecosystems located at the interface between terrestrial and aquatic systems, characterized by the presence of:

- Water, which may be present on the surface or within the root zone for significant periods of the growing season.
- Specific soil conditions, such as saturated or hydromorphic soils that differ from the surrounding environments.
- Adapted biota, including hydrophilic vegetation and the absence of organisms intolerant to flooding.

These ecosystems play a crucial role as ecotones (transition zones), sources, sinks, and transformers of nutrients, contributing to stabilizing water resources, protecting shorelines, purifying water, and providing habitats for a wide range of biodiversity.

As the Mississippi River approaches its final stretch before entering the Gulf of Mexico in southeastern Louisiana, it transitions into one of the most wetland-rich areas globally. This region encompasses over 36,000 km² of marshes, swamps, and shallow coastal lakes. As the river's distributaries extend toward the sea, forested wetlands gradually transition into freshwater marshes and ultimately into salt marshes. These salt marshes are among the largest and most productive in the United States, benefiting from the upstream flow of fresh water, nutrients, sediments, and organic material from swamps. However, both freshwater and saltwater wetlands in coastal Louisiana have been shrinking at an alarming rate, with a total loss of 4,800 km² since the 1930s and annual rates of 60–100 km² per year. This decline is attributed to both natural and human-induced factors, with the primary cause being the disconnection of the river from its delta. Another notable wetland region in the delta is the Barataria Bay estuary in Louisiana. This interdistributary basin, now separated from the river

by flood-control levees, spans 6,500 km² and contains approximately 700 km² of wetlands, including cypress-tupelo swamps, bottomland hardwood forests, marshes, and shallow lakes [39].

Coastal wetlands are shaped by the interplay between tidal flooding and oceanic processes. Near the coastline, water salinity resembles that of the ocean, while further inland, tidal effects persist even as salinity approaches freshwater levels. Coastal wetlands encompass tidal salt marshes, tidal freshwater wetlands, and mangrove swamps. Tidal freshwater wetlands are typically found upstream in areas where salinity is below 0.5 ppt, while salt marshes and mangroves thrive downstream in polyhaline and mesohaline estuarine waters with salinity levels exceeding 5 ppt. Coastal wetlands are situated along gradients of decreasing salinity from the ocean toward inland areas [39].

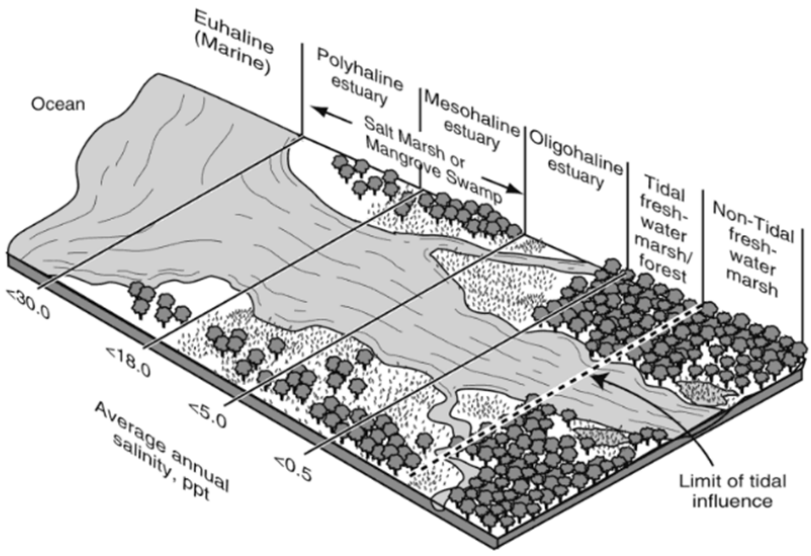

Figure 1.5: Coastal Wetlands lie on gradients of decreasing salinity from inland to the ocean [39].

This research focuses primarily on salt marshes, which are distributed globally along protected coastlines in mid- and high-latitude regions. Salt marsh ecosystems are largely

detritus-based, supporting diverse fauna that depend on detrital productivity either directly or indirectly. Grazing accounts for a small portion of marsh grass productivity [39].

The formation and extent of salt marshes within their geographical range are determined by factors such as tides, sediment availability, freshwater inputs, and shoreline configuration. Most salt marshes are intertidal, meaning they are periodically submerged by high tides but remain exposed during low tides. Gentle shoreline slopes, rather than steep ones, facilitate tidal flooding and vegetation stability. Protection from wave and storm energy is also crucial for their development. The sediments that form salt marshes originate from upland runoff, marine reworking of coastal shelf materials, or organic matter produced within the marsh [39].

Salt marshes typically extend inland to the highest tide line, between mean high water and the peak of spring tides. They are often divided into two zones: the upper or high marsh, which is irregularly flooded and exposed to the atmosphere for at least 10 consecutive days, and the lower or intertidal marsh, which is flooded almost daily and rarely exposed for more than 9 days. In areas with large tidal ranges, salt marsh salinity often reflects marine conditions despite significant rainfall[39].

In regions adjacent to major rivers, freshwater inputs dilute marine salinity, resulting in brackish or even freshwater marshes. Extreme salinity conditions, however, can occur in subtropical regions like the Texas Gulf Coast, where limited freshwater input and narrow tidal ranges lead to reduced flushing. As a result, evaporation concentrates marine water, sometimes doubling salinity levels compared to seawater. Lateral salinity gradients, shaped by flooding frequency, influence vegetation productivity[39].

As marsh elevation increases, flooding frequency decreases, and finer sediments retain water poorly. In salt flat zones, spring tides bring saltwater that is concentrated through evaporation. Insufficient flushing allows salts to accumulate to toxic levels. At higher elevations, tidal flooding is rare, and rainwater flushing prevents salt buildup. These interactions between marsh elevation, tides, and precipitation create salinity gradients that shape vegetation

zonation and productivity. However, within the salt marsh itself, all plants are salt-tolerant, making it insufficient to attribute plant zonation and productivity solely to salinity. Salinity is the result of various hydrodynamic factors, including slope, elevation, tides, rainfall, freshwater inputs, and groundwater flow. For example, Spartina thrives in the intertidal zone, where tides reduce salinity, remove toxins, supply nutrients, and alleviate soil anoxia. These combined factors lead to variations in productivity and growth forms between the intertidal and high marsh zones[39].

1.2.1 Vegetation in the Bird-foot

As demonstrated by the data collected from the Coastwide Reference Monitoring System (CRMS), the vegetation along the Birdfoot Delta has experienced significant changes over the analysis period from 2007 to 2023, largely due to the increasing stress factors affecting plant health (refer to Section 1.2). The vegetation plays a critical role in coastal wetlands; indeed, the vulnerability of the ecosystem is closely linked to the tolerance and response of plant species to major stressors such as flooding and salinity [60].

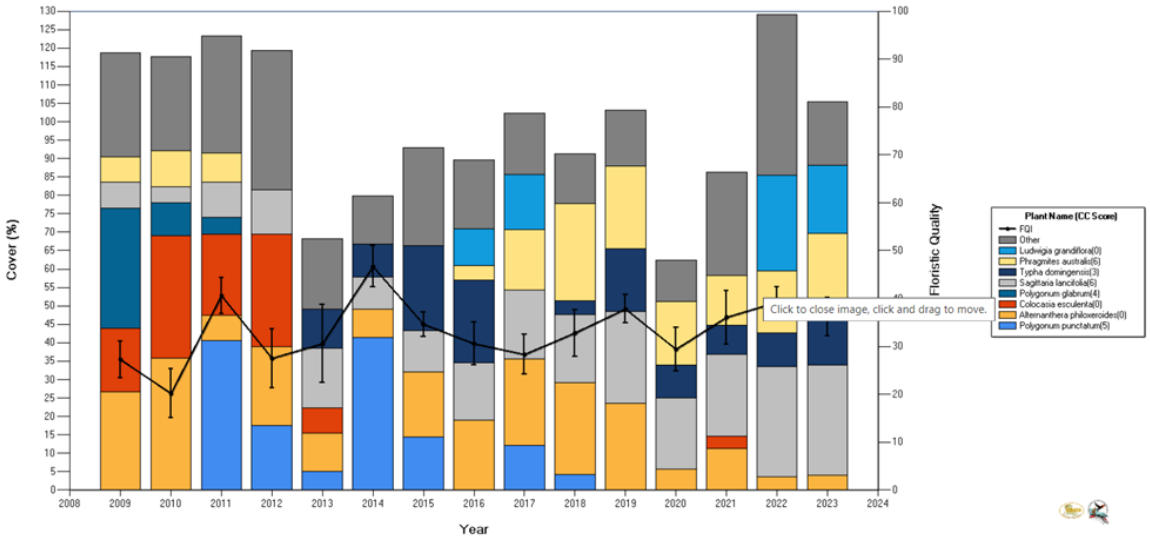

Figure 1.6: Herbaceous Marsh Vegetation Data; site CRMS2608 [50]

By examining the multiple vegetation types recorded across all stations, it becomes apparent that the two dominant species are: *Phragmites australis* and *Sagittaria lancifolia*.

(a) (b)

Figure 1.7: (a)*Phragmites australis*,(b)*Sagittaria lancifolia*[50].

Phragmites australis, commonly known as the common reed, is a flowering plant in the Poaceae family. It serves as a transitional species between aquatic and terrestrial ecosystems, thriving in wetlands and swamps. This species is globally recognized for its ecological importance, environmental resilience, and tolerance to salinity. Its growing season is extended in subtropical and mild temperate regions, allowing the plant to adapt to fluctuations in temperature, soil nutrients, and oxygen availability, particularly in wetland environments. Physiological traits, such as transpiration rates, also adjust to seasonal changes.[16].

Regardless of location, *P. australis* provides food and habitat for various organisms and helps stabilize soils against erosion. Additionally, its biological characteristics make it effective as a biological filter for pollutants. Compared to other emergent aquatic plants, *P. australis* features annual cane-like stems that can grow up to 6 meters high, with diameters ranging from 4 to 10 mm and internodes measuring 10 to 25 cm. It possesses an extensive rhizome system, with both horizontal and vertical components. Horizontal rhizomes contribute to the expansion of the clone, while vertical rhizomes produce the annual upright stems[30].

Sagittaria lancifolia L, commonly known as duck potato, is a native North American wetland plant species. It grows in inland and coastal freshwater marshes, around margins of lakes and ponds, and along rivers and streams. It is highly adaptable to a wide range of water conditions, making it an ideal candidate for restoring degraded aquatic habitats [20].

Sagittaria lancifolia L., commonly known as duck potato, is a native North American wetland plant that thrives in freshwater marshes, lakes, and riverbanks. It is highly adaptable to various water conditions, making it suitable for restoring degraded aquatic habitats. The plant features arrow-shaped leaves that can range from 5 to 40 cm in length and 2 to 25 cm in width. It produces small, white, three-petaled flowers on erect stalks and reproduces both sexually through seeds and asexually via rhizomes, allowing for rapid colonization. [20].

Sagittaria lancifolia provides essential habitat and food for wildlife, including waterfowl and invertebrates, while its dense growth enhances wetland biodiversity. It is commonly used in environmental restoration projects for its ability to stabilize soil, reduce erosion, and improve water quality. [20].

1.3 Saltwater Intrusion in the Mississippi River Delta: Impacts of Drought Conditions

The Mississippi River Delta, as a coastal ecosystem, is naturally subject to spatial and temporal variations in salinity, referred to as primary salinization. These variations are influenced by the geographical location of the delta and the continuous exchanges between terrestrial and oceanic environments. The spatial factors that determine salinity primarily include the distance from salt sources, such as proximity to the coast. Temporal variations can occur on short scales (hours) or extended scales (years). Climatic conditions, including temperature, precipitation, and wind regimes, interact with salt deposition, significantly influencing salinity over time and shaping plant responses to such salinity, often more so than other environmental factors [35].

In addition to primary salinization, the Mississippi Delta faces secondary salinization, which refers to the increase in salt concentration due to human intervention [35]. Activities such as oil and gas extraction directly impact wetlands, contributing to habitat loss through the creation of transport channels and the installation of pipelines. These channels disrupt the natural flow of water, increasing the risk of flooding and reducing sediment deposition, thus facilitating the intrusion of saline water into areas previously dominated by freshwater [42].

Saltwater intrusion occurs when seawater slowly rises along freshwater systems, such as rivers and aquifers. Typically, the underground layers beneath the land are filled with freshwater, while the soil beneath the oceans contains saltwater. When these layers meet, a pressure differential develops between the freshwater and saltwater. Since saltwater is denser, it tends to move inland, gradually invading freshwater systems. This process is accelerated by reductions in freshwater levels, often caused by drought or excessive exploitation of water resources [35].

In recent years, climate change has amplified the factors contributing to rising salinity in the Delta. Between 2022 and 2023, the region experienced severe droughts, characterized by exceptionally low river flows, allowing saltwater to rise up the river to New Orleans. This drought fits into a long-term trend of progressively decreasing annual minimum water levels in the lower river, a phenomenon that has intensified over the past century [27].

There are two main causes of this decline in water levels. First, the construction of dams, locks, and levees for flood control, initiated in the 1930s, has progressively blocked an increasing portion of the river's flow upstream, reducing the natural variability of the hydrological regime and exacerbating low flow conditions. Second, higher atmospheric temperatures increase evaporation, contributing both to drought and more intense precipitation. Historical river records from North America indicate that approximately 1,000 years ago, higher temperatures resulted in much more variable precipitation patterns, with prolonged drought periods alternating with extreme flooding, conditions similar to those observed today in the lower Mississippi [27].

The lack of significant precipitation has led to a drastic reduction in the river's volume, which reached record low levels in 2022. Concurrently, chronic relative sea-level rise, exacerbated by subsidence, results in more frequent and prolonged flooding of wetland areas. These combined factors create a favorable environment for saltwater intrusion. Without the normal river flow to counteract the saltwater flowing from the Gulf of Mexico, the latter slowly rises along the riverbed, forming a "wedge" of saltwater that, as it advances, contaminates internal aquifers, polluting the water systems of local communities [15].

The consequences of these processes are devastating for vegetation. Marsh plants are adapted to living in freshwater or low-salinity environments and have limited tolerance for salinity changes. The sudden increase in salinity, due to drought and rising sea levels, undermines their ability to absorb water and nutrients, causing water stress and, in the long term, plant death [17].

The decline of vegetation leads to the loss of vital ecological functions for the delta, such as soil stabilization and erosion protection. In the absence of vegetation, wetland areas are more vulnerable to coastal erosion and saltwater intrusion, accelerating the degradation of delta ecosystems and reducing the entire system's capacity to adapt to future extreme events. This degradation compromises the resilience of wetlands, making them more susceptible to future episodes of decline and loss of biodiversity [17].

1.4 Effects of salt stress on the plant

High saline concentrations impose severe osmotic and ionic stress at both cellular and systemic levels. Plants respond to salt stress in two phases:

1. A rapid, osmotic phase that inhibits the growth of leaf shoots;

2. A slower, ionic phase that accelerates senescence in mature leaves.

To tolerate the presence of salt, plants employ various interconnected strategies [65],[8]:

1. Tolerance to osmotic stress (homeostasis maintenance);

2. Mechanisms of exclusion of Na+ and Cl- ions from tissues;

3. Detoxification of cellular Na+ and Cl- accumulation.

Genetic variability enables plants to respond differently to increasing salt stress. The physiological, morphological, and molecular mechanisms that plants adopt in response to salt stress are often similar. As reported by [65], halophytes' salt tolerance mechanisms are similar to those found in glycophytes, but small differences in their regulation result in significant variations in salt tolerance or sensitivity. However, prolonged exposure leads to growth inhibition and molecular damage, which, depending on the plant's salt sensitivity, can result in irreversible cellular damage and ultimately, death.

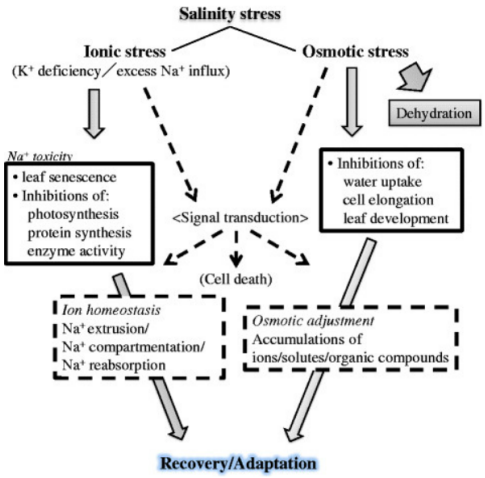

Figure 1.8: Schematic summary of the stresses to which plants are subjected under high-salinity growing conditions and the corresponding responses that plants enact to survive these damaging effects [43].

1.4.1 Morphological and physiological aspetcts

Water potential refers to the potential energy of water per unit volume relative to pure water under reference conditions. It quantifies the tendency of water to move toward a region with the most negative osmotic potential.

The total water potential ψ_{tot} is given by the sum of the contributions of osmotic potential ψ_{π}, piezometric potentialψ_{hw} and matrix potential ψ_{s}.[47]

$$\psi_{\text{tot}} = \psi_{s} + \psi_{hw} + \psi_{\pi} \tag{1.1}$$

Osmotic potential, or solute potential, is generated by osmotic pressure, the force with which a solute binds water. Water in soil is never in a pure state but instead exists as a solution, where dissolved molecules and ions exert electrostatic forces on water molecules, reducing their activity. Osmotic pressure is always negative.

Under normal conditions, water potential drives water from the soil into the roots and through the conducting tissues to the leaves, where it is released as vapor. Osmotic stress induced by salt acts quickly when the ionic concentration outside the roots exceeds that inside. This stress can lead to rapid changes in root tip expansion, leaf growth, stomatal aperture, stomatal density and area, gas exchange, and photosynthetic activity [41].

An increase in soil salinity causes a decrease in water potential, driving water out of the roots toward the hypertonic medium. The resulting loss of turgor is temporary, as the plant can restore turgor by increasing the production of osmoprotectant solutes in the apoplast. Osmoprotectants are compounds involved in osmoregulation during salt stress and help mitigate the effects of salt in several ways. When ion concentrations rise, osmoprotectants balance the osmotic imbalance that forms in the intracellular space.

In addition to the ion concentration in the apoplast, salt is also excluded from the cell interior. This accumulation in intercellular spaces creates an osmotic potential across the cell wall and membrane. In response to high apoplastic concentrations, compatible solutes

are accumulated in the cytoplasm to prevent cellular dehydration. Besides their role in osmotic adjustment, many compatible solutes, such as mannitol, trehalose, proline, and glycine betaine, have been shown to function as scavengers of reactive oxygen species (ROS).

Regulation of Leaf Area

Regulating leaf area is a crucial plant response to minimize the transpiring surface, thereby preserving turgor in the mesophyll cells and preventing the upward transport of high ion concentrations from the roots. Various mechanisms contribute to reduced leaf expansion and overall plant growth. The decrease in leaf growth is likely controlled by long-distance signals originating from the roots, which are transmitted in the form of hormones or their precursors.

Abscisic acid (ABA) plays a pivotal role in root-to-shoot communication and likely influences both growth and stomatal conductance [41]. The reduction in leaf growth may be attributed to the accumulation of cytoplasmic solutes, which help maintain osmotic balance in high-salinity conditions.

A less pronounced response to osmotic stress could lead to increased leaf expansion and stomatal conductance, but this would be advantageous only in plants with sufficient water availability.

Inhibition of Growth

Salt stress, like many other abiotic stresses, inhibits development. Plant growth responds to salinity in two phases related to the time [41]:

- a rapid response to the increase in external osmotic pressure. In the osmotic phase which starts immediately after the salt concentration around the roots increases to a threshold level (40mM NaCl), the rate of shoot growth falls significantly.

- a slower response due to the accumulation of Na+ in leaves. The second, ion-specific, phase starts when salt accumulates to toxic concentrations in the old leaves and they die. If the rate at which they die is greater than the rate at which new leaves are produced, the photosynthetic capacity of the plant will no longer be able to supply the

carbohydrate requirement of the young leaves, which further reduces their growth rate.

These responses vary strongly among genotypes, salinity levels, soil, and other abiotic factors.

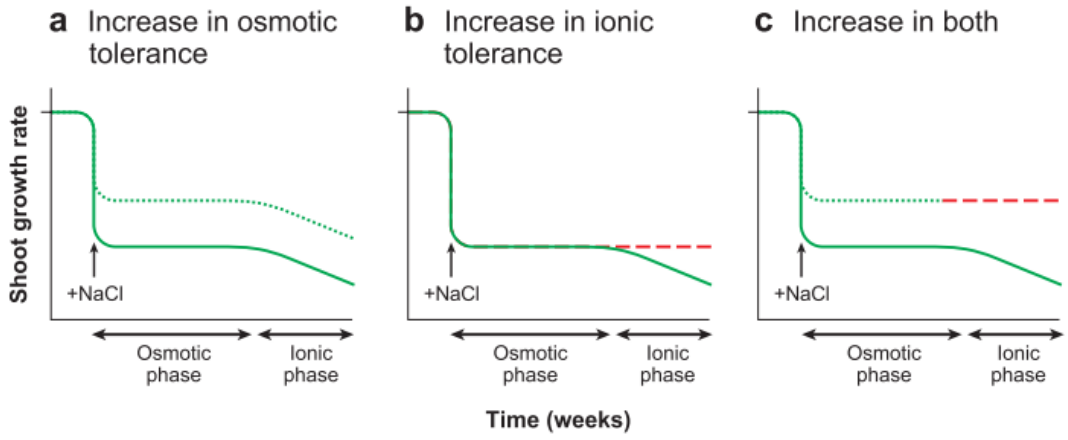

Figure 1.9: The growth response to salinity stress occurs in two phases: a rapid response to the increase in external osmotic pressure (the osmotic phase), and a slower response due to the accumulation of Na+ in leaves (the ionic phase). The solid green line represents the change in the growth rate after the addition of NaCl. (a) The broken green line represents the hypothetical response of a plant with an increased tolerance to the osmotic component of salinity stress. (b) The broken red line represents the response of a plant with an increased tolerance to the ionic component of salinity stress (based on Reference 93). (c) The green and red line represents the response of a plant with increased tolerance to both the osmotic and ionic components of salinity stress.[41]

Osmotic Control

The most significant damage to salt-stressed plants arises from water loss due to inadequate stomatal closure. Regulating transpiration through stomatal control is crucial in high-salinity environments. Salt stress increases abscisic acid (ABA) production in the roots, which, once transported to the leaves, reduces transpiration within hours [18].

Salt-tolerant species, particularly halophytes, exhibit lower water loss and reduced transpiration than glycophytes. Decreasing stomatal aperture helps limit water loss and slows the movement of ions from roots to shoots during salt exposure, serving as a defense against dehydration [41].

Photosynthesis and Stomatal Conductance

Stomata are tiny pores on leaves responsible for regulating gas exchange, permitting carbon dioxide intake for photosynthesis while releasing oxygen and water vapor. Stomatal conductance refers to how easily gases move through these pores.

Salinity impacts stomatal conductance quickly—first by disrupting water balance, followed by the synthesis of abscisic acid (ABA), which signals stomatal closure to reduce transpiration within hours [19]. This leads to lower carbon dioxide levels and a reduced photosynthetic rate. However, despite reduced gas exchange, photosynthesis per leaf area often remains stable due to structural changes, such as smaller leaves with a higher chloroplast density [41].

The mechanisms that allow the exclusion of ions at high concentrations include:

- Plants compartmentalize Na+ into the vacuoles of most tissues so as to reduce the toxic concentration of Na^+ in the cytosol [28], allowing the plant to continue its metabolic and enzymatic functions until the vacuole reaches saturation.

- The exclusion of salt from the cytoplasm. During salt stress, the cell activates $H^+ -$ ATPase pumps, which generate the proton energy needed to activate the H^+/Na^+ antiport pumps. This process allows the transport of Na^+ out of the cell and maintains a low concentration of Na^+ inside the cell [14].

- The development of salt glands, specialized epidermal trichomes, which sequester salt from metabolically active tissue.

A failure or reduced function of the aforementioned mechanisms would result in the accumulation of high levels of Na^+ in the cytoplasm. This would lead to the inhibition of

various enzymes and, consequently, to disruptions in cellular metabolic activities. Therefore, the entry of sodium ions into the cell must always be minimized or avoided. An important goal in studying salt tolerance is to determine which transporters are involved in the entry of Na^+ into the cell. The main gene implicated in Na^+ transport in plants is SOS1, which encodes for an Na^+/H^+ antiporter located on the plasma membrane [41].

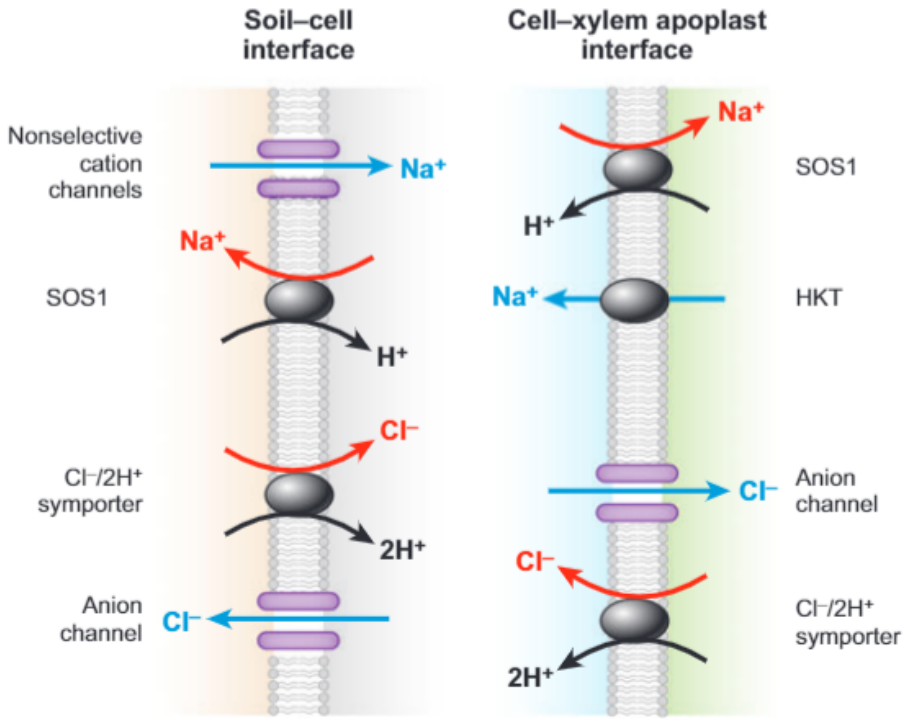

Figure 1.10: Thermodynamics and mechanisms of Na^+ and Cl^- transport at the soil-root and stelar cell–xylem vessel interfaces in roots. The proposed mechanisms of passive and active Na^+ and Cl^- transport at the two interfaces, are mediated by ion channels and carriers (uniporters and H^+-coupled antiporters and symporters). Abbreviations: SOS1, salt overly sensitive mutant 1; HKT, high-affinity K^+ transporter [41].

The last strategy is the **Detoxification of salt accumulation** . Ionic toxicity affects tissues more slowly compared to the onset of osmotic disturbances. In tissues, tolerance to the accu-

mulation of Na^+, or in some cases Cl^-, depends on genetic traits in responding to increased intracellular ions when compartmentalization mechanisms lose their effectiveness.

When extrusion and compartmentalization mechanisms fail, intracellular levels of Na^+ and Cl^- reach high concentrations, especially in the mesophyll of leaf cells. Toxicity gradually increases over time, first affecting older leaves and then younger ones. High saline concentrations cause damage to cellular structures, inhibit enzymatic activities, and disrupt both nutrient uptake and photosynthetic activity.

Many of these disturbances are associated with the generation of reactive oxygen species (ROS), which can signal and/or exacerbate physiological stress. To protect themselves from the toxic effects of ions, plants respond with the synthesis of proteins, organic acids or bases, and osmolytes (such as proline) that, in addition to providing osmotic protection, also have detoxifying actions [32].

1.5 Different Drivers and Effects of Hydraulic Stress on Plants

Plants experience different types of hydraulic stress depending on environmental conditions and soil water availability. A clear distinction exists between terrestrial forests and tidal wetlands in terms of the limiting factors affecting water uptake and the adaptive strategies employed by plants. In terrestrial forests, hydraulic stress is primarily driven by soil water availability, whereas in tidal wetlands, it is governed by salinity.

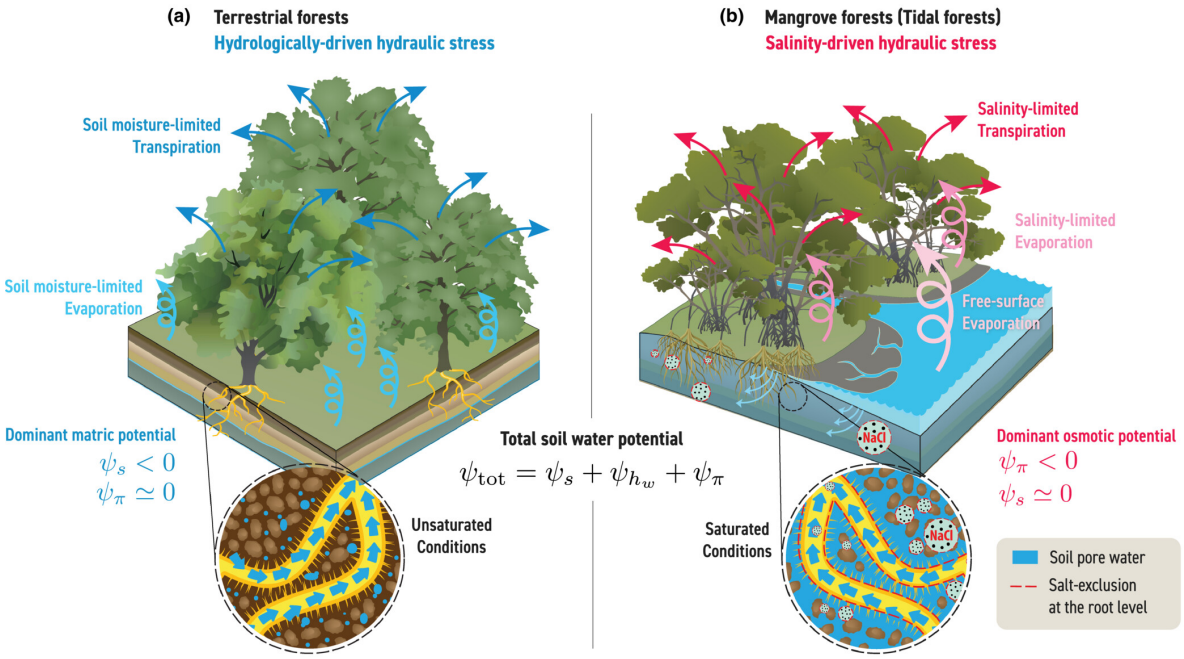

Figure 1.11: Hydrologically driven versus salinity-driven hydraulic stress. Conceptual representation of water stress in terrestrial (a) and tidal (b) forests [48].

In terrestrial forests, hydraulic stress is regulated by soil moisture availability (hydrologically-driven hydraulic stress). These ecosystems are typically characterized by unsaturated soils, where water content fluctuates based on precipitation patterns and the substrate's water retention capacity.

Plant transpiration is constrained by soil water scarcity, leading to a reduction in stomatal conductance. Under extreme drought conditions, stomatal closure prevents excessive water loss. Soil evaporation is also limited by water availability, decreasing during prolonged dry periods. The soil water potential (Ψ_s) is predominantly negative, as water is retained within the soil matrix by adhesion and cohesion forces (matric potential dominance). The osmotic potential (Ψ_π) is negligible since salinity levels in terrestrial forest soils are typically low.

The intensity and duration of drought determine the severity of these effects. Additionally, the nutrients needed for plant growth and biomass production generally come from the

internal cycle of stored materials, which requires water for solubilization and translocation. In drought conditions, nutrient absorption decreases because the reduction in soil water potential slows the diffusion rate of nutrients from the soil matrix to the roots. A low transpiration rate and compromised active transport, due to reduced available energy and altered membrane permeability, further limit nutrient absorption by the roots[1].

Water stress can have similar aspects to Salinity stress in plant growth, except for the addition of ion cytotoxicity, which appears with salt excess in soil [43].The plant responses to water stress are different between the species, and also depends of the time exposition. In the table below could be observed the plant response to salinity,as a water stress, at different time scales [40].

Table 1.1: Plant response to salinity at different time scales. The effects on a salt-tolerant plant are basically identical to those due to soil water deficit [40].

Time	**Water stress effects** (Observed effect on growth of a salt-tolerant plant)	**Salt-specific effects** (Additional effects on growth of a salt-sensitive plant)
Minutes	Instant reduction in leaf and root elongation rate then rapid partial recovery	
Hours	Steady but reduced rate of leaf and root elongation	
Days	Leaf growth more affected than root growth; Reduced rate of leaf emergence	Injury visible in oldest leaf
Weeks	Reduced final leaf size and/or number of lateral shoots	Death of older leaves
Months	Altered flowering time, reduced seed production	Younger leaves dead, plant may die before seed matures

Photosynthesis is particularly sensitive to drought. The reduction in leaf size and number, stomatal closure, impaired carboxylation enzyme activity, altered ATP synthesis, and damage to the photosynthetic apparatus significantly reduce carbon fixation. The effects of drought on

photosynthesis can be divided into stomatal and non-stomatal limitations. Stomatal closure is one of the primary responses to drought, limiting water loss but also reducing CO2 intake. Reduced stomatal size is the main factor limiting photosynthesis under mild to moderate drought stress, while reduced water potential and loss of turgor decrease stomatal opening. Additionally, alterations in essential enzymes, photosynthetic pigments, ATP synthesis, and oxidative stress cause non-stomatal limitations to carbon fixation [1].

Finally, when plants under drought stress are exposed to high radiation, the overproduction of reactive oxygen species (ROS) can lead to photoinhibition. All abiotic stresses, including drought, lead to increased oxidative stress with an overproduction of ROS, which are highly toxic molecules that damage proteins, lipids, carbohydrates, and DNA. Under these conditions, water deficit stimulates the production of abscisic acid (ABA), which reduces stomatal conductance to limit water loss through transpiration [1].

Wetlands exhibit a fundamentally different hydrological context compared to terrestrial ecosystems. Here, hydraulic stress is driven by salinity (salinity-driven hydraulic stress), as the soil remains constantly saturated but with a high salt concentration. Moreover, during extreme drought periods, surface water becomes even more saline. This occurs because the freshwater body is unable to counterbalance lateral water fluxes, leading to a further increase in soil salinity levels. Transpiration is limited by high salinity, as the presence of NaCl lowers the osmotic potential of soil water, making it less available for root uptake. Evaporation is influenced by the presence of surface water, which contributes to increased soil salinity through free-surface evaporation and salt deposition. The osmotic potential (Ψ_π) is strongly negative, due to the high salt concentration. This creates a steep osmotic gradient between the soil and plant roots, requiring plants to develop strategies for salt tolerance or exclusion to survive. The matric potential (Ψ_s) is close to zero, as the soil is water-saturated, meaning there is no significant tension within the soil matrix. To cope with these conditions, wetland plants have evolved specific salt-exclusion mechanisms at the root level, as discussed previously.

However, these adaptations can further amplify hydraulic stress, as they restrict water uptake while managing ion toxicity, ultimately shaping the physiological and ecological responses of these plant communities.

While in terrestrial forests water scarcity is the primary limiting factor, in tidal wetlands the main challenge is the presence of water that is too saline to be readily utilized by plants. The difference between these two types of hydraulic stress is reflected in the distinct mechanisms plants employ to regulate water uptake:

Table 1.2: Comparison of hydraulic stress in terrestrial forests and tidal wetlands

Characteristic	**Terrestrial Forests (Hydraulically-driven stress)**	**Tidal Wetlands (Salinity-driven stress)**
Water Availability	Limited by soil moisture	High, but reduced by salinity
Dominant Potential	Matric ($\psi_s < 0$)	Osmotic ($\psi_\pi < 0$)
Limitation to Transpiration	Soil water scarcity	High soil water salinity
Adaptation Strategies	Stomatal regulation, deep root growth	Salt exclusion, accumulation of compatible solutes, salt excretion

This distinction is crucial for understanding the physiological responses of plants in different environments and for accurately modeling water dynamics and productivity in both terrestrial and tidal forests.

1.6 Soil-Plant-Atmosphere Continuum (SPAC)

The Soil-Plant-Atmosphere Continuum (SPAC) is a framework that illustrates the flow of water from the soil, through plants, and into the atmosphere. Understanding this continuum

is essential for grasping how plants maintain hydration and overall health, as it encompasses various physiological processes and environmental factors. For a more detailed view of water flow, refer to Appendix A.

- Soil: In the soil, water is retained in the spaces between soil particles, influenced by factors such as texture, structure, and moisture content. The amount of available water in the soil plays a crucial role in determining both plant growth and rates of transpiration [59].

- Plant: Water absorption takes place through the roots and moves through the plant's vascular system, specifically the xylem. This movement is primarily driven by capillary action and osmotic potential. During transpiration, plants lose water vapor through stomata, which generates a negative pressure that aids in the upward movement of water from the roots to the leaves [59].

- Atmosphere: The concluding phase of this continuum involves the evaporation of water from the leaf surfaces into the atmosphere. Factors such as temperature, humidity, and wind speed significantly affect the rates of transpiration and evaporation, thereby influencing the overall water balance[59].

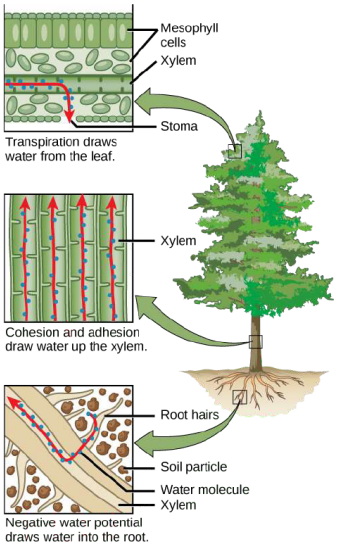

Figure 1.12: Water Flow in the Soil-Plant-Atmosphere Continuum (SPAC)

Plants play a vital role in ecohydrological processes. They are not only the primary conduits for transferring water from the soil to the atmosphere but also rely on water to carry out photosynthesis, maintain turgor pressure, and support growth [2]. The balance of water within plants is a complex interplay of various physiological and physical mechanisms, encompassing everything from water presence in the soil to its eventual loss through transpiration.

Water movement in the Soil-Plant-Atmosphere Continuum occurs along a gradient of decreasing water potential. SPAC provides a framework for interpreting water balance using both physical and physiological models, demonstrating how the soil, plant, and atmosphere interact in a cohesive flow.

To simplify the mathematical representation, the water movement within SPAC can be modeled as a series of steady states between compartments where water is in local thermodynamic equilibrium. With these assumptions, the flow of water is treated as a current traversing a network of nodes connected by resistors. Each node represents a specific water potential, and the transport of water between them is dictated by the gradients of water potential, proportional to their resistances (or inversely, their conductances) [2].

Previous analyses have shown that salinity influences plant-water interactions in two primary phases: the osmotic phase and the ionic phase. The osmotic phase occurs almost immediately (within minutes to hours) [40] following an increase in salt concentration at the root level. As salt concentration rises, it reduces the water potential in the soil, making it more challenging for plants to absorb water. This leads to a gradual decline in stomatal conductance and a swift inhibition of growth in young leaves.

Osmotic stress has a more immediate and pronounced effect on transpiration and growth compared to ionic stress, which primarily impacts older leaves, leading to senescence and a reduction in photosynthesis [41].

To cope with both osmotic and ionic stress, plants have developed various strategies and adaptations collectively referred to as osmoregulation. These adaptations contribute to a plant's salt tolerance, defining how salinity affects its water interactions, growth, and overall health. Salt tolerance varies significantly among species and results from a combination of diverse adaptations to osmotic and ionic stress that operate across different temporal scales [45].

Estimating water pathways is a complex endeavor that involves multiple compartments soil, plant, and atmosphere and requires precise characterization of water dynamics in an anisotropic medium under variable external influences. This complexity is further heightened for intertidal species, which experience unique environmental conditions such as high salinity, tidal fluctuations, and alternating waterlogged and unsaturated soil conditions, often unrepresented in standard models [47].

Moreover, gathering environmental data in tidal settings presents additional challenges, leading to a lack of extensive datasets necessary for model validation. The parameterization and validation of ecohydrological models demand comprehensive experimental data, which are often unavailable for these salt-tolerant ecosystems [47].

To address these challenges, three zero-dimensional models (i.e., single-layer models without time dependency) have been created to capture the complex effects of salinity on

plant-water relations at the plant scale. These models are presented in increasing order of difficulty and complexity (Figure 1.11). The results concerning transpiration rates (T_r) were derived from various stationary salt concentrations, along with fixed environmental and soil conditions, focusing on short- to medium-term exposure to salinity.

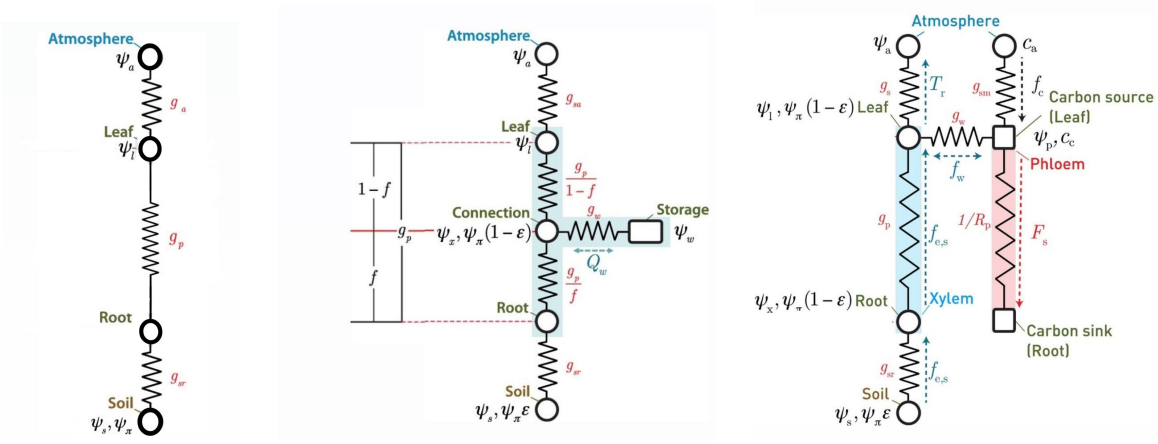

(a) (b) (c)

Figure 1.13: Conceptual representation of the SPAC with soil salinity dependence. (a)SPAC model with salinity limiting function, without capacitance[47]; (b)SPAC model with osmoregulation[45]; (c) Xylem–phloem hydraulic coupling[46].

1.6.1 SPAC model with salinity limiting function

The model proposed by [47] is a straightforward soil-plant-atmosphere continuum model, aimed at offering a conceptual one-dimensional view of how water transfers from the soil to the atmosphere through vegetation.

This model primarily focuses on replicating the mechanisms of salt tolerance, particularly concerning salt filtration at the root level. It does not account for secondary water-saving strategies, such as regulating leaf temperature or non-stomatal uptake of CO_2. The model evaluates plant transpiration using a macroscopic approach, analyzing the water flux from the soil to the plant, from the plant to the leaves, and the leaves to the atmosphere, along with

the leaf energy balance. According to the continuity principle of water potential, the total transpiration must equal these three water fluxes. Since the model excludes any storage term, the continuity assumption results in a constant water flux, which remains uniform across all plant compartments [47] (Figure 1.11 (a)).

Stomatal conductance is also influenced by the salinity of the soil pore water, independent of other conditions. Specifically, salinity leads to an initial increase in conductance as the concentration transitions from 0 (freshwater) to an optimal value (m_0), after which stomatal conductance declines for salinity levels exceeding m_0. The reduction in stomatal conductance at sub-optimal salinity is likely due to turgor loss, particularly in older leaves, while supra-optimal salinity introduces significant abiotic stress. Similar to conditions of water stress, the decrease in stomatal opening serves as a water-conserving measure. Additionally, g_s may decline due to reduced turgor or changes in cell wall elasticity resulting from high ion concentrations in the apoplastic water. In this model, the relationship between stomatal conductance and salt concentration is partly represented through its dependence on salt concentration, as depicted in the modified Jarvis equation f_m:

$$f(m) = \begin{cases} a_1 + b_1 m & \text{per } m < m_0 \\ a_2 - b_2 m & \text{per } m \geq m_0 \end{cases} \tag{1.2}$$

where :

- m_0 is equal to 150 mol/m^3;
- a_1,a_2,b_1 and b_2 are the function parameters

Salt concentration has been shown to impact transpiration rates. Specifically, as salinity increases from zero (freshwater) to an intermediate critical threshold, transpiration initially rises. However, once salinity surpasses this threshold, transpiration begins to decline. This phenomenon arises from the combined effects of salinity on macroscopic water balances.

Nevertheless, this simplified model does not consider small-scale dynamics such as ion balance and osmoregulation within the plant, which could significantly influence the overall

response to salinity. These internal mechanisms play a crucial role in modulating how plants manage water loss and maintain physiological functions under saline conditions.

This model thus represents a starting point for the next [45], which takes into account the adjustment of internal water potential in response to salt stress.

1.6.2 SPAC model with osmoregulation

The model presented by [45] is a streamlined soil-plant-atmosphere continuum (SPAC) that differs from its predecessor by incorporating both salt exclusion at the root level and osmoregulation. This model emphasizes the scale of osmoregulation, which involves phases of passive dehydration and active osmotic adjustment. It demonstrates that the direct water flux modifications employed by salt-tolerant species can account for the observed peak in transpiration.

This updated model [45], an advancement over the previous version [47], is divided into six primary compartments: (a) soil, (b) root, (c) connection (the intermediate section of the plant), (d) leaf, (e) atmosphere, and (f) the osmoregulation compartment (mid-plant storage; refer to the diagram in Figure 1.11 (b)).

Stomatal conductance is modeled using Jarvis' equation, which does not introduce any limiting function equation to account for salinity effects as previously done in [47].

In the osmoregulation component of the model, the salt concentration, denoted as C_w, is treated as a constant parameter within the soil-plant-atmosphere continuum (SPAC). This value represents the storage potential that enables the plant to optimize its water usage and counteract a specific gradient of salt concentration between the interior and exterior of the plant. When external salinity levels approach C_w, an isotonic symplastic solution is established, resulting in no storage flux. However, any variation leads to a disparity in water potential between the plant and the storage, which is balanced by the storage flow Q_w or by adjusting the plant's water uptake [45]. $C_{T_{\mathrm{r,MAX}}}$ The elements that influence $C_{T_{\mathrm{r,\,MAX}}}$ have been examined through a series of approximations that enhance the analytical feasibility of

the problem. This simplified model enables the derivation of an analytical expression for the optimal concentration as a function of various environmental, morphological, and physiological factors. It was found that $C_{T_{\mathrm{r,\,MAX}}}$ increases with C_w: the greater the plant's capacity for osmoregulation (a proxy for salt tolerance), the higher the $C_{T_{\mathrm{r,\,MAX}}}$ value. The modeled relative transpiration results align well with experimental data. However, by neglecting CO_2 assimilation, the model limits the ability to estimate the impacts of salinity and salt tolerance on productivity. The subsequent model [46] aims to incorporate these factors for a more comprehensive analysis.

1.6.3 Xylem–phloem hydraulic coupling

At the whole-plant level, salinity significantly impacts yield by limiting several key processes: (1) the movement of water from the soil to the leaves, (2) the uptake of CO_2 in the leaves, and (3) the production and translocation of carbohydrates in the phloem to meet the plant's carbon demands (Figure 1.11 (c)).

The underlying hypothesis suggests that different species respond to salt exposure based on their ability to regulate osmolyte concentrations in the xylem-leaf-phloem system. Building on this premise, a physically based model [46] has been proposed to represent the short-term effects of salinity on plant-water relations and the hydraulic coupling between xylem, leaf, and phloem. This model is grounded in three main theories: (a) the cohesion-tension theory applicable to the root-plant system, (b) the balance between biochemical demands and the atmospheric supply of CO_2 at the leaf level, and (c) the Münch osmoregulation theory that describes carbohydrate movement within the phloem.

Despite this framework, the combination of these theories remains mathematically unclosed, necessitating an additional constraint that connects soil salinity with leaf water potential (Ψ_l. To address this, four different closure assumptions are explored to enhance the coupled equations governing CO_2, water, and carbohydrate transport in the xylem-leaf-phloem system. The primary notion is that plants have evolved to rapidly optimize one of the follow-

ing: (1) sap flow to maintain leaf turgor, (2) CO_2 assimilation in the leaves, (3) carbohydrate production and loading (primarily sucrose), or (4) the trade-off between carbon gain and hydraulic cost.

Table 1.3: Summary of the four optimality hypotheses [46].

Hypothesis	**Formulation**
(1) Water uptake maximization	$\frac{\partial f_{e,s}}{\partial \psi_{v,l}} = 0$
(2) CO_2 maximization	$\frac{\partial f_c}{\partial \psi_{v,l}} = 0$
(3) Sucrose transport maximization	$\frac{\partial f_s}{\partial \psi_{v,l}} = 0$
(4) Profit maximization	$\frac{\partial}{\partial \psi_{v,l}}(G-R) = 0$

This proposed model marks an essential initial step toward describing the interconnected transport of water, carbon, and sucrose within the soil-plant system in saline environments. It encompasses the primary processes that may be affected by soil salinity and enables the exploration of various optimality rules needed to mathematically close the system and determine leaf water potential. While rigorous validation of the model is not feasible at this stage, the approach can help interpret observed patterns of transpiration and photosynthesis in halophytes and glycophytes. From this analysis, hypotheses regarding the influence of salinity on photosynthesis and plant-water interactions can be formulated, paving the way for future experimental assessments of the model [46].

1.6.4 Model Limitations

All of the approaches introduced above have several important limitations:

- The separation between osmotic and ionic phases simplifies the model structure but limits its applicability to time scales at which morphological modifications are negligible [45].

- At longer time scales, salt mass, and soil moisture balance are expected to play a crucial role and need to be included to account for salinity fluctuations[45].
- At longer time scales, the dynamics of water storage flux can significantly affect the plant response to salinity, hence the flux cannot be assumed stationary [45].
- Fluctuating environmental conditions could affect stem water storage dynamics assumed to be constant [46].
- Processes such as hydraulic redistribution (i.e. passive water movement from wet to dry soil in the root zone) and 3D gradients in soil moisture and salinity that may impact the overall plant response to salt stress are not considered [46].

A possible extension of the model may also include longer timescale dynamics and stochastic external forcing to analyze the feedback effect of salinity on the water balance [47].

The objective of this study is to develop a transient model of the soil-plant-atmosphere continuum (SPAC), which incorporates the water storage capacity of the different system components. This model will be developed in a dynamic context, where environmental conditions are not fixed, and soil moisture varies over time. Specifically, it will take into account fluctuations in meteorological conditions, soil-plant interactions, and the overall water balance, to achieve a more accurate and realistic representation of water transport processes.

Finally, the model will be used to observe and analyze the plant's response when subjected to dual stress factors, namely the combination of salinity and drought. This approach will provide a better understanding of how the plant's physiological processes are affected by the simultaneous presence of these two adverse conditions, offering insights into the sustainable management of natural ecosystems in environments prone to such stressors.

2. Case Study Introduction

This study focuses on data collection from two wetland sites in coastal Louisiana, selected to represent two marsh types (fresh and brackish). The coastal zone of Louisiana encompasses approximately 2144 km² of brackish marsh and about 2837 km² of freshwater marsh. Both sites feature vegetation assemblages and hydrological signatures consistent with these wetland types. Many brackish marshes in Louisiana are experiencing stress and peat collapse due to persistent submersion and saltwater intrusion, and our brackish marsh site is representative of such degradation. Additionally, the continuous marsh cover within a 200-meter radius ensures reliable EC measurements [31].

Two sites were selected for this study, although not directly part of the Bird Foot Delta—the primary area of interest—to address the lack of stations capable of providing meteorological data required for model validation and verification. These eddy covariance stations enable the collection of CO_2 fluxes, evapotranspiration, and meteorological data to be used as model inputs. Additional salinity, biomass, and water level data will be obtained from CRMS stations.

The analyzed data show discontinuities, with periods where data are not consecutively available. For this reason, the selected observation period spans from 2021 to 2023, during which there is a more continuous data coverage sufficient for meaningful analyses. This timeframe provides an opportunity to study the behavior of ecosystem fluxes, such as evapotranspiration, CO2, and CH4 fluxes, during a significant climatic event: the drought that occurred in 2022. The 2022 drought event represents an opportunity to examine the combined effects of water stress and high salinity conditions on ecosystem fluxes.

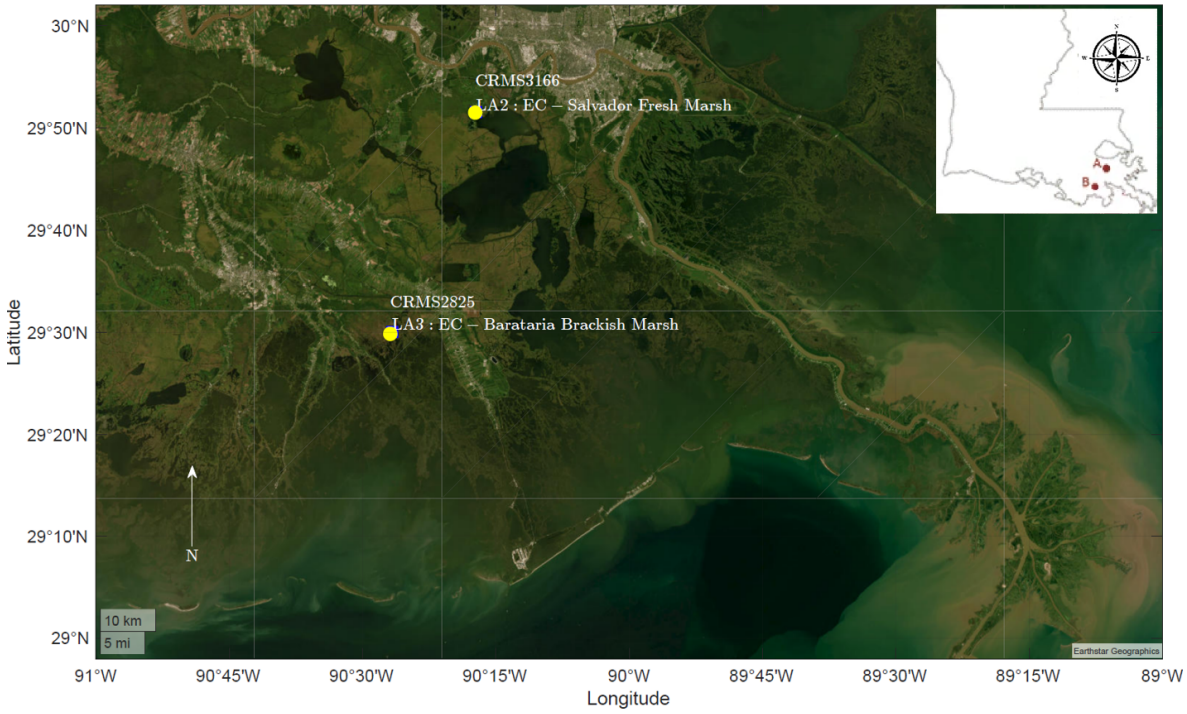

(a)

(b)

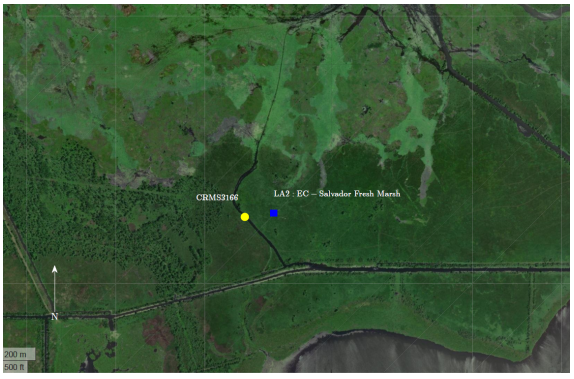

(c)

Figure 2.1: Geographical context of the two marshes (a) with enlargement of the brackish (b) and freshwater(b) eddy covariance study sites (blu) in coastal Louisiana and the location of Coastwide Reference Monitoring System stations (yellows).

The first site (hereafter referred to as "brackish marsh") is located adjacent to the Pointe-aux-Chenes Wildlife Management Area (WMA), approximately 24 km southeast of Houma ($29^\circ 30' 04.77'' \mathrm{N}; 90^\circ 26' 41.65'' \mathrm{W}$; Coastwide Reference Monitoring System (CRMS-Wetlands) site 2825). The soils are organic (40–70% organic content) with a low bulk density ($< 0.2\,\mathrm{g\,cm^{-3}}$) and a live rooting depth $\leq 30\,\mathrm{cm}$. The site is classified as mesohaline and is dominated by *Spartina patens* [24].

The second site (hereafter referred to as the "freshwater marsh") is located in the Salvador Wildlife Management Area (WMA), approximately 19 km southeast of New Orleans ($29^\circ 51' 31.29'' \mathrm{N}, 90^\circ 17' 12.80'' \mathrm{W}$; CRMS-Wetlands site 3166). The freshwater marsh, with a salinity of 0.23 ± 0.1 psu (SE) during the study period, represents lowland deltaic freshwater wetlands. The dominant species in this area is *Sagittaria lancifolia*. The soils consist of more than 75% organic matter, with a bulk density of $< 0.10\,\mathrm{g\,cm^{-3}}$ and live rooting depths reaching up to 60 cm [24].

Both sites are microtidal (range < 30 cm) with major wind events influencing the duration of flooding. From the water table levels shown below, it is clear that, for both sites, the vegetation remains submerged most of the time. The period during which the sites experience prolonged non-flooded conditions coincides precisely with the drought event.

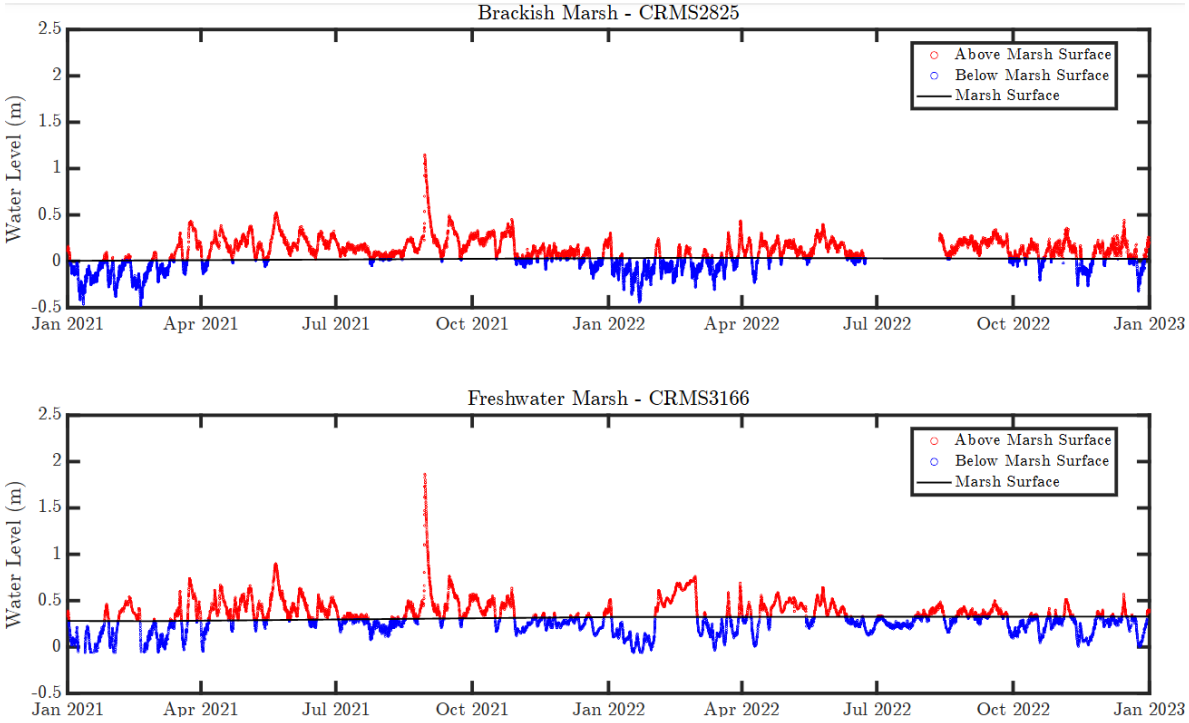

Figure 2.2: Water Level for the two CRMS stations of interest

As a result, the soil in these environments consistently exhibits near-saturation soil moisture, a finding further confirmed by the EC data, indicating a water content ranging between 80% and 100%. The soil moisture value was also extracted from the EC station. Unfortunately, for the entire observation period, the only available data is for a single day for a single EC station LA3 , as shown in the figure below. However, this value can be considered representative and provides an indication of how, under these conditions, the soil remains saturated or near saturation for most of the time.

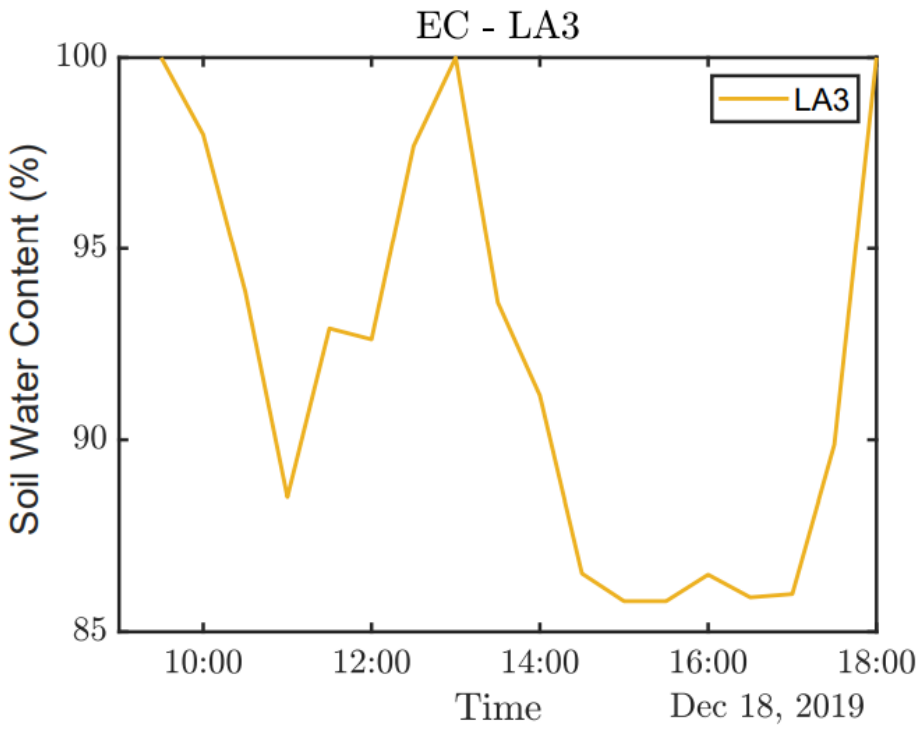

Figure 2.3: Daily variation of soil moisture, for the EC- LA3

Air temperature, precipitation (mm/h), relative humidity, and net radiation for both sites are shown in the following figure. These parameters will be used as input data in the model to define dynamic rather than fixed boundary conditions.

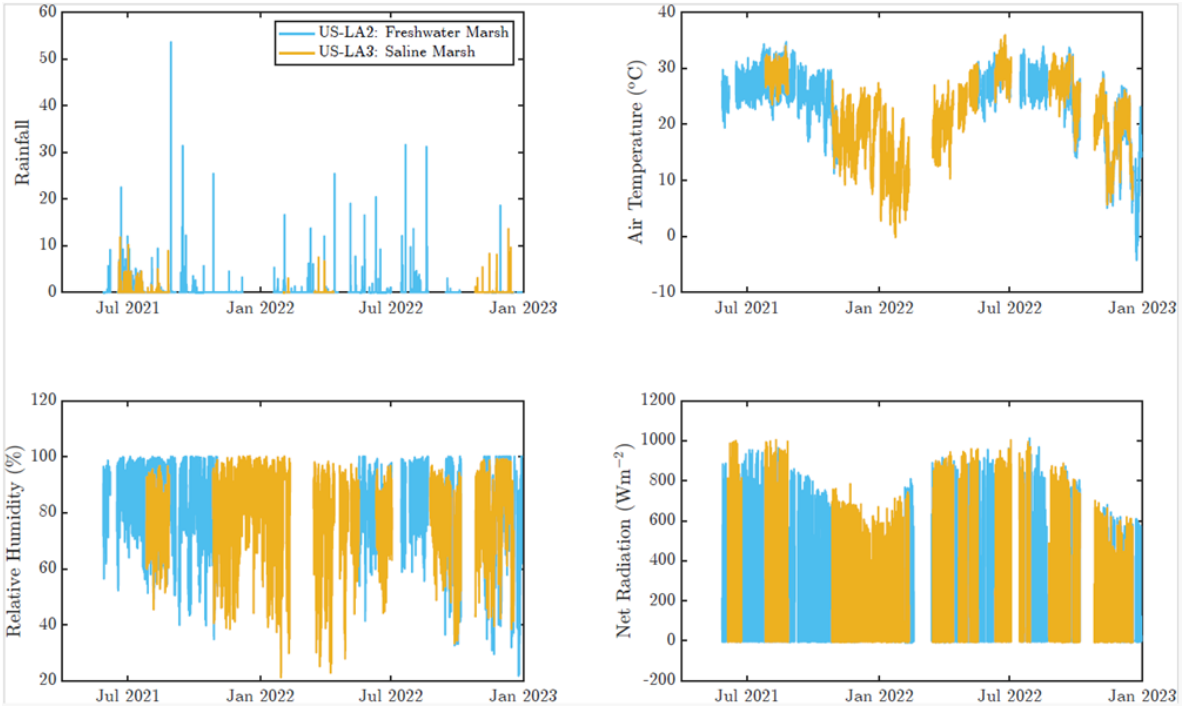

Figure 2.4: Time Series of Meteorological Data from the two EC stations (Rainfall, Air Temperature, Relative Humidity, and Net Radiation

Soil temperature data were also extracted from both EC stations. However, only station LA2 provided a continuous data series spanning from 2012 to 2014. An average was calculated from these values, which will be used as a fixed variable within the model. The resulting average temperature of soil (TS) is 23°C.

2.1 Data Collection EC

Both sites are equipped with towers featuring an open-path methane sensor (LI-COR LI-7700, LI-COR Biosciences, Nebraska, USA), a closed-path CO2/H2O sensor (LI-COR LI-7200), and a sonic anemometer (Gill Windmaster Pro, Gill Instruments Ltd., Lymington, UK), along with a data logger and an air pump. The Eddy Covariance (EC) systems are in-

stalled on 3×3 m platforms elevated 1.0 m above the ground surface. The towers are centrally located within a homogeneous wetland area with similar roughness (or canopy height) within a 200 m fetch, ensuring that wind directions can be captured from all sides to maximize data acquisition. Both sites feature similar heights of emergent herbaceous canopies, ranging from 0.5 to 1.2 m throughout the year. Measurement heights above the ground surface were 3.6 m and 3.4 m for the freshwater and brackish sites, respectively [24].

Figure 2.5: Eddy Covariance (EC) systems installed at the selected sites [24].

See the following section (2.1.1) to understand better how the EC technique collects measurements. Data were downloaded from the AmeriFlux platform, which provides detailed information on greenhouse gas, energy, and water exchanges between terrestrial ecosystems and the atmosphere, obtained using Eddy Covariance (EC) techniques. The data were downloaded with an hourly aggregation. These datasets are the result of continuous, high-resolution measurements subjected to standardization and quality control. Advanced processes such as gap-filling to address missing data and the partitioning of total fluxes into key

components like Gross Primary Production (GPP) and Ecosystem Respiration (RECO) were also applied.

These data are suitable for ecological, climatic, and hydrological modeling, as they integrate additional meteorological parameters such as temperature, relative humidity, and net radiation.

2.1.1 Eddy Covariance Method

Eddy covariance (also referred to as eddy correlation or eddy flux) is a fundamental atmospheric measurement technique employed to quantify vertical turbulent fluxes within atmospheric boundary layers. This method involves the analysis of high-frequency scalar atmospheric data, wind velocity, gases, energy, and momentum to derive flux values for these properties. As a statistical technique, eddy covariance is widely used in meteorology, micrometeorology, oceanography, hydrology, agricultural sciences, and in regulatory and industrial applications to determine trace gas exchange rates over natural ecosystems and agricultural fields, as well as to quantify emission rates from other terrestrial and aquatic surfaces. It is frequently applied to estimate momentum fluxes, heat, water vapor, carbon dioxide, and methane [64].

Airflow can be conceptualized as a horizontal movement comprised of numerous rotating eddies, each with three-dimensional components, including vertical air motion. Although this process may initially appear chaotic, these components can be effectively measured using instrumentation mounted on a tower. In the accompanying diagram, the airflow is depicted as a large arrow passing through the tower, consisting of eddies of varying sizes. This framework forms the basis of atmospheric eddy transport [7].

Turbulent eddies are primarily generated by the interplay of shear forces and buoyancy. Mechanical shear arises when the horizontal wind encounters obstacles such as vegetation canopies, buildings, or topographical features, disrupting the flow. Additionally, larger ed-

dies induce wind shear that creates smaller eddies, transferring turbulent energy from larger to smaller scales in a process known as the turbulent energy cascade. Buoyancy, on the other hand, occurs when warmer, lighter air rises (upwelling) or cooler, denser air descends (downwelling), further contributing to turbulence. In some instances, significant water vapor fluxes may enhance buoyancy through the upward movement of lighter, moisture-laden air. These mechanisms collectively drive atmospheric eddy transport [7].

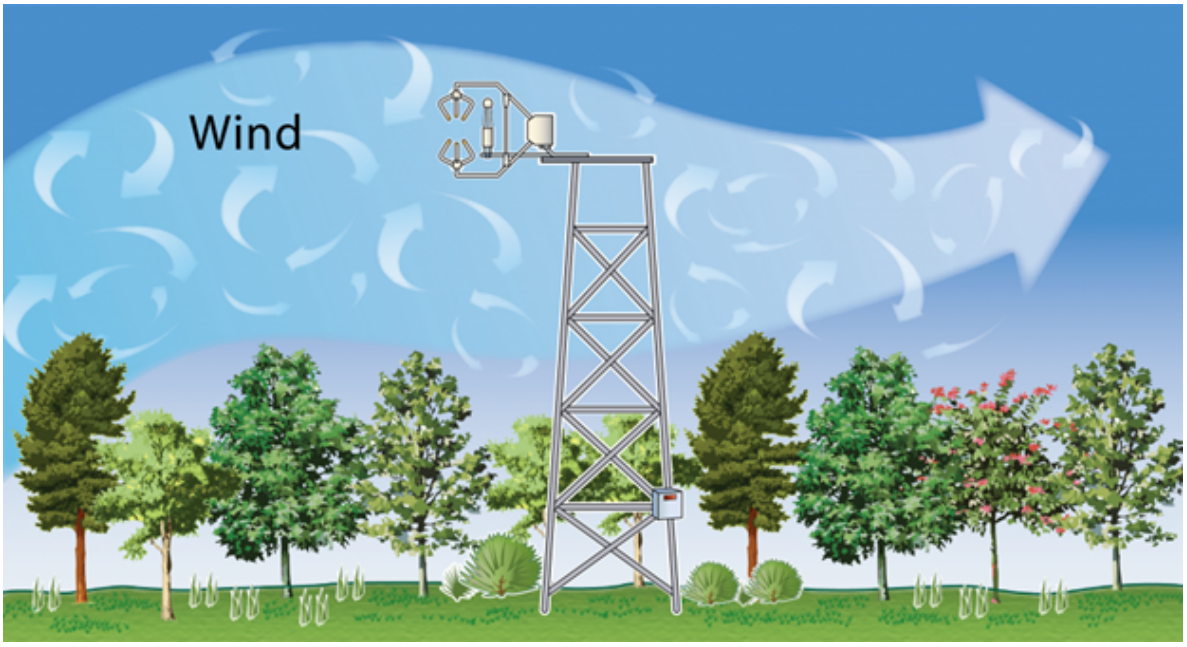

Figure 2.6: Tower of Eddy covariance [47]

From the perspective of a single point on the tower, at one moment (time 1), eddy number 1 moves air parcel c_1 downward with the speed w_1. At the next moment (time 2) at the same point, eddy number 2 moves air parcel c_2 upward with speed w_2. Each air parcel has its characteristics, such as gas concentrations, temperature, humidity, etc. If we can measure these characteristics and the speed of the vertical air movement, we will know the vertical upward or downward fluxes of gas and water vapor concentrations, temperature, and humidity. This is the general principle of eddy covariance measurements: covariance between

the concentration of interest and vertical wind speed [7].

$$\mathrm{COV}_{x,y} = \frac{\sum(x_i - \bar{x})(y_i - \bar{y})}{N-1} \tag{2.1}$$

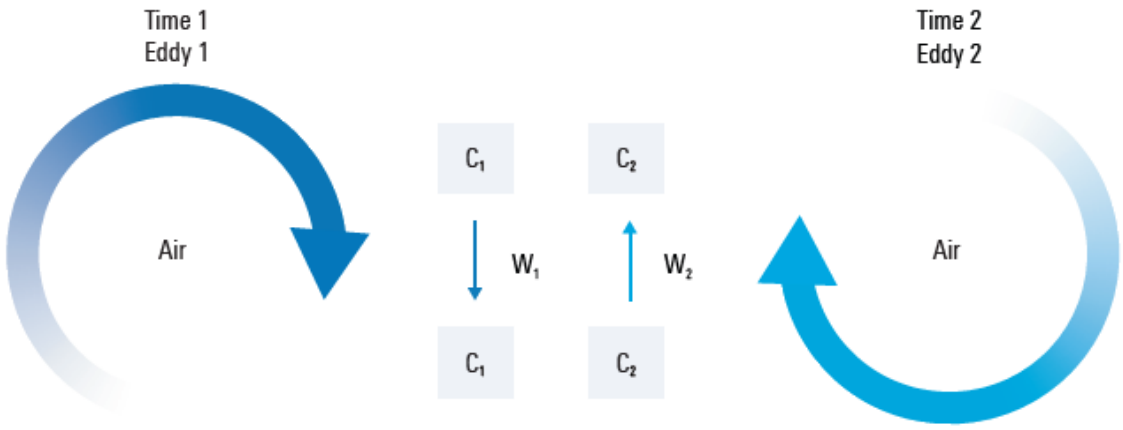

Figure 2.7: Eddies at a single point [7].

The mathematical foundation of the method is as follows and the major assumptions: In turbulent flow, vertical flux can be expressed as the mean product of dry air density (ρ_d), vertical wind speed (w), and the dry mole fraction of the gas of interest (s).

$$F = \overline{\rho_d w s} \tag{2.2}$$

Reynolds decomposition is applied to separate the equation into mean values and deviations from these means. Air density is represented as the sum of a mean value, averaged over a specific period, and an instantaneous deviation from that mean. A similar approach is applied to vertical wind speed and the dry mole fraction of the substance of interest. Considering that the average deviations from the average are removed since the average deviation from an average is zero, the simplified and final equation is given by

$$F = \overline{\rho_d}\,\overline{ws} + \overline{\rho_d}\,\overline{w's'} + w\overline{\rho_d s'} + s\overline{\rho_d w'} + \rho_d\overline{w's'} \tag{2.3}$$

In the conventional eddy covariance method, two key assumptions are made. First, it is assumed that air density fluctuations are negligible. This assumption is generally valid when eddy covariance is applied to large, relatively flat areas, such as fields or plains, where air density variations do not significantly affect the results. Second, it is assumed that the mean vertical flow is negligible in horizontally homogeneous terrain, meaning that there are no flow diversions or conversions. With these two assumptions, the classic equation for eddy flux is derived. The flux is defined as the product of the mean air density and the mean covariance between the instantaneous deviations of vertical wind speed and dry mole fraction. And accordingly, for the scalar fluxes of heat, water, and carbon we have:

Flux Type	**Equation**
Sensible Heat Flux	$F_{c_pT} = H = \rho c_p \overline{w'T'}$
Latent Heat Flux	$F_q = \rho_w E = \rho \overline{w'q'}$
Carbon Flux	$F_{CO_2} = \rho \overline{w'c'}$

Table 2.1: Flux Equations

In addition to the assumptions given thus far, there are other important assumptions in the eddy covariance method. Measurements at a point are assumed to represent an upwind area. Measurements are also assumed to be done inside the boundary layer of interest and the constant flux layer. Fetch and footprint are assumed adequate, so flux is measured from the area of interest. It is assumed that flux is fully turbulent, the terrain is horizontal and uniform, and flow divergences and convergences are negligible. It is also assumed that air density fluctuations are negligible, and the instruments can detect very small changes at a very high frequency. Finally, it is assumed that mean airflow and turbulence at the measurement point are not appreciably distorted by the installation structure or the instruments themselves. The degree to which some of these assumptions hold depends on proper site selection and instrument setup [7].

2.2 Data Collection CRMS

While EC stations provide us with meteorological data, the Coastwide Reference Monitoring System (CRMS) stations in the Mississippi Delta are designed to monitor and assess the health of coastal wetlands through an integrated monitoring network. These stations collect data on key environmental variables, including salinity, water level, soil moisture, vegetation biomass, soil quality, and water fluxes. This data is recorded at regular intervals to provide a comprehensive and detailed view of environmental conditions and their variations over time [50].

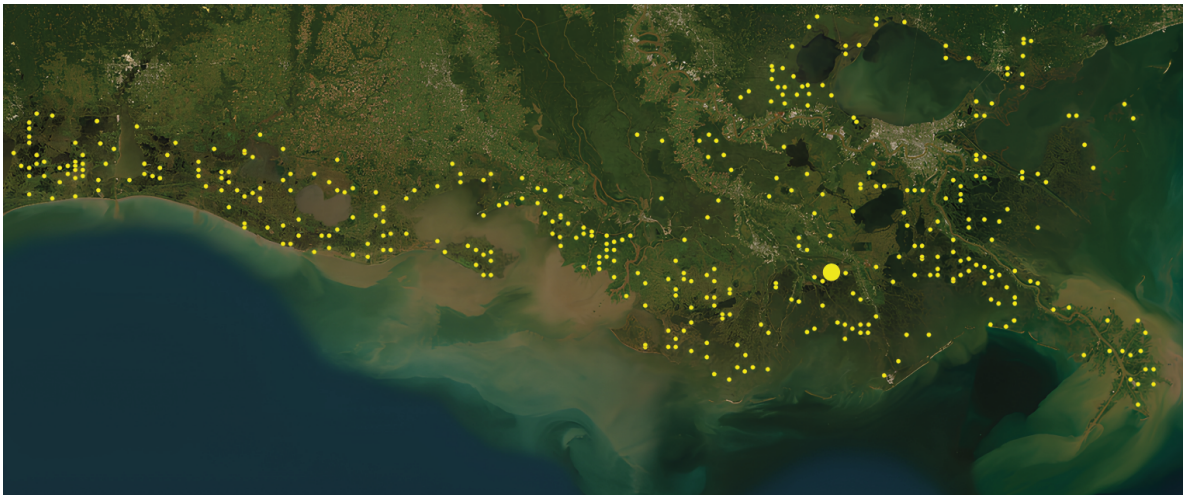

Figure 2.8: Coastal Reference Monitoring System (CRMS) network stations along the Mississippi Delta .

The primary goal is to understand how natural and human-induced factors, such as saline intrusion, soil subsidence, erosion, and alterations in water flow, affect the health of wetland areas. Through this monitoring network, the CRMS stations support the development of environmental management and restoration strategies, providing data to predict the impact of extreme events, such as storms and droughts, and to evaluate the effectiveness of conserva-

tion interventions over the long term. This system is a critical resource for the sustainable management and conservation of wetlands in the Mississippi Delta.

From the CRMS station, it was possible to extract the water level, the elevation of the marsh, the Total biomass, and the salinity.

The baseline measurements of wetland conditions are based on biomass or productivity measurements to enhance the understanding of the system's structure and function (within a given location) and its responses to restoration activities or natural trajectories. Aboveground and belowground biomass samples, along with other plant and soil characteristics, are collected for the System Wide Assessment and Monitoring Program (SWAMP). These samples are gathered at selected CRMS sites within each hydrological basin. Peak standing biomass serves as an indicator of wetland production or productivity. Belowground biomass measurements, obtained from soil samples at CRMS stations, are designed to document changes in both aboveground and belowground biomass in wetlands. After the collection of baseline samples, vegetation parameters will be sampled every 5 years from 3 plots per CRMS site at a subset of CRMS locations. These sites represent specific vegetation communities containing at least one of the seven target taxa, whenever possible. The whole plot parameters include total aboveground live and dead biomass. The plots measure 0.5 x 0.5 m.

Three aboveground biomass clip-plots (replicates) are collected at each selected CRMS site. The mean and standard error (SE) are calculated for both "Total live aboveground biomass (g/m2)" and "Total dead aboveground biomass (g/m2)" for each year and site. Three belowground biomass cores are collected from each site. The mean and SE are calculated for both "Belowground live biomass (g/m2)" and "Belowground dead biomass (g/m2)" for each year and site. This is done for each of the three biomass cores by summing the biomass across depths and then calculating the mean and SE of the sums.

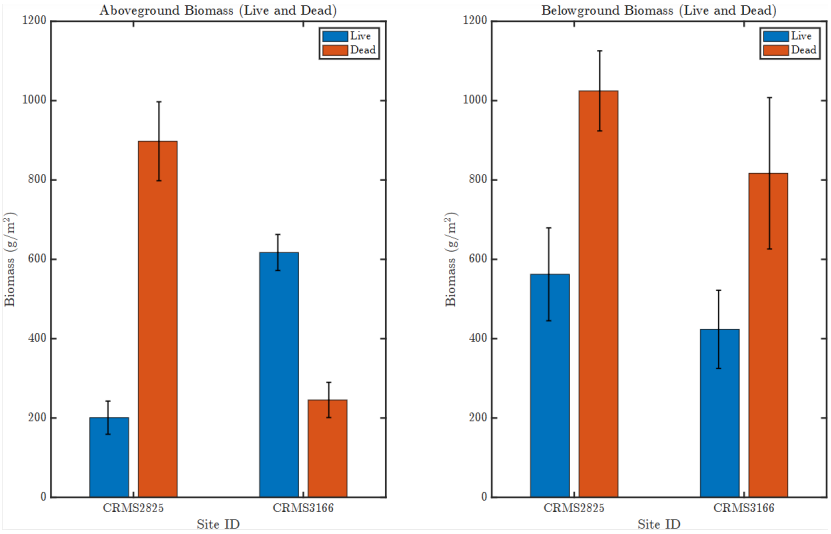

Figure 2.9: Aboveground and Belowground Biomass (Leave and Dead)

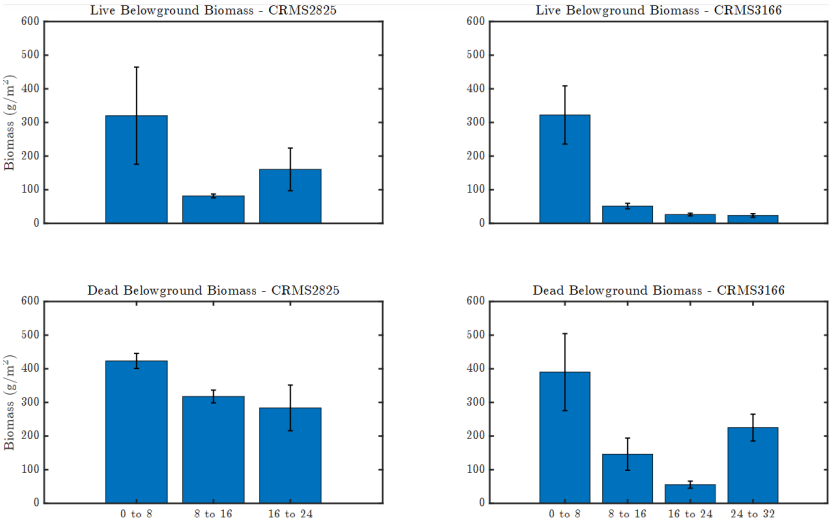

Figure 2.10: Aboveground and Belowground Biomass (Leave and Dead), in relation to depth

The biomass levels vary depending on the site considered. When a plant is exposed to higher salinity levels, as in the case of site CRMS2825, it may trigger various physiological and adaptive responses, leading to increased belowground biomass production despite the water and salt stress induced by salinity.

Plants in saline environments develop mechanisms to maintain osmotic balance within their cells. To achieve this, they accumulate compatible solutes (such as sugars and amino acids) within their roots and vascular system. This adaptation enhances the plant's ability to absorb water even under high salinity conditions, allowing it to invest more resources in belowground growth to improve water and nutrient uptake.

Exposure to salinity can stimulate root growth as a response to the increased need for water and nutrients. Root growth in saline environments is often associated with greater root depth and density, enhancing access to less saline water resources at greater soil depths or enabling solute accumulation to regulate osmotic pressure.

An increase in belowground biomass under high salinity conditions is often accompanied by a reduction in aboveground biomass. In saline stress conditions, plants may redirect resources, such as energy and nutrients, from aboveground growth to root development. This strategy enhances water and mineral absorption efficiency—crucial in saline environments—but implies a reduction in aerial biomass, as fewer resources are dedicated to leaf and stem growth. In saline environments, plants may reduce leaf area to limit water loss through transpiration, an adaptive mechanism to minimize further water stress. A smaller leaf area limits evaporation but results in lower aboveground biomass. Exposure to high salinity can also inhibit metabolic processes in the aboveground parts of the plant, reducing photosynthetic efficiency. This limitation leads to stunted growth of aerial parts, which are less equipped to compete for light and space compared to less saline conditions.

2.3 Fluxes and their relation with Salinity

For the salt marsh site, compared to the freshwater site, the vegetation is exposed to salinity stress, requiring more detailed considerations. The increase in salinity presents additional challenges to the vegetation, affecting its productivity, physiology, and species composition. This salinity stress alters the plants' ability to absorb water and nutrients, leading to either continuous adaptation or a reduction in vitality. Therefore, it is necessary to carefully consider the interaction between salinity, vegetation, and other ecological factors such as inundation, which together determine the overall behavior of the salt marsh ecosystem.

Below are the salinity levels, evapotranspiration fluxes, and CO_2 assimilation fluxes for both sites. Both the saltwater marsh and the freshwater marsh experienced an increase in salinity during 2022, attributed to heightened saline intrusion resulting from an extreme drought event. In the first case, salinity levels reached very high values, which will negatively impact the vegetation, as the levels far exceed the maximum tolerance thresholds. In the second case, for the freshwater site, this does not occur, as salinity levels only increase during the drought event, remaining well below the critical tolerance limits.

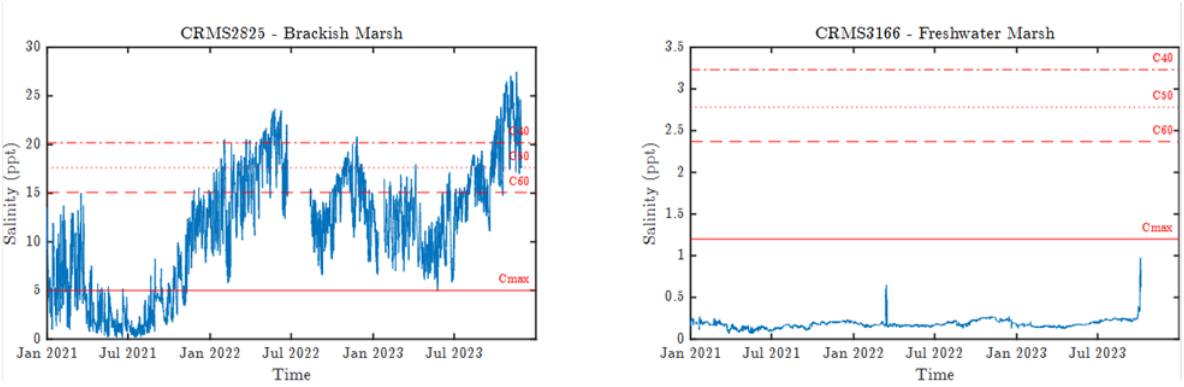

Figure 2.11: Salinity (Blue) time series with different thresholds (Red) for each dominant vegetation

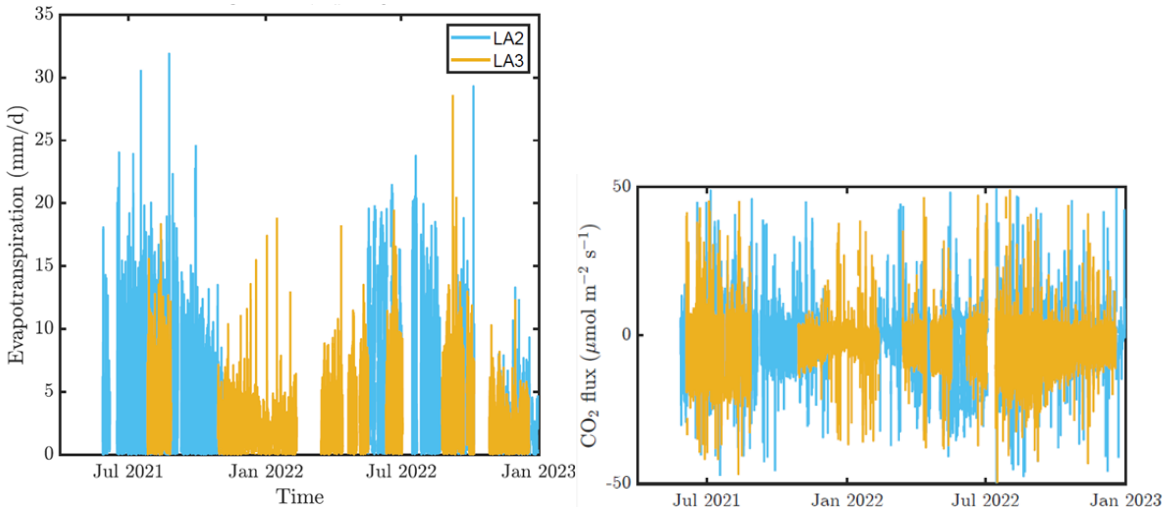

(a) (b)

Figure 2.12: Fluxes exchange of Evapotranspiration (a) and Assimilation of CO_2 (b) for both EC station.

The salinity threshold values (C_{max}, C_{60}, C_{50}, C_{40}), shown in Figure 2.9, are critical parameters that define the tolerance of a specific plant species in relation to productivity. These values represent the salinity levels beyond which significant changes occur in the plant's ability to perform photosynthesis, absorb nutrients, and maintain a balanced metabolism. For *Spartina Patens*, as shown in the figure, the maximum productivity level occurs at a salinity of approximately 5 ppt, beyond which productivity decreases almost linearly with increasing salinity.

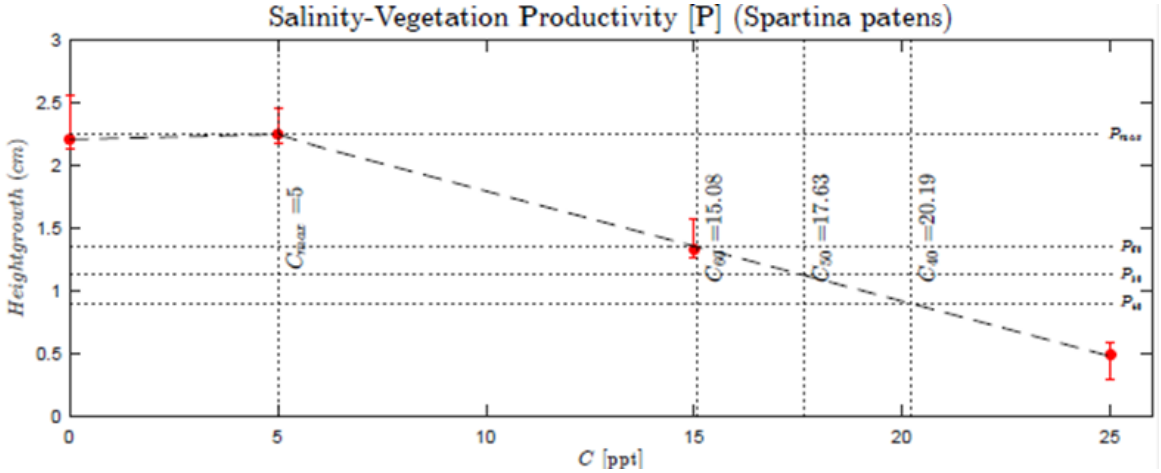

Figure 2.13: Salinity Threshold values in relation with productivity for *Spartina Patens*

By comparing the threshold values of *Spartina Patens* with the continuous salinity data provided by the CRMS (Coastwide Reference Monitoring System), significant observations emerge regarding two drought events that occurred during the observation period: the first in 2012 and the second in 2022 (Figure 2.12).

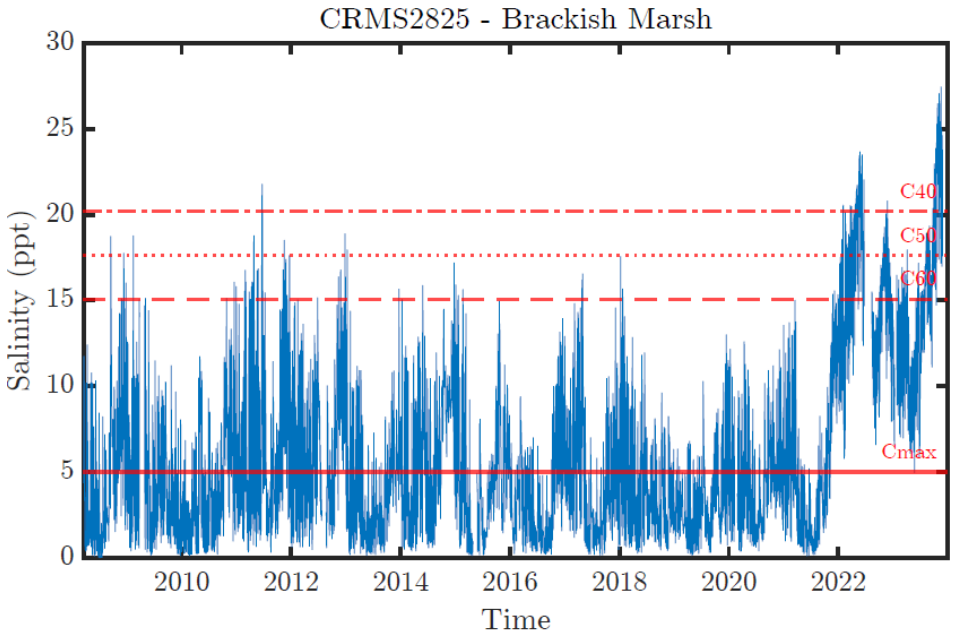

Figure 2.14: Salinity Levels for the Brackish Marsh Over the Entire Time Period Recorded by CRMS2825

As explained in the previous chapter, drought intensifies soil and water salinity, profoundly influencing plant productivity. During the 2012 drought event, salinity levels reached peaks that exceeded the C_{50} threshold value. However, once the event concluded, salinity progressively returned to near-normal levels, allowing the vegetation, dominated by *Spartina Patens*, to recover and re-establish its cover.

The second drought event presented significantly different dynamics. Starting from the end of 2021, salinity levels showed a marked increase, reaching peak values during the most intense period of the drought. After the event, instead of decreasing, salinity continued to rise, surpassing the C_{40} threshold value. This prolonged salinity stress had severe effects on the vegetation, leading to a substantial change in the site's floristic composition.

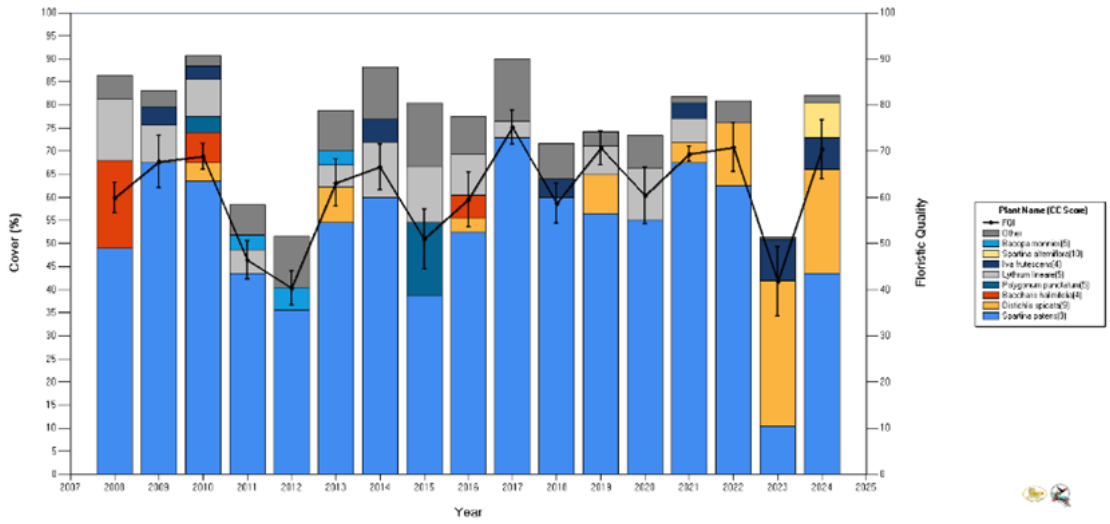

Figure 2.15: % Cover vegetation for Brackish Marsh, CRMS2825 [50].

Analyzing the percentage of vegetation cover during the two drought events, a marked difference in species response emerges:

- First event (2012): The vegetation remained dominated by *Spartina Patens*, despite temporary salinity stress.
- Second event (2022): A significant reduction in *Spartina patens* cover was observed, along with a substantial increase in the percentage of *Distichlis Spicata*.

This sudden change in vegetative composition could be explained by the different salinity tolerance thresholds of the two species. *Distichlis Spicata* is known for its ability to tolerate higher salinity conditions compared to *Spartina patens*. The replacement of the dominant species thus reflects the site's adaptation to an increasingly saline-stressed environment. The shift from a plant community dominated by *Spartina Patens* to one characterized by *Distichlis Spicata* involves changes not only in vegetation structure but also in the ecological functions of the marsh. The reduction of *Spartina Patens*, which contributes significantly to soil stability and primary productivity, could lead to increased vulnerability of the site to

erosive phenomena and a reduction in carbon sequestration. The analysis of salinity data and vegetation composition highlights how more intense and prolonged drought events can trigger significant changes in the dynamics of tidal ecosystems. The replacement of dominant species represents an adaptive response, but it raises questions about the long-term stability of these ecosystems under the influence of extreme climatic events and the rising salinity associated with climate change.

The daily average fluxes of evapotranspiration (ET) and CO_2 extracted from the EC station were analyzed concerning salinity levels. The graphical data show that for salinity levels below the minimum threshold value (C_{max}), the fluxes remain stable. However, for salinity levels between C_{max} and C_{60}, there is an average reduction in fluxes of approximately of 2 mm/day for ET and 4 $\mu\text{mol}\,\text{m}^{-2}\,\text{s}^{-1}$ for CO_2 flux. This reduction, which appears to be modest daily (few mm/day for ET or minimal variations in greenhouse gas fluxes), when extrapolated over the entire year, can have a significant impact on the overall balance of the wetland.

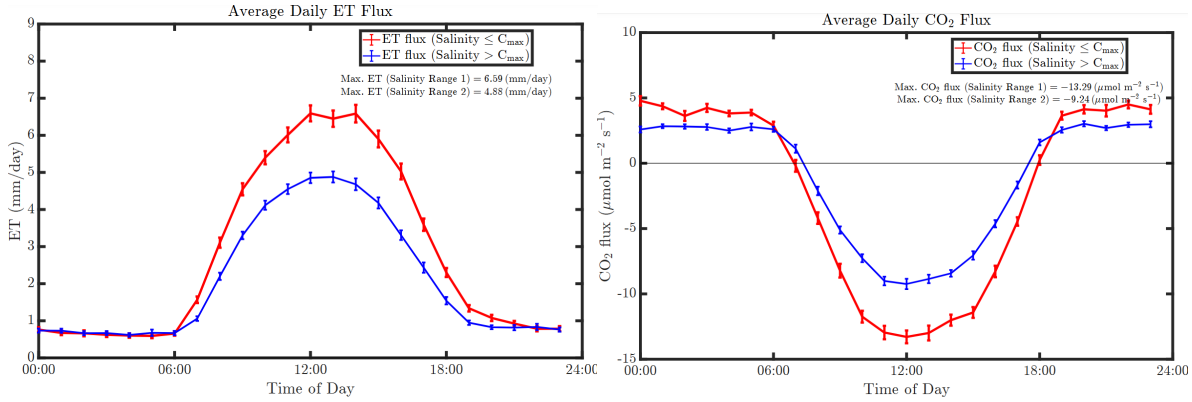

(a) (b)

Figure 2.16: Fluxes exchange in relation with the salinity of Evapotranspiration (a) and Assimilation of CO_2 (b) for Brackish Marsh, CRMS2825

An interesting observation concerns the fluxes corresponding to salinity levels above (C_{max}). Contrary to the expectation of a continuous decline in fluxes with increasing salinity, the data show that extreme salinity levels do not result in further significant reductions. The fluxes for salinities above (C_{max}) are similar to those recorded for salinity levels just above the threshold. For this reason, only two flux ranges are reported: one representing the maximum flux under conditions below stress levels, and another showing peak values under stress conditions. This behavior suggests that, in addition to salinity, other environmental factors, such as stress from inundation, may play a crucial role in modulating the fluxes.

Wetlands, being subject to periodic flooding, experience simultaneous stress from both salinity and inundation. Their interaction differs in how they influence the various fluxes:

- CO_2 Assimilation: It shows a constant impact from both stress factors. Salinity limits photosynthetic efficiency through stomatal closure, while inundation further reduces assimilation due to decreased oxygen availability in the soil and leaf photosynthesis under hypoxic conditions.

- Evapotranspiration (ET): It responds differently. In the presence of inundation, the evaporation component increases due to the free water on the surface, compensating for the losses caused by reduced plant transpiration. This behavior might explain why, at high salinity levels combined with continuous inundation, ET fluxes do not show a continuous decline.

To isolate the specific effects of inundation, a comparison was made by removing periods when the system was submerged. This analysis allowed for a clearer distinction between the relative contributions of salinity and inundation to changes in the daily average fluxes.

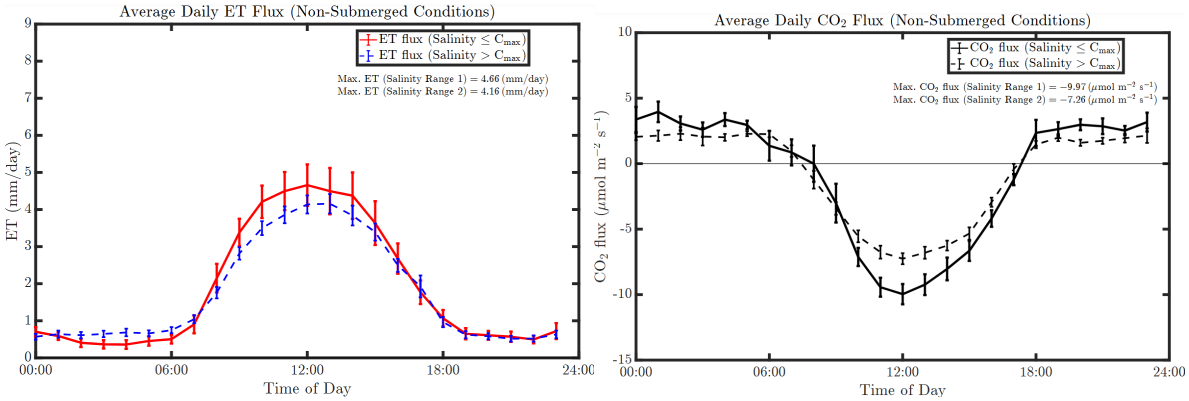

(a) (b)

Figure 2.17: Fluxes exchange in relation with the salinity of Evapotranspiration (a) and Assimilation of CO_2 (b) for Brackish Marsh, CRMS2825, without period of submersion

The results confirm that inundation plays a significant role in modulating the fluxes, particularly for evapotranspiration and, to a lesser extent, for assimilation. Including inundation in simulation models is essential for accurately representing ecosystem fluxes in tidal wetlands. The combination of salinity and inundation effects, as well as their interactions, must be parameterized to correctly predict the impact of future scenarios, such as sea-level rise or increased drought events. A model that integrates both factors will allow for a better representation of the hydrological and ecosystemic balance, which is crucial for management and conservation strategies.

As will be introduced later, it is unfortunate that in the model that will be presented, we have only been able to include salinity effects, thus not considering submergence. but once the results are obtained, they will be considered in order to manipulate the results and make important considerations.

3. Approach and Model

As introduced in the first chapter, the primary objective of this work is to develop a dynamic model capable of representing the impact of salinity on plant productivity. This impact will be analyzed regarding transpiration, carbon assimilation, and biomass production. Unlike previously discussed cases, the model will integrate not only osmotic stress, representing the immediate effect of salinity but also ionic stress, significantly limiting plant physiological performance over the long term.

An innovative aspect of the model is the water balance, where soil moisture is not treated as a fixed variable but evolves dynamically over time, oscillating within a predefined minimum range. Additionally, boundary climatic conditions will be variable and not imposed as static parameters, enhancing the model's alignment with real environmental scenarios.

The methodological foundation of this work is the Photo3 model [22], implemented in Python. This model describes photosynthesis in C3, C4, and CAM species consistently, using the Farquhar et al. model for carbon assimilation. Photo3 also calculates stomatal conductance and transpiration based on stomatal optimization theory, integrating soil and atmospheric conditions through a representation of the soil-plant-atmosphere continuum, with the option to include plant water storage. Using variables such as soil moisture, air temperature, relative humidity, and solar radiation, the model determines net carbon assimilation and transpiration, among other variables of interest.

In this study, Photo3 is employed to parameterize two representative species from the study areas described in the previous chapter: *Spartina patens* (C4) and *Sagittaria lancifolia* (C3). The aim is to adapt the model to the specific conditions of wetland ecosystems, characterized by saline soils and submersion, as discussed in earlier chapters. Integrating these key parameters will enhance the model's accuracy and predictive capabilities, making it more suitable for representing the ecological dynamics typical of these habitats.

3.1 Transpiration and soil water balance

According to the classical framework of the soil–plant–atmosphere continuum (see Appendix A), the water is taken up by the roots, flows through the xylem, and exits through the leaf stomata to the atmosphere, following a path of decreasing water potential, from the soil at Ψ_s, through the leaves at Ψ_l, to the atmosphere at Ψ_a. Typically, the water flow inside the plant is assumed to take place as a succession of steady states (i.e., considering the system adjustment to the time-varying equilibrium conditions as practically instantaneous). The exchanges between vegetation and atmosphere are simply modeled using the standard big-leaf schematization [22]. Under these assumptions, the soil moisture be provided as a model input or determined through the balance equation,

$$n \cdot ZR \cdot \frac{ds}{dt} = -E - EV - L \tag{3.1}$$

where n is the soil porosity, Z_r is the rooting depth and s is the volumetric soil moisture averaged over the rooting depth. Total losses from the soil are due to plant water uptake qs(s,w), leakage loss L(s), and evaporation Ev (s). The Evapotranspiration, E, represent the sum of the losses resulting from plant transpiration and evaporation from the soil. When soil moisture is high, the evapotranspiration rate depends mainly on the type of plant and climatic conditions (e.g., leaf area index, wind speed, air temperature and humidity, etc.). As long as soil moisture content is sufficient to permit the normal course of the plant physiological processes, evapotranspiration is assumed to occur at a maximum rate Emax, which is independent of s. When soil moisture content falls below a given point, which depends on both vegetation and soil characteristics, plant transpiration (at the daily time scale) is reduced by stomatal closure to prevent internal water losses and soil water availability becomes a key factor in determining the actual evapotranspiration rate. Is possible also to considere the rainfall R(t), may be specified either as a model input or may be generated within the model as a stochastic process that requires the mean rainfall depth and frequency as input parameters [22].

Soil Evaporation :

$$\text{evap}(s) = \begin{cases} \text{EVMAX} \cdot \frac{s-\text{SH}}{1-\text{SH}} & \text{if } s > \text{SH} \\ 0 & \text{otherwise} \end{cases} \tag{3.2}$$

Where :

- EVMAX is the maximum soil evaporation rate;
- SH is the soil moisture threshold below which evaporation is zero

For reasons of mathematical convenience, EV is assumed to be equal to EVmax for s higher than the wilting point s_w and to decrease linearly to zero at the hygroscopic point s_h.

Soil Water Leakage Equation: Leakage losses are assumed to happen by gravity at the lowest boundary of the soil layer, neglecting possible differences in matrix potential between the soil layer under consideration and the one immediately below. The loss rate is assumed to be at its maximum when soil is saturated and then rapidly decays as the soil dries out, following the decrease of the hydraulic conductivity K(s) [1]. The decay of the hydraulic conductivity is usually modeled using empirical relationships of different forms.

$$\text{leak}(s) = 0.11574 \cdot K_S \cdot s^{(2B+3)} \tag{3.3}$$

Where:

- KS is the saturated soil hydraulic conductivity.
- s is the soil moisture saturation fraction.
- B is an empirical coefficient.

Since it is a transient model, soil moisture is updated at each time interval to reflect dynamic changes in water content. In this study, given that the soil remains predominantly near saturation for most of the time, as confirmed by both site data and water table levels, a constant

soil moisture value close to saturation will be adopted. This approach, which will be detailed in the following chapter, highlights the persistent saturation of the soil and allows for a significant simplification of the model.

The SPAC system is solved using a soil, root, plant formulation combined with a stoma, atmosphere formulation using the continuity assumption that the water flux through the plant is equal to the evaporation out, and finally coupling with an energy balance [22].

The transpiration flux E from the stomata is given by the difference between the specific humidity internal to the leaf and that of the atmosphere, i.e.:

$$E = \frac{g_{sa} \cdot \rho}{\rho_w} \left[q_i(T_l, \psi_l) - q_a \right] \tag{3.4}$$

where g_{sa} is the series of atmospheric conductance and the combined stomatal-cuticular conductance, ρ is the density of air, ρ_w is the density of water, q_i is the specific humidity internal to the leaf, and q_a is the specific humidity of the atmosphere. At the same time, the transpiration must be equal to the flux of water through the plant, i.e. the flux per unit of ground area from the roots to the leaves :

$$E = g_{srp} \left(\psi_s - \psi_l \right) \tag{3.5}$$

where g_{srp} is the series of the soil-root and plant conductances, ψ_s is the soil water potential, ψ_l is the leaf water potential.Because of this choice of units, g_{srp} depends on both LAI (leaf area index, i.e., the leaf area per unit ground area) and RAI (root area index, i.e., the root area per unit ground area), which express the relative importance of root and xylem conductance, determining which part contributes more to the limitation of water flow [1].

For the calculation of stomatal conductance, no empirical formulation is used. The stomatal conductance to water g_s, is closely related to stomatal conductance for CO_2 and here is given by $g_s = 1.6 g_{s,CO2} + g_{cut}$, where 1.6 accounts for the differences between the diffusivity in air of CO_2 and H_2O.

Following [12], the soil - root conductance g_{sr}, is given by $g_{sr}(s) = \frac{K(s)\sqrt{RAI}}{\pi g \rho_w Z_r}$,, where RAI is

the root area index, Z_r is the rooting depth and K(s) is the hydraulic conductivity, g represents gravitational acceleration and ρ_w denotes the density of water. Given that roots continuously adapt to fluctuations in soil moisture, plant water availability (and consequently soil-root conductance) cannot be assessed purely based on soil properties. It is therefore logical to infer that, as soil dries, the reduction in g_{sr} caused by K is partially offset by the plant's response through root proliferation. Consequently, under moderate soil water deficits, the distance decreases as soil water availability diminishes. This relationship can be modeled by adjusting the Root Area Index (RAI) with a multiplicative factor that mitigates the decline induced by K. Specifically, RAI_w under optimal watering conditions can be scaled by a parameter a, which varies depending on the plant species, $RAI = RAI_w s^{-a}$ [1].

Plant conductance, g_p, drops when the water potential is too low because of xylem cavitation; this decay is modeled by a vulnerability curve, $g_p = g_{p,\max} \exp\left[-\left(-\frac{\Psi_l}{d}\right)^c\right]$. The parameters d and c are such that g_p is equal to g_{pmax} for high values of Ψ_l and close to 0 for low Ψ_l.

The SPAC model integrates the energy balance at the leaf level to achieve closure. A comprehensive representation of the leaf energy balance should account for radiative processes, as well as convection and conduction, while considering radiation heterogeneity and its penetration through leaf layers. Despite this, SPAC models often employ a simplified framework, utilizing the "big sunlit leaf" approximation. This assumes a flat and uniform canopy, which simplifies the calculations.

Under this approximation, the leaf energy balance is described by equating the net radiation (R_n) to the sum of the sensible heat flux (H), the latent heat flux ($\lambda_w \rho_w E$), and the conductive heat flux to lower layers (G):

$$R_n = H + \lambda_w \rho_w E + G$$

where λ_w is the latent heat of vaporization of water, ρ_w is the water density, and E represents the water flux per unit area. Since G is negligible for canopies, the equation simplifies to:$R_n = H + \lambda_w \rho_w E$

The sensible heat flux (H) depends on the ambient temperature (T_a) and the leaf temperature (T_l) [K], and is expressed as: $H = c_p \rho (T_l - T_a)$

where c_p is the specific heat capacity of air and ρ is the air density. Substituting this relationship into the leaf energy balance, the equation becomes:

$$\phi = g_a \cdot \rho \cdot c_p (T_l - T_a) + \lambda_w \rho_w E \tag{3.6}$$

These three equations are solved simultaneously for the three unknowns: the transpiration E, the leaf temperature T_l, and the leaf water potential ψ_l.

The code [22] also includes a section with the capacitance. Plant water storage is represented in this model as a capacitor located at the height which is a fraction f of the total plant height. Using this scheme, the change in the plant's relative water content w is given by the balance equation :

$$\text{LAI} \cdot Z_w \cdot \frac{dw}{dt} = q_s(s,w) - E \tag{3.7}$$

When plant water storage is included, the formulation of hydrology balance is altered, and a fourth variable, ψ_x , is introduced, which describes the water potential at the storage connection node.

$$E = \frac{g_p}{1-f} \cdot (\psi_x - \psi_l) \tag{3.8}$$

The evapotranspiration evf is defined by the relationship between soil water flow and xylem storage flow:

$$\text{evf} = \frac{\text{gsrfp} \cdot (\psi_s - \psi_l) + \text{lai} \cdot \text{gw} \cdot (\psi_w - \psi_l)}{1 + \left(\frac{\text{gsrfp} \cdot (1 - \text{F\_CAP})}{\text{lai} \cdot \text{gp}}\right) + \left(\frac{\text{gw} \cdot (1 - \text{F\_CAP})}{\text{gp}}\right)} \tag{3.9}$$

Now the resulting system is composed by: (3.4),(3.6),(3.9) .

3.2 Assimilation

Photosynthesis is the process by which green plants capture light energy and convert it into carbohydrates using carbon dioxide and water. This process occurs in the chloroplasts of leaf cells and involves two consecutive stages. The first stage, known as *light reactions*, directly depends on light, whereas the second stage, referred to as *dark reactions*, does not directly involve light. Below is a structured overview of the process, introducing key concepts and terminology [1]:

1. 1. Light Reactions: Light energy is absorbed by pigment molecules, primarily chlorophyll, and transferred to reaction centers. Here, a sequence of biochemical reactions generates reducing power in the form of NADPH (reduced nicotinamide adenine dinucleotide phosphate) and chemical energy in the form of ATP (adenosine triphosphate). Water is essential in this phase as it undergoes photolysis, breaking down into protons, electrons, and oxygen. Well-hydrated leaf cells with high leaf water potential (ψ_l) are critical for this process, as photosynthesis decreases when water availability is limited. This is particularly significant in ecosystems governed by water availability but is often overlooked in models. The high water content in leaf cells also leads to substantial water loss through evaporation when stomata are open to allow carbon dioxide uptake [1].

2. Dark Reactions: NADPH and ATP produced during the light reactions drive the conversion of carbon dioxide, taken up via the stomata, into carbohydrates through the Calvin cycle. This cycle has three main stages:

    - **Carboxylation**: The five-carbon sugar RuBP (ribulose-1,5-bisphosphate) reacts with carbon dioxide and water, forming three-carbon compounds (in C3 plants). This reaction is catalyzed by the enzyme rubisco (ribulose bisphosphate carboxylase-oxygenase). The rate of CO_2 fixation by carboxylation is denoted as A [1].

- **Reduction**: The three-carbon compounds are modified using ATP and NADPH, with some transformed into carbohydrates [1].
- **Regeneration**: The remaining three-carbon compounds combine with ATP to regenerate RuBP, allowing the cycle to continue [1].

During the Calvin cycle, rubisco also facilitates the oxygenation of RuBP, a process known as photorespiration or RuBP oxygenation. This process consumes oxygen and releases carbon dioxide, reducing net CO_2 uptake by 30–50%. The rate of photorespiration is represented as P.

In contrast to photosynthesis, respiration involves the oxidation of organic molecules to release energy for maintaining plant functions and supporting new tissue growth. This process occurs continuously, day and night, across most plant parts. In leaf cells during daylight, respiration occurs concurrently with photosynthesis and is facilitated through the stomata. Known as *dark respiration* or *daytime respiration*, this process is distinct from photorespiration. The rate of dark respiration is denoted as R_d.

The net carbon uptake is modeled as a steady-state Fickian diffusion through the stomata:

$$A_n = g_{s,CO_2}(c_s - c_m) \tag{3.10}$$

where g_{s,CO_2} is the stomatal conductance to CO_2, c_s is the concentration of CO_2 at the leaf surface, and c_m is the concentration of CO_2 in the mesophyll cytosol. The stomatal conductance is assumed :

$$g_{s,CO_2} = \frac{(a_1 A_n)}{(c_s\sqrt{D})} \tag{3.11}$$

Where a_1 is an empirical constant adjusted to account for the differences in the c_m/c_a ratio and D is the vapor pressure.

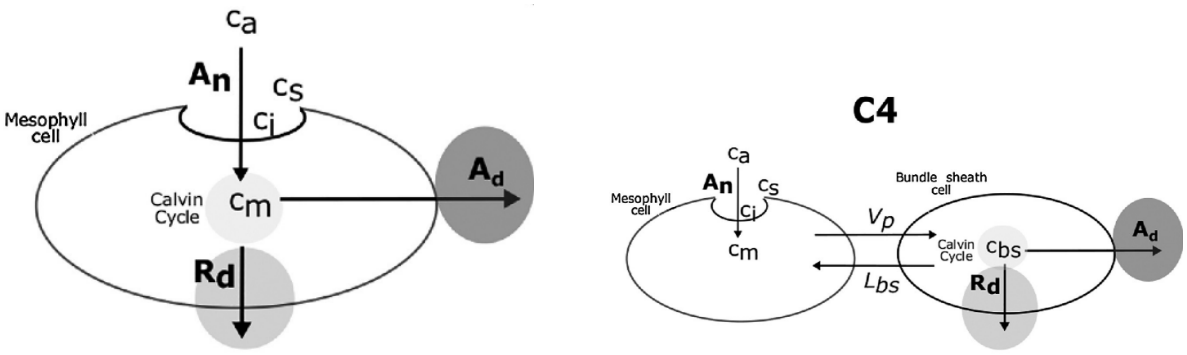

(a) C3 (b) C4

Figure 3.1: Representation of carbon fluxes[22].

The net photosynthetic demand for CO_2, A_d, is modeled with an adjustment to account for plant water stress,

$$A_d = A(\phi, c_x, T_l) f(\psi_l) \tag{3.12}$$

Due to the lack of temporal separation of CO_2 uptake and assimilation in C3 and C4 photosynthesis, the net carbon uptake An equals the net photosynthetic demand Ad for these photosynthetic types.

$$A(\phi, c_x, T_l) = min[A_c(c_x, T_l), A_q(\phi, c_x, T_l)] \tag{3.13}$$

where A_c is the Rubisco-limited photosynthetic rate, A_q is the light-limited photosynthetic rate, Tl is the leaf temperature, cx is the CO2 concentration at the site of the Calvin cycle, and ϕ is the incoming solar radiation. The relevant CO_2 concentration c_x varies based on the photosynthetic type. For C3 plants, c_x is the mesophyll concentration c_m; for C4 plants, it is the bundle sheath concentration c_{bs}.

The effects of water stress reduce the photosynthetic demand according to a 'vulnerability' function of the leaf water potential, here represented for simplicity as a piecewise linear function that decreases between the point of onset of water stress, ψ_{lA1}, and the point of

stomatal closure ψ_{lA0}, i.e

$$f_{\psi_l}(\psi_l) = \begin{cases} 0, & \text{if } \psi_l < \psi_{lA0} \\ \frac{(\psi_l - \psi_{lA0})}{\psi_{lA1} - \psi_{lA0}}, & \text{if } \psi_{lA0} < \psi_l \leq \psi_{lA1} \\ 1 & \text{if } \psi_l > \psi_{lA1} \end{cases} \tag{3.14}$$

In the C4 plant, the influx of CO_2 to the bundle sheath cell is driven by the C4 pump and is modeled by Michaelis-Menten type dependence on the mesophyll cytosol CO_2 concentration, c_m. The PEP regeneration rate, V_P is :

$$V_P(c_m) = \min\left(\frac{c_m V_{P,\max}}{c_m + K_p}, V_{Pr}\right) \tag{3.15}$$

Leakage of CO_2 from the bundle sheath cell is modeled as a diffusion flux from the bundle sheath to the mesophyll cell, i.e.,

$$L_{bs}(c_{bs}, c_m) = g_{bs}(c_{bs} - c_m) \tag{3.16}$$

It introduced a balance equation for the CO_2 fluxes into and out of the bundle sheath cell, i.e.,

$$V_P(c_m) = A_d(\Phi, c_{bs}, T_l, \psi_l) + L_{bs}(c_{bs}, c_m) \tag{3.17}$$

and solve for the CO_2 concentration in the bundle sheath cell, c_{bs}.

To estimate carbon assimilation given several input data variables, the above equations were solved using the Photo3 model [22], python code solving the SPAC model for a given simulation period.

Table 3.1: Photo3 Input Data Variables.

Parameter	**Units**	**Description**
Net Radiation	W/m^2	Net Radiation
T	°C	Temperature
RH	%	Relative humidity

3.3 Updating the Photo3 Model

Before beginning work on the code, extensive research was conducted in the scientific literature to understand how the plants present at the site respond, in terms of biomass reduction, to salinity and submersion conditions. This preliminary study identified the main ecological and physiological dynamics characterizing the plant species at the site, providing a solid foundation for adapting the model. Subsequently, considerations were made on how to modify the model to integrate this information and improve its ability to represent plant responses to such environmental stressors. The simulations conducted using site-specific data will then be presented. The goal of these simulations is to evaluate the model's response to observed conditions, aiming to identify potential interventions or further modifications needed to refine the model and achieve a more accurate representation of the studied system for future challenges.

However, in the specific case under examination, the soil is almost constantly in saturated conditions due to the presence of a shallow water table.

In this context, it is more appropriate to reformulate the water balance, shifting the focus from soil moisture to the dynamics of the shallow water table. This approach allows for a more accurate description of the hydrological processes characterizing the system, including the interactions between the water table position and soil saturation.

The objective is to develop a water balance that considers the shallow water table as the main variable, integrating input and output components such as precipitation, evapotranspiration, infiltration, capillary rise, and lateral drainage. This modification enables a more realistic representation of water dynamics in a system dominated by persistent saturation conditions.

Given the complexity of implementing a stochastic variation of the water table, a significant simplification was introduced in this study's water balance: instead of focusing on soil moisture variation, soil moisture was treated as a constant variable. This decision was

made considering that, for most of the time, the soil remains saturated at the study site, as mentioned earlier, rendering soil moisture variations negligible. Although this represents a significant approximation, it provides a functional starting point, leaving the implementation of a water balance based on the variation of the shallow water table as a potential future challenge, which could offer a more realistic representation of hydrological dynamics.

For this simplification, a new soil class was developed in which soil moisture is maintained constant, and salinity is introduced as an input. Salinity values, expressed in ppt (g/L) and later converted to mol/m³, were provided through an Excel file containing data collected from the CRMS 2825 station. Simultaneously, data on temperature, relative humidity, and net radiation, required for the model, were obtained from the eddy covariance station EC.

In the water balance, rainfall was not considered, as in the presence of saturated soil and constant soil moisture, the impact of precipitation is negligible. This simplified approach allows for a greater focus on the influence of salinity and other environmental parameters on plant behavior, providing a solid foundation for future, more complex analyses.

With the introduction of the new class, it was observed that the code initially only read the first value from the file containing salinity data. This behavior limited the dynamic updating of values throughout the simulation. To address this issue, a solution was implemented that integrates the salinity value directly into the main Soil class.

The most important change therefore is to consider the soil water potential governed by the osmotic potential introduced through Vant'Hoff's law and the salt filtration coefficient (ε). This implementation allows for a more realistic representation of the effects of salinity on soil dynamics and plant water status, making the model more suitable for saline environments.

The soil water potential (ψ_s) now is expressed as:

$$\psi_s = \psi_{ss} \cdot s^{-B} - \varepsilon \cdot C_s \cdot R \cdot IV \cdot T_S \tag{3.18}$$

In the updated version, the Soil class includes salinity among its initialization parameters, defined as the salt concentration in the soil expressed in mol/m^3. Upon initialization, an

empty list associated with the class is created to record all salinity values read during the simulation progressively. This allows verification that all values have been read correctly.

The potential values are obtained at each iteration, as the salinity concentration is correctly read and recorded. In addition, a dedicated list for the water potential has been introduced, which is iteratively updated with the values calculated at each simulation step.

```
class Soil(object):
    EVMAX = 1.0
    TS = 296.  # Soil water temperature (K)
    IV = 2.    # Van't Hoff coefficient for NaCl
    E = 0.95   # Emissivity constant
    R = 8.314  # Universal gas constant (J/mol K)

    def __init__(self, stype, dynamics, zr, s, cs):
        self.PSI_SS = stype.PSI_SS
        self.B = stype.B
        self.KS = stype.KS
        self.N = stype.N
        self.SH = stype.SH
        self.ZR = zr
        self.s = s
        self.s_a = []
        self.psi_s_a = []
        self.dynamics = dynamics
        self.cs = cs  # Salt concentration in soil (mol/m  )
        self.cs_a = []

    def update(self, dt, zr, qs, cs):
```

```
23          self.s = self.dynamics.snew(self, dt, zr, qs)
24          self.s_a.append(self.s)
25          self.psi_s_a.append(self.psi_s(self.s))
26          self.cs = cs
27          self.cs_a.append(self.cs)
28
29      def output(self):
30          return {'s': self.s_a, 'psi_s': self.psi_s_a, 'cs': self
                .cs_a}
31
32      def leak(self, s):
33          """Leakage (mm/day)"""
34          try:
35              return 0.11574 * self.KS * s**(2. * self.B + 3.)
36          except OverflowError:
37              return 0.0
38
39      def psi_s(self, s):
40          """Soil Potential (MPa)"""
41          return self.PSI_SS * (s**-self.B) - self.E * self.cs *
                self.R * self.IV * self.TS * 1e-6
42
43      def evap(self, s):
44          """Soil evaporation rate, per unit ground area (mm/day)
                """
45          if s > self.SH:
46              return self.EVMAX * (s - self.SH) / (1. - self.SH)
47          else:
48              return 0.0
```

In the main file (Main), the modification consists of integrating the salinity value ‘csInp[i]‘ within the iteration. This value represents the current element of the list containing salinity data, previously read and recorded.

This change allows the salinity parameter to be dynamically updated at each iteration, ensuring that the model accounts for the temporal variation of salinity values throughout the simulation.

```
# Initialize the simulation object with relevant modules
plant = Simulation(species, atmosphere, soil, photo, hydro)

# Loop through simulation steps
for i in range(steps(duration, int(timestepM))):

    # Update the plant model at each timestep with the provided
       inputs
    plant.update(
        dt,         # Timestep duration (\si{\second})
        phiInp[i],  # Incoming solar radiation (\si{\watt\per\
           metre\squared})
        taInp[i],   # Air temperature (\si{\degreeCelsius})
        qaInp[i],   # Specific humidity (\si{\kilogram\per\
           kilogram})
        csInp[i]    # Soil salinity concentration (\si{\mole\per
           \metre\cubed})
    )
```

The data available from the EC stations have been compiled into two Excel files (”Dati

LA3" and "Dati LA2"). In these files, some values are labeled as 'NaN', indicating missing or unavailable data. Since the original code did not account for missing data, a new section was implemented to handle this issue. The modified code reads all values from the Excel files and, when encountering a missing value (NaN), skips it and proceeds to the next available data point. This approach ensures uninterrupted iterations and extends the visualization period, providing a more comprehensive analysis of the dataset.

The primary goal is to ensure that:The model's iterations skip invalid values without interrupting the simulation.

- The model's iterations skip invalid values without interrupting the simulation;
- The model's outputs retain the temporal gaps to preserve the consistency of the time series.

To address this issue, a modification was made to the simulation's main loop. When one of the inputs is identified as NaN, the model:

- Skips the calculations for the current iteration.
- Records a NaN value for all model outputs, thereby maintaining the temporal structure of the results.

This approach ensures the robustness of the simulation while accurately representing missing data within the output.

```
results = {}
initial_output = plant.output()  # Retrieve the structure of the
    output keys

# Initialize the dictionary with output keys and empty lists
for key in initial_output.keys():
    results[key] = []
```

```
7
8  # Main iteration loop
9  for i in range(steps(duration, int(timestepM))):
10     # Check if any input is NaN
11     if np.isnan(phiInp[i]) or np.isnan(taInp[i]) or np.isnan(
           qaInp[i]) or np.isnan(csInp[i]):
12         # Add NaN to all output keys
13         for key in results.keys():
14             results[key].append(np.nan)
15         continue  # Skip to the next iteration
16
17     # Update the model with valid values
18     plant.update(dt, phiInp[i], taInp[i], qaInp[i], csInp[i])
19
20     # Save the updated outputs
21     current_output = plant.output()
22     for key in current_output.keys():
23         results[key].append(current_output[key][-1])  # Append
              the latest updated value
```

Regarding the species class, the Photo3 model was originally designed for tall trees living in arid climates. Therefore, a key adjustment involved developing a new class adapted to plant species at our study site, with a particular emphasis on creating a specific class for *Spartina Patens*, the dominant vegetation in the salt marsh ecosystem. In the following, information from the literature on this plant species is provided [54]. *Spartina Patens*, also known as saltmeadow cordgrass, is a perennial bunchgrass characterized by a summer growth cycle and a photosynthetic mechanism of C4. The plant height typically ranges from 0.3 to 1.5 m, with growth occurring individually or in small clumps derived from thin, threadlike, and widely

spread rhizomes. This species is adapted to a variety of coastal environments, including salt meadows, low dunes, sandy flats, beaches, overused areas, and high salt marshes.

The edaphic conditions in which *S. Patens* thrives are broadly categorized into two types: (1) peat deposits of variable depth and (2) mineral soils formed from washout materials or deposits left by tidal and wave action. In Louisiana, *S. Patens* is a dominant species exclusive to salt meadows, where it constitutes over 50% of the total vegetation. Although abundant in salt meadows, its presence in saline marshes is relatively rare.

The soil water salinity in which *S. Patens* grows range from 0.12% to 3.91%, with the species being most abundant in environments characterized by relatively low salinity and water levels. This tolerance and adaptability make *S. Patens* a crucial component of salt marsh ecosystems, contributing to soil stability and the mitigation of coastal erosion.

Assigning specific hydrological and photosynthetic parameters for *S. Patens* posed a challenge due to the limited availability of species-specific studies in the scientific literature. For photosynthetic parameters, it was necessary to refer to generally accepted values for C4 species, using previously identified parameters as a reference. For hydrological parameters, values reported in the literature for plants with similar characteristics or for *S. Patens* themselves were initially assigned, and subsequently adjusted to optimize the fit of the model to the observed data from the study site. This iterative approach allowed for the refinement of parameters, ensuring a more accurate representation of the hydrological and photosynthetic behavior of the species within the model's context.

For the soil classification, the LOAMYSAND type was chosen, and the parameters are form [12]. This decision is based on the analysis conducted in the previous chapter, which considers the characteristics of the two study sites and aligns with the data provided by the CRMS.

Table 3.2: Parameter values, units, descriptions, and references for *Spartina patens*.

Parameter	Value	Units	Description	Reference
Z_r	0.3	m	Mean Root Depth	CRMS site
LAI	1.8	-	Leaf Area Index	[34]
g_{cut}	0	mm s^{-1}	Cuticular conductance per unit ground area	N/A
g_a	61	mm s^{-1}	Atmospheric conductance per unit ground area	[26]
RAI_w	5.6	-	Root area index (well-watered)	N/A
g_{pmax}	0.075	μm $MPa^{-1}s^{-1}$	Maximum plant conductance	[52]
g_{wmax}	0	μm $MPa^{-1}s^{-1}$	Maximum xylem-phloem conductance	N/A
v_{wt}	0	m^3 m^{-2}	Maximum depth of water storage (phloem)	N/A
CAP	0.5	-	Location of storage in plant	N/A
V_{cmax0}	39	μm m^{-2} s^{-1}	Max carboxylation rate	[11]
J_{max0}	180	μm m^{-2} s^{-1}	Electron transport rate	[11]
ψ_{LA0}	-3.11	MPa	Point of max plant water stress	[53]
ψ_{LA1}	-0.19	MPa	Onset of plant water stress	[53]

Table 3.3: Soil parameters.

Parameters	K_s (cmd^{-1})	ψ_s (MPa)	**b**	**n**	s_h
Values	100	-1.7 $\times 10^{-4}$	4.38	0.42	0.08

4. Results

The results presented below will demonstrate the model's adaptation to the data observed from the EC station, recalling that it is a validation of a qualitative nature. This will provide a reference to assess whether the model can be considered representative.

As previously described, the model allows the evaluation of transpiration and assimilation fluxes over a one-year period during which the vegetation is subjected to saline stress. It is important to emphasize that the fluxes derived from the data do not exclusively account for contributions from the vegetation in the specific study area. Instead, these fluxes represent a larger spatial area, defined as the "footprint," which includes inputs from various elements within the observed domain. Consequently, it is expected that discrepancies may arise, and a perfect correspondence between the estimated fluxes and those specific to the individual vegetation cannot be achieved. Moreover, as will be emphasized later, while the model simulates only transpiration values, the fluxes provided by the EC station represent evapotranspiration. This will require further analysis to better compare the values. Nevertheless, the collected data provide a valuable order of magnitude that remains comparable and useful for the analyses. This comparability allows the results to be contextualized within a broader spatial scale, offering meaningful insights into eco-physiological processes and environmental dynamics. Moreover, as can be observed from the following graphs, when a larger area is considered, significant data gaps emerge. This phenomenon is primarily due to the numerous missing values in the input data provided to the model, such as temperature, relative humidity, and radiation. Additionally, it is important to note that the values used in the salinity model do not represent soil salinity but rather the salinity of the water body. This, in turn, constitutes another important assumption to consider. For the Breakmarsh site, in the year 2022, the simulations for both transpiration and assimilation are as follows.

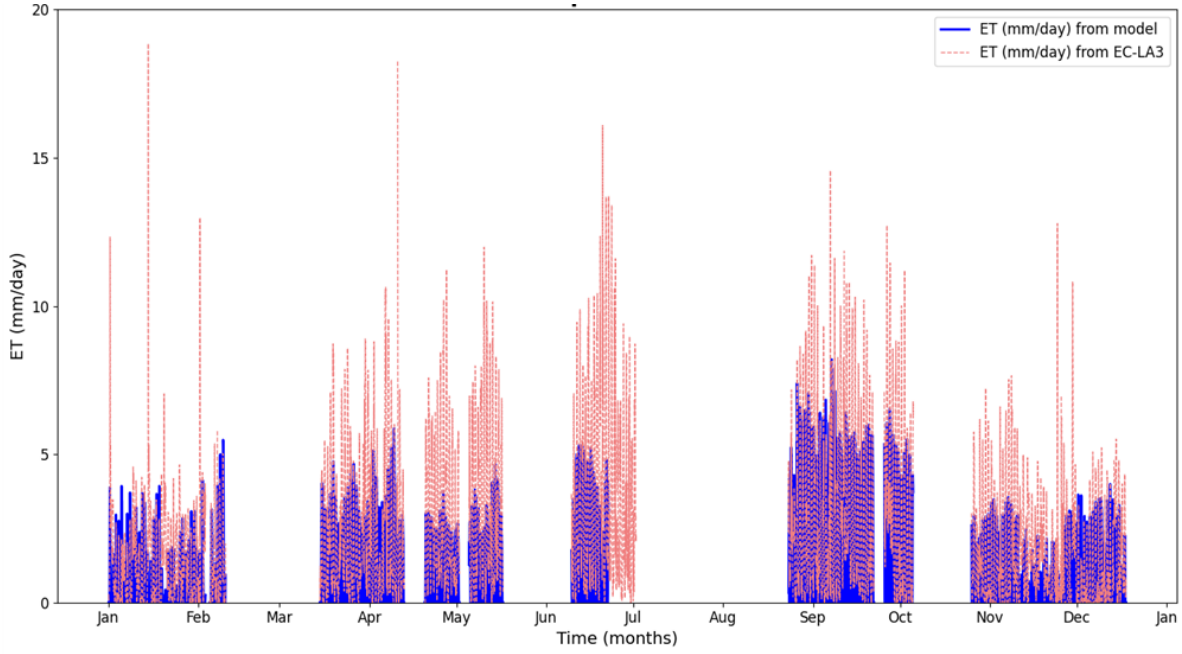

Figure 4.1: Transpiration rate form the model and from EC-LA3 for the entire year of 2022.

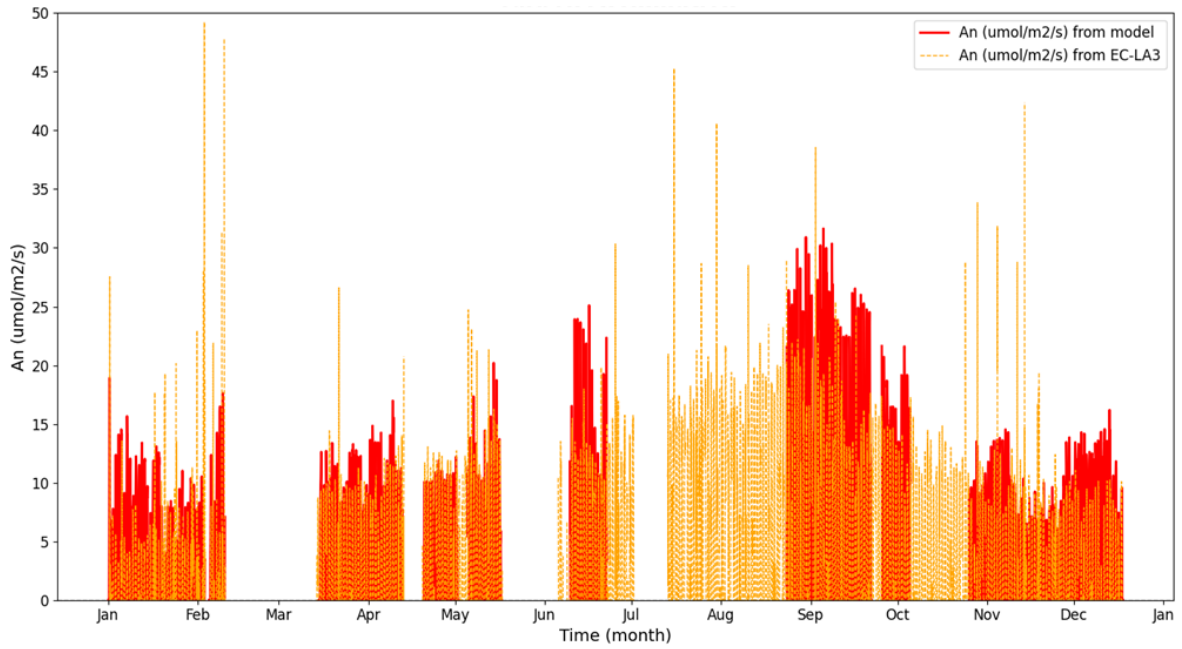

Figure 4.2: Carbon Assimilation rate form the model and from EC-LA3 for the entire year of 2022

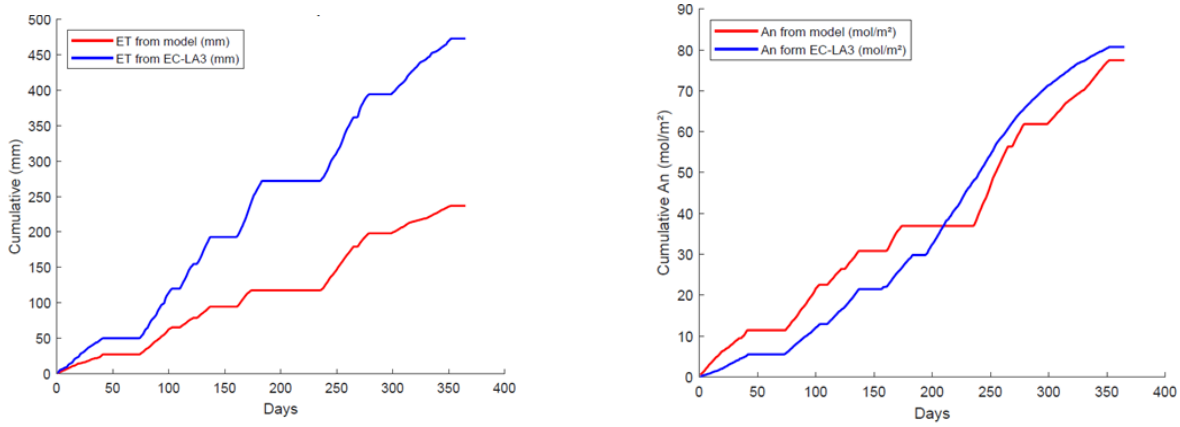

(a) (b)

Figure 4.3: (a) Cumulative Transpiration and (b) Cumulative Carbon Assimilation.

The first two graphs depict the comparison between the daily values obtained from the EC station under examination and the model outputs, while the subsequent graphs illustrate the cumulative values to provide a long-term perspective on productivity trends. This initial result, as presented, does not clearly allow us to assess whether the model performs well. The simulation's time span is too extensive, making it challenging to closely observe the detailed dynamics. Therefore, a second analysis was conducted.

The objective of the second analysis was to compute and visualize the daily average fluxes for each hour of the day based on the recorded dataset. The methodology was structured as follows.

Data processing :

- The dataset containing flux measurements and corresponding temporal information was loaded.
- Missing values (NaN) were removed to ensure the accuracy and reliability of statistical computations.
- Each timestamp was analyzed to extract the hour of the day, enabling the data to be

grouped into hourly intervals.

Statistical Analysis: For each hour of the day (ranging from 0 to 23), the following statistical metrics were calculated:

- Mean Flux: To determine the central tendency of the flux values for each hour.
- Standard Deviation: To quantify the variability of the flux data within each hourly group.
- Standard Error of the Mean (SEM): To represent the statistical uncertainty associated with the computed mean flux values.
- Handling Missing Hours
- To ensure a comprehensive representation, all hours of the day were included in the analysis, even if no data were available for some intervals.
- For hours with missing data, the mean flux and standard error values were set to zero, enabling a uniform and complete depiction of the flux patterns across the day.

Results Visualization:

- A detailed graph was produced to illustrate the average daily flux pattern across all hours of the day.
- Error bars were included to visually represent the standard error of the mean, providing an indication of the uncertainty associated with the calculated hourly flux averages.

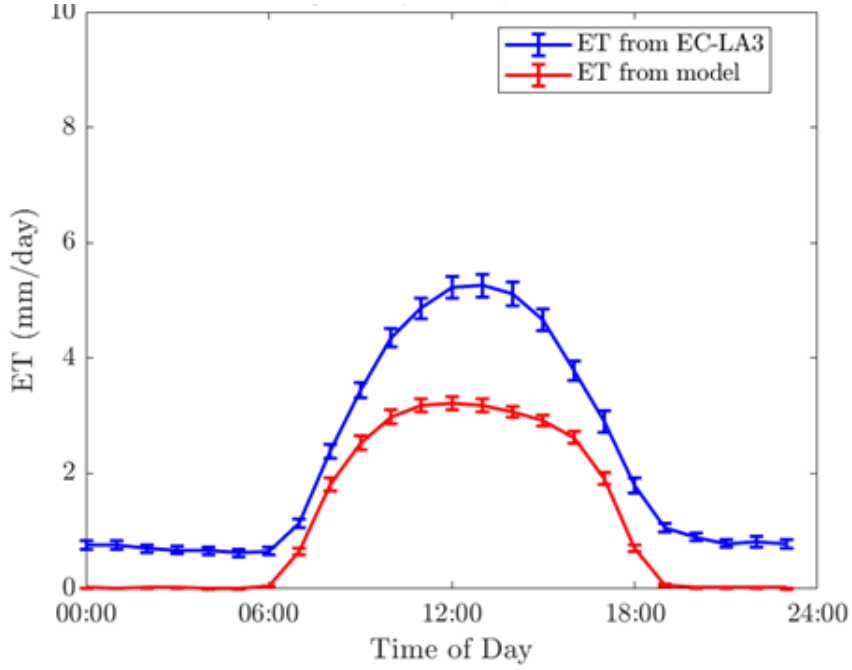

(a)

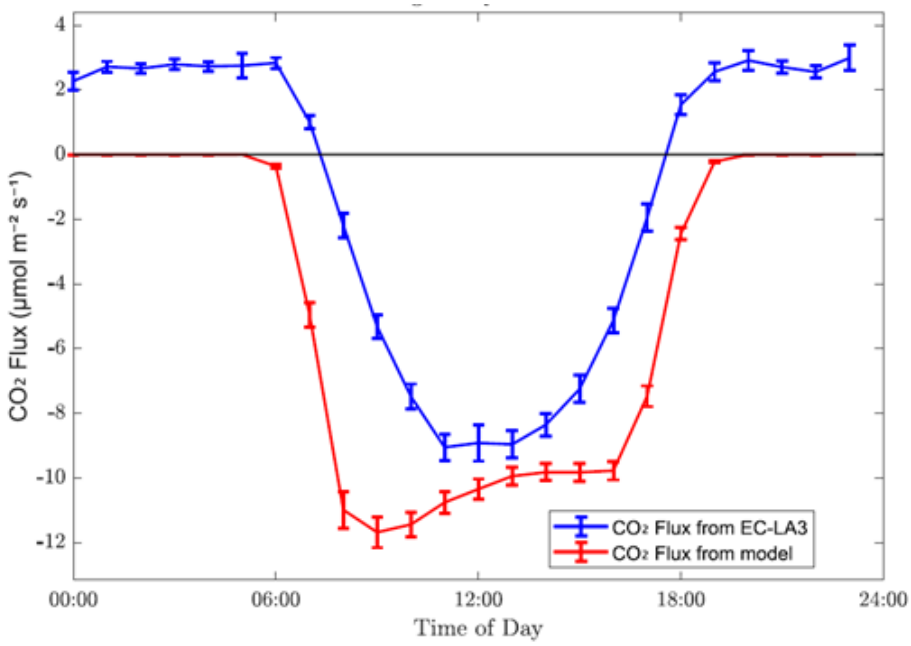

(b)

Figure 4.4: (a) Average Daily Transpiration Flux (b) Average Daily CO_2 Flux.

A daily average of the respective fluxes was computed to better visualize the trend and the deviations between the model and the EC station data. As mentioned earlier, the model outputs represent transpiration alone, without accounting for evaporation. To provide a more detailed analysis, the same computation was repeated, dividing the data across the four seasons. This seasonal breakdown allows us to observe how the model performs during periods when evaporation is minimal—particularly in winter—offering an opportunity to evaluate whether the model can more accurately reproduce the EC station data under such conditions.

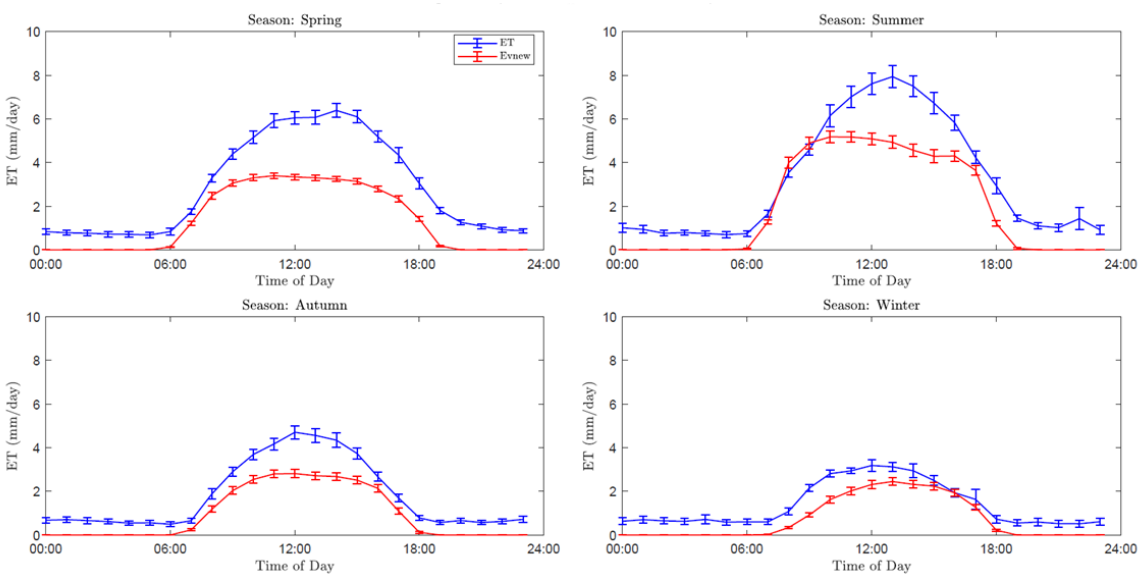

Figure 4.5: Average Daily Transpiration Flux by season.

The figure above illustrates the seasonal average daily flux patterns for evapotranspiration (ET) and transpiration (Tr) across four seasons: spring, summer, autumn, and winter. The fluxes derived from the EC station (ET, blue line) represent total evapotranspiration, which includes both vegetation transpiration and soil evaporation. In contrast, the fluxes simulated by the model (Tr, red line) exclusively represent transpiration from vegetation.

Seasonal Observations:

Spring and Summer:

- Both evapotranspiration and transpiration fluxes exhibit a pronounced diurnal cycle, with peak values occurring around midday.
- The model underestimates the total flux (ET), as expected, since it does not account for soil evaporation. This difference is more pronounced during summer, likely due to higher soil evaporation rates caused by elevated temperatures and greater solar radiation.

Autumn:

- The diurnal patterns are still evident but with reduced peak values compared to spring and summer. This consists of shorter daylight hours and lower temperatures.
- The gap between ET and Tr remains present, though slightly narrower than in summer, suggesting reduced soil evaporation during cooler conditions.

Winter:

- Both ET and Tr show significantly lower flux values, reflecting reduced vegetation activity and limited evaporation due to low temperatures and potentially higher soil moisture levels.
- The model aligns more closely with EC data during winter, as soil evaporation is likely minimal in these conditions.

This comparison highlights the need for further analysis to isolate and quantify the soil evaporation component from the EC fluxes. Incorporating this distinction could enhance the model's applicability in representing the overall water fluxes in the system. Additionally, the observed seasonal differences emphasize the importance of accounting for environmental variables such as temperature, solar radiation, and soil moisture when interpreting evapotranspiration and transpiration dynamics.

The analysis was also conducted for carbon assimilation focusing on the seasonal dynamics of CO_2 uptake by vegetation.

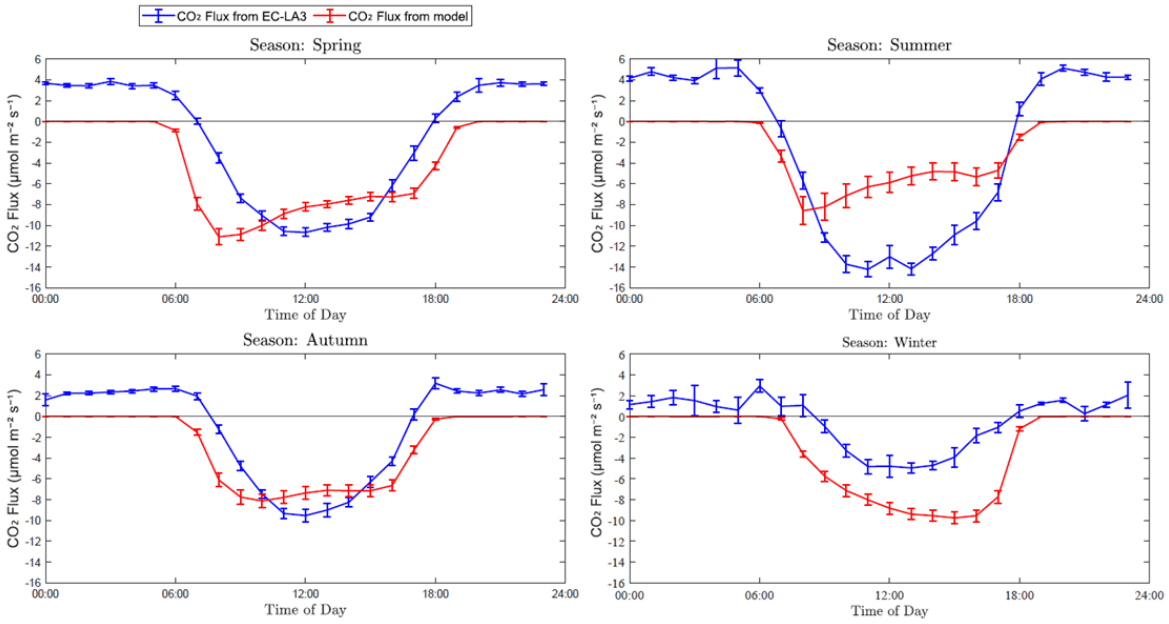

Figure 4.6: Average Daily CO_2 Flux by season.

4.1 Winter Season, without Submersion

During the winter season, characterized by minimal evaporation, the model exhibits a closer alignment with the observed data. To further explore the impact of submersion on the accuracy of the model's predictions, a focused analysis was performed.

As illustrated in the graph below, by excluding days in the time series when the plants were submerged, a marked improvement in the model's ability to approximate the observed data was achieved. This observation underscores the role of submersion as a critical factor introducing variability that the current model framework is not fully equipped to account for. The results suggest that submersion dynamics should be explicitly incorporated into the model to enhance its capacity to simulate the complex interactions between hydrological conditions

and plant physiological responses.

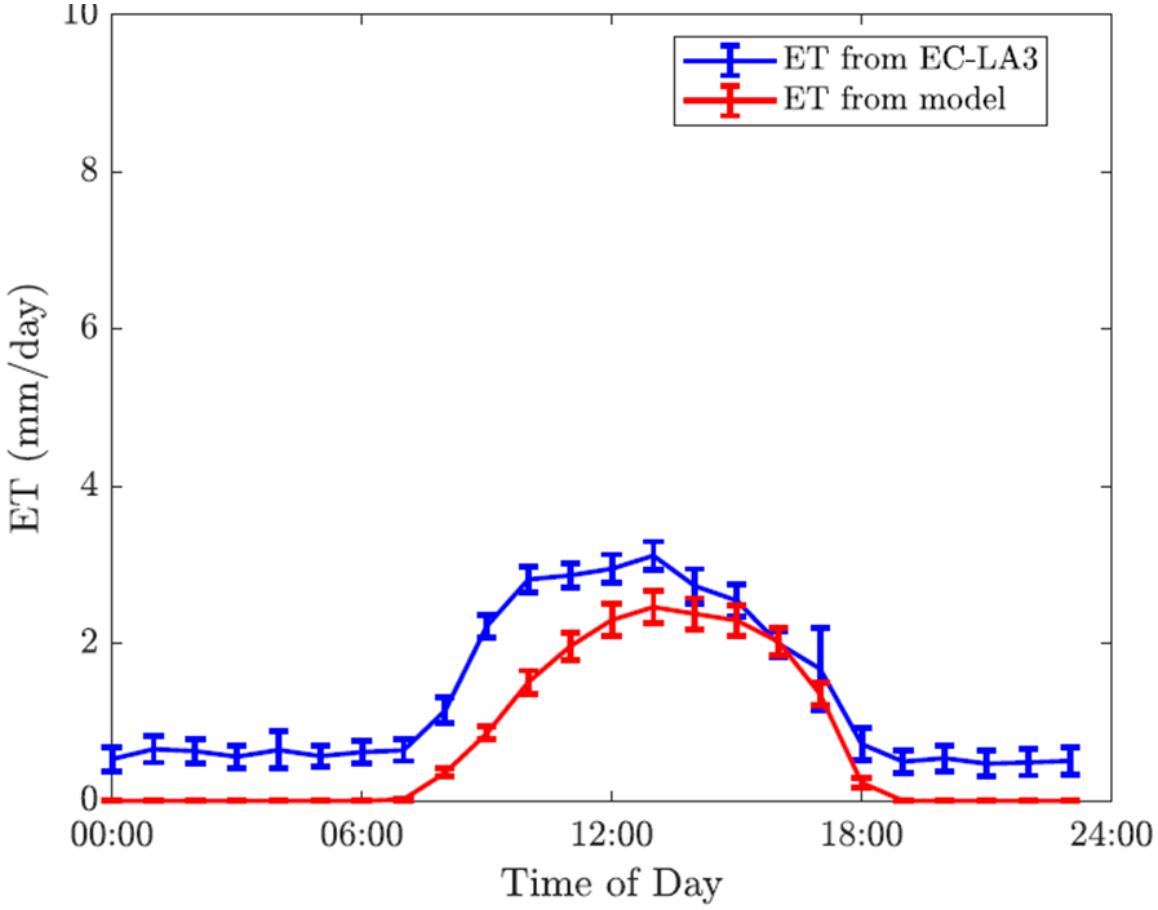

Figure 4.7: Average Daily Transpiration Flux, during the winter season in which the submersion period is removed.

To better visualize the effect of salinity on transpiration, six winter days were selected during which the model exhibited a better approximation to the observed data. These days were then compared with a separate set of winter days recorded at the station where Sagittaria lancifolia is present.

This comparative analysis aims to highlight the influence of salinity under similar seasonal conditions, providing a clearer understanding of how this stressor impacts transpiration

dynamics in the two scenarios.

A period was selected to isolate the effects of stress attributable solely to salinity characterized by lower salinity levels, ranging from 8 to 14 ppt, and the absence of significant submersion. This choice enabled an exclusive evaluation of the plant's response to salt stress. In the first phase of the analysis, the class of halophytes, an experimental framework derived from [37] study, was considered by introducing a minimal reservoir into the model. This choice was justified by the limited ability of *S. Patens* to tolerate high salinity levels. However, due to the complexity of quantifying the reservoir capacity and the fact that *S. Patens*, being a smaller plant compared to species like mangroves, possesses a minimal capacitance, so it was concluded that its impact on the model would be negligible. Furthermore, the salinity levels recorded during the drought were still far above the species' maximum tolerance threshold.

Consequently, the analysis focused on the **HydroNC** class, which does not include any reservoir. In this approach, a simplified SPAC model was used, as illustrated in Figure 1.11 (a). In this configuration, no salinity reduction functions were applied; instead, salinity data were directly integrated into the model using values collected from the CRMS site, as previously described.

By directly introducing salinity levels and modifying the soil class to include osmotic potential, using Van't Hoff's law as previously described, it was possible to significantly reduce the total soil water potential due to the presence of salts. Additionally, for all analyses, a constant soil moisture value of 0.9 was assumed. As a result, the soil water potential depended almost exclusively on the osmotic component, which in turn was determined by the salt concentration.

This approach allowed for a more precise analysis of the effects of salinity, eliminating interference from submersion and improving the understanding of the model's behavior under specific site conditions.

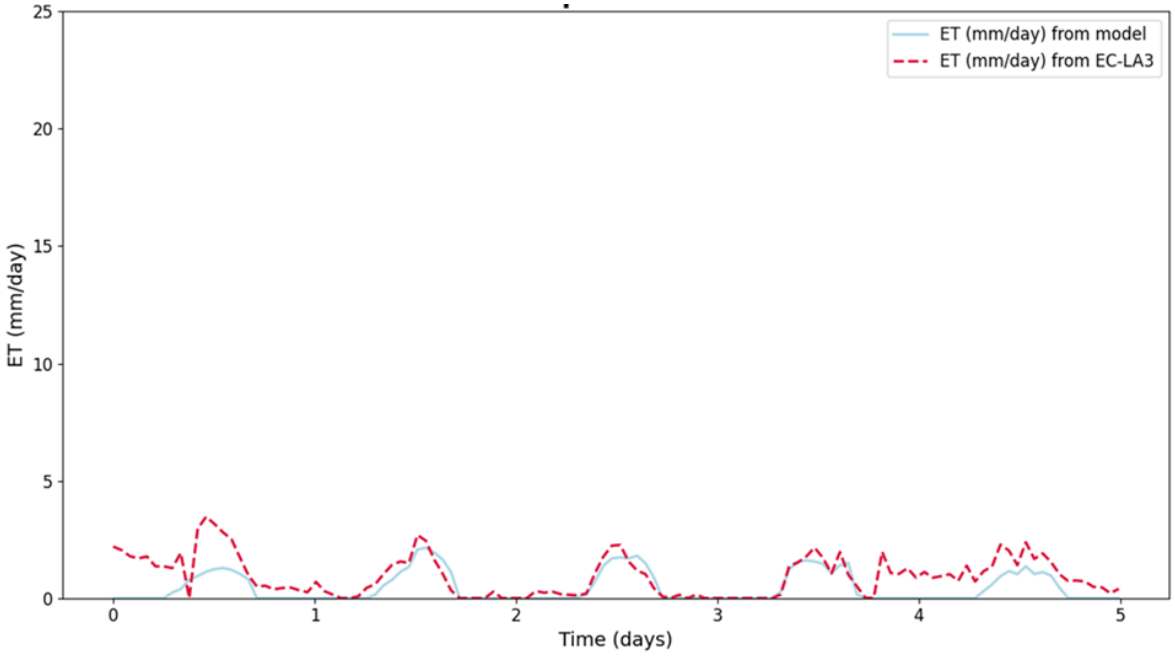

Figure 4.8: Transpiration Rate from EC-LA3 and model for during six days of winter season, without submersion period.

To gain a deeper understanding of the program's functionality and to analyze more concretely the impact of high salinity levels, data from the EC-LA2 station, located in a "fresh marsh" environment, were used. In this context, the dominant species is *Sagittaria lancifolia*, a plant belonging to the C3 photosynthetic group.

In this site, salinity levels are relatively low, ranging between 0.15 and 0.17 ppt, values that do not induce salinity stress, as described in Chapter 2. For the specific case of *S. lancifolia*, the default parameters of the Photo3 model for C3 plants were primarily used, with some adjustments. Specifically, the average root length was set to 0.6 m, based on CRMS data, and the Leaf Area Index (LAI) was fixed at 4, consistent with values reported in the literature [61].

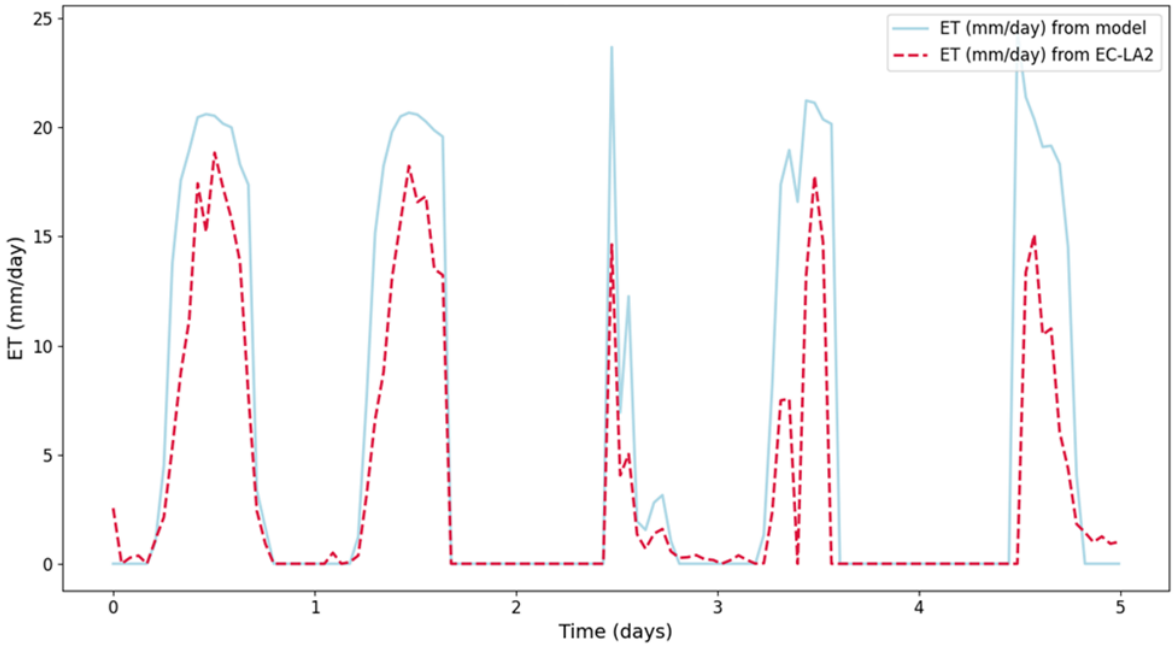

Figure 4.9: Transpiration Rate from EC-LA2 and model for during six days of winter season, without submersion period.

The graphs below illustrate the model's response for the "fresh" site case. A time period was selected in which all necessary data were available and coincided with a period without submersion, to highlight how very low salinity levels can produce effects different from the previous case.

This is particularly evident in the evapotranspiration (ET) values, which are significantly higher compared to the site characterized by higher salinity levels. These results confirm that salinity negatively affects the physiological processes of plants, reducing ET rates, and emphasize the importance of considering such parameters in simulations to achieve an accurate representation of the environmental effects on the vegetative system.

As shown in the graphs, in the case of ET, the model tends to slightly overestimate the observed data. This discrepancy could be attributed to the fact that the parameters used in the model are not fully representative of the plant species present at the site. However, this

still provides a valid point of comparison and allows for useful observations in the overall analysis.

This comparison highlights that transpiration is significantly lower at the site where vegetation is subjected to stress throughout the entire study period, in contrast to the second site, where vegetation never experiences saline stress.

4.2 Estimation of Evaporation

An additional analysis was conducted to estimate evaporation from free water surfaces using data provided by the eddy covariance (EC) station. EC data provide evapotranspiration (ET) values, while the model considers transpiration only. This discrepancy represents one of the main causes of divergence between the model results and observed data. To reduce this gap, evaporation was estimated and subtracted from the ET values to achieve a better match between the model and the observations.

Wetlands are considered free water surfaces. These are transitional areas between aquatic and terrestrial ecosystems, characterized by soils that are saturated or submerged for significant periods [39]. In contrast, a free water surface typically refers to uncovered water bodies (such as lakes, ponds, or channels) where evaporation occurs directly from exposed water, without the direct influence of vegetation or soil.

In wetlands, evaporation can be influenced by:

- The presence of emergent vegetation, which reduces direct evaporation from water but contributes to transpiration [39];
- The coverage of saturated soil, which interacts with the overall water balance [39].

A more precise analysis should differentiate between evaporation from free water surfaces and transpiration by vegetation, integrating both into the water balance. However, to obtain

an approximate estimate for practical considerations, a combined Aerodynamic method and Energy balance method was employed.

The two main factors influencing evaporation from an open water surface are the supply of energy to provide the latent heat of vaporization and the ability to transport the vapor away from the evaporative surface. Solar radiation is the main source of heat energy. The ability to transport vapor away from the evaporative surface depends on the wind velocity over the surface and the specific humidity gradient in the air above it. [9]

To develop continuity and energy equations applicable to the evaporation phenomenon, we consider the case of evaporation measured using an evaporation pan, as illustrated in figure below . An evaporation pan is a circular container filled with water, where the evaporation rate is determined by monitoring the lowering of the water surface. A control surface is defined around the pan, encompassing both the contained water and the overlying air [9].

Considering a unit of water surface area, the primary source of thermal energy is the net radiation flux R_n, measured in watts per square meter. The water transfers a sensible heat flux H_s to the overlying air and a ground heat flux G. Therefore, the energy balance equation is expressed as:

$$\frac{dH}{dt} = R_n - H_s - G \tag{4.1}$$

Assuming that the water temperature within the control volume remains constant over time, the only change in stored energy within the control volume is represented by the variation in the internal energy of the evaporated water, equal to $\lambda_v m_v$, where λ_v is the latent heat of vaporization [9].

Replacing m_v with $A = 1\,m^2$ and neglecting the ground heat flux G, evaporation can be expressed as:

$$E = \frac{R_n - G}{\lambda_v \rho_w} \tag{4.2}$$

However, this method does not provide reliable and usable results, as it represents an estimate with overly simplified assumptions.

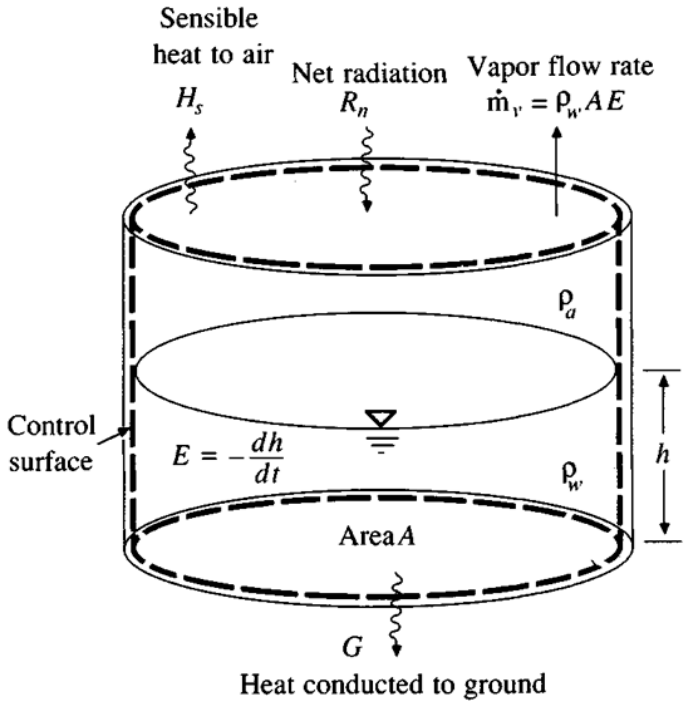

Figure 4.10: Control Volume defined for continuity and energy equation development for an evaporation pan [9].

Subsequently, the aerodynamic method [9] was applied, providing results more consistent with local conditions. This approach allowed for a refinement of the modeled transpiration estimate, thereby improving comparability with observed data.

The aerodynamic method is based on the supply of thermal energy, the second factor controlling the evaporation rate from a free water surface is the ability to transport vapor away from the surface. The transport rate is determined by the humidity gradient in the air near the surface and the wind speed blowing over it. These two processes can be analyzed by coupling the equations for mass transport and momentum in the air[9]. In the control volume shown in figure below, we consider a horizontal plane of unit area located at a height z above the surface. The vapor flux, per unit area, which corresponds to the evaporation rate

E_a, moving upward across the plane by convection, is described by the equation:

$$E_a = B(e_{as} - e_a) \tag{4.3}$$

Where the evaporation rate E_a as proportional to the difference between the saturated vapor pressure e_{as} and the actual vapor pressure e_a, multiplied by a coefficient B:

$$B = \frac{0.622k^2\rho_a u_2}{p\rho_w \left[\ln\left(\frac{z_2}{z_0}\right)\right]^2} \tag{4.4}$$

Where:

- k: von Kármán constant,
- ρ_a: air density,
- u_2: wind speed at height z_2,
- p: atmospheric pressure,
- ρ_w: water density,
- z_2: wind height above the surface,
- z_0: surface roughness length.

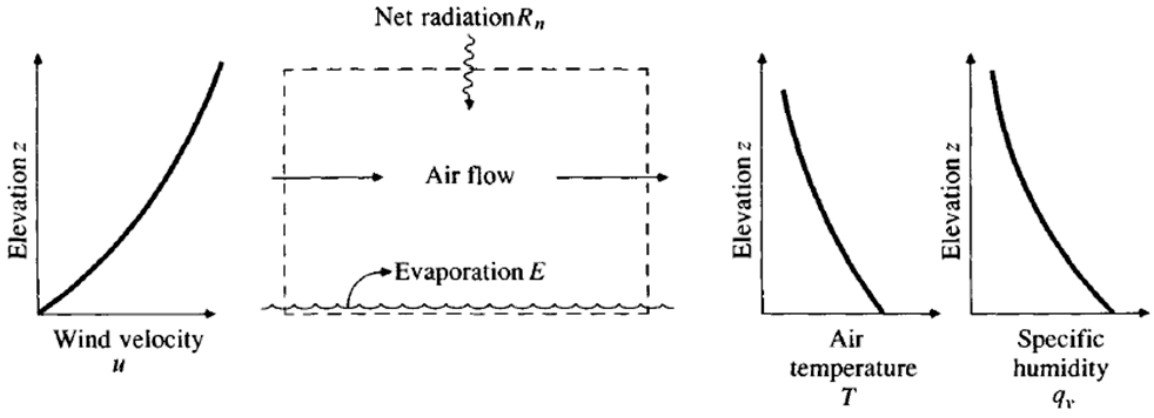

Figure 4.11: Evaporation from an open water surface [9].

The parameters, such as wind speed, height z_2, atmospheric pressure, and temperature, used to calculate evaporation, were obtained from the eddy covariance (EC) station.

The combined method is given by:

$$E = \frac{\Delta}{\Delta+\gamma}E_r + \frac{\gamma}{\Delta+\gamma}E_a \tag{4.5}$$

where γ is the psychrometric constant and Δ is the gradient of the saturated vapor pressure curve at air temperature T_a.

Following this analysis, the comparison between the daily average of the various fluxes was revisited, incorporating the evaporation estimate calculated using the aerodynamic method, which was subsequently subtracted from the evapotranspiration flux. As shown in the following result, the model appears to slightly overestimate the transpiration data compared to the observed values.

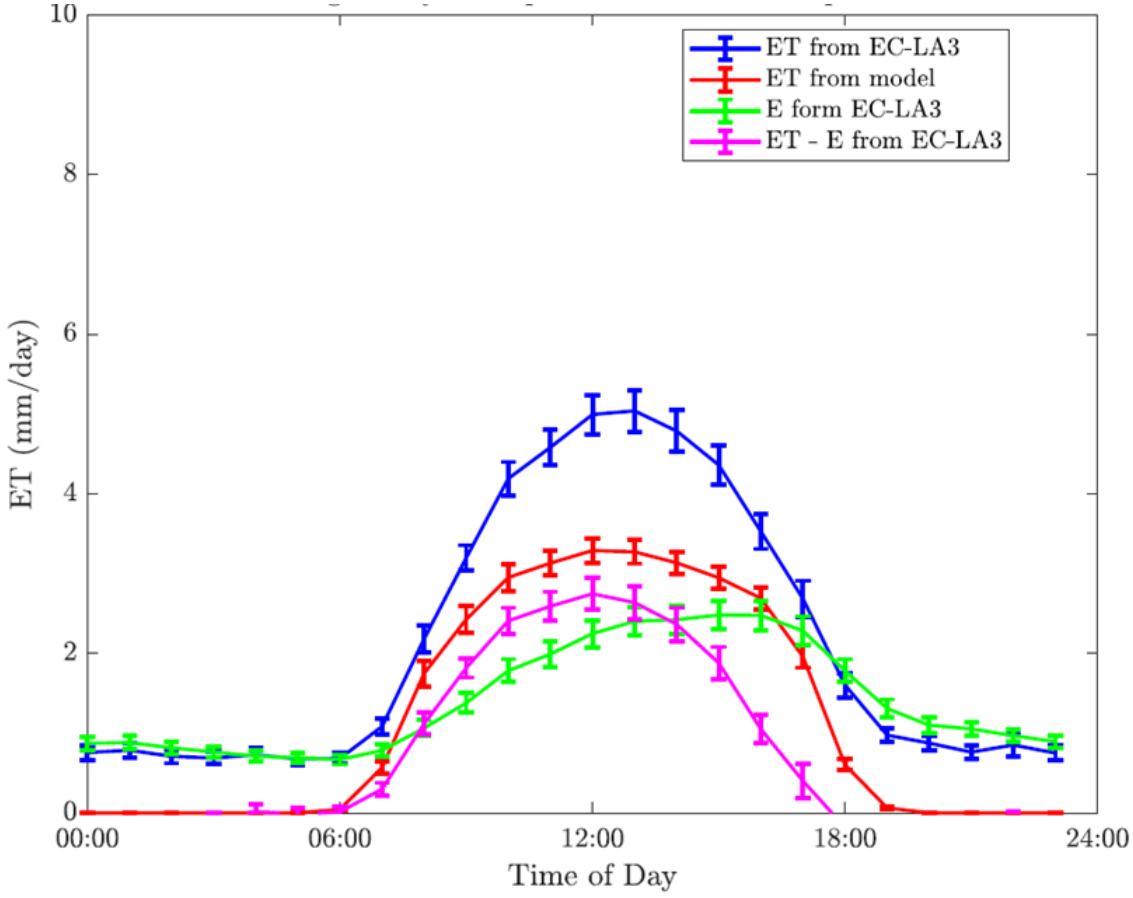

Figure 4.12: Average Transpiration flux and Evaporation.

As noted earlier, when using an estimate of evaporation based on a free water surface, the model accurately represents environments with large submerged areas or open water bodies. However, in wetland areas, the presence of vegetation, saturated soils and micro soils introduces variables that can alter evaporation rates. This leads to discrepancies between estimated and actual values, as the contribution of vegetation (e.g. transpiration), uneven surfaces and land cover alters the microclimate and, consequently, evaporation.

By only considering periods when the surface is actually submerged (water level ¿ marsh elevation), the estimation becomes more representative of actual wetland conditions, as it excludes data on non-submerged conditions, where evaporation follows different dynamics.

The improvement in accuracy is modest due to the limited amount of data available, which may adversely affect the robustness of statistical analyses.

Although the filtered data are not perfect, the decision to focus only on the submergence period reduces the noise introduced by unrepresentative conditions (e.g. transpiration of dominant vegetation) and strengthens the correlation between the evaporation model and the reality of submerged wetlands.

A limited dataset makes it difficult to draw firm conclusions, but still supports the idea that the filter slightly improves the quality of the estimate.

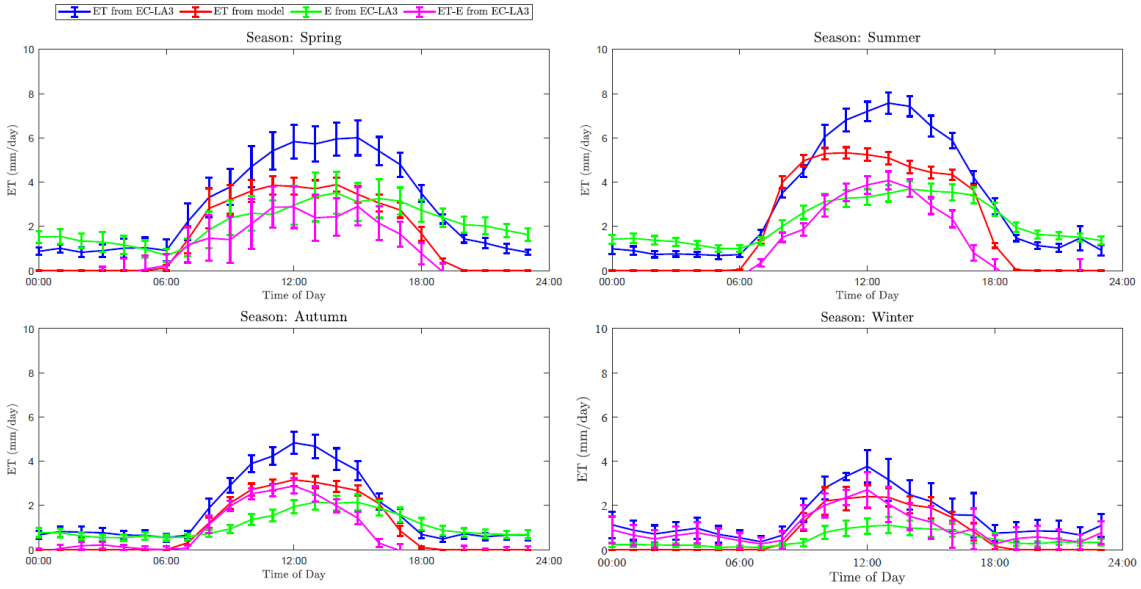

Figure 4.13: Average Daily Transpiration and Evaporation flux by season, during submersion time.

5. Model Limitations and Future Considerations

5.1 Model Limitations

This study represents a preliminary step in research focused on wetlands, an ecosystem that remains underexplored. The adopted approach aimed to provide a simplified description of the system, acknowledging the inevitable gaps and limitations. During the research period, additional investigations were conducted to identify potential improvements to the applied model. However, due to the uncertainty and lack of site-specific data, a simplified methodology was employed, allowing for the development of a model that could be representative of the system, despite its known limitations.

The Photo3 model, used in this thesis to simulate transpiration and carbon assimilation values for the two plant species under investigation, was applied in a context characterized by high salinity stress caused by the severe drought of 2022. While effective in certain aspects, the model presents several limitations that require attention.

One major limitation lies in its water balance approach, which is based on soil moisture variation. This approach proves inadequate for the study area, where soils are frequently saturated or submerged. Such a simplification introduces significant errors. To address this issue, strategies are proposed in this work, including the introduction of reduction functions to account for plant submergence.

Another significant limitation is that the model was originally developed for plants adapted to arid or semi-arid climates and not for species typical of wetlands. The absence of mechanisms to represent the effects of submergence—a critical stressor for wetland plants—affects the model's ability to accurately capture the physiological dynamics of the studied species.

Additionally, the model was designed primarily for shrubs with significant height, whereas the plants analyzed in this thesis, such as *S. Patens* and *S.Lancifolia*, exhibit distinct morpho-

logical characteristics. This discrepancy inevitably led to divergences between the model's simulations and the observed data.

The treatment of salinity is another area for improvement. In the current version of the model, salinity is directly introduced as a salt concentration without explicitly considering osmoregulation mechanisms or the complex interactions between salinity and plant physiology. Throughout this work, alternative functions have been proposed to better integrate salinity into future model developments.

A further limitation pertains to the data used for model validation. Although the initial intent was to focus the study on the Bird Foot Delta area, the available data primarily originated from EC and CRMS stations located further north. This choice was dictated by the instability and frequent submergence of the Bird Foot area, which made the installation of monitoring stations impractical. Additionally, the collected data contained numerous temporal gaps, preventing complete coverage of the year 2022.

The data observed from the eddy covariance (EC) station correspond to a spatial scale significantly larger than the one under study. Moreover, the EC provides measurements of total evapotranspiration, which were used for comparisons with the transpiration-only values simulated by the model. Although an attempt was made to estimate the evaporation component through approximations and simplifications, this introduced additional limitations, hindering the ability to achieve a fully reliable comparison.

Finally, it is important to highlight the challenges in obtaining specific parameters for the species *S. Patens* and *S. Lancifolia* The literature on these plants is limited, and in most cases, general values or data derived from studies on similar species had to be used. This compromises the model's ability to accurately reflect the reality of the studied system.

5.2 Future Considerations

5.2.1 Dynamic of Water Table

Wetlands are areas inundated or saturated by surface water at a frequency and duration sufficient to support a prevalence of vegetation typically adapted for life in saturated soil conditions. They are characterized as having a water table that stands frequently at or near the land surface [51].

To better represent the hydrologic function of vegetation in coastal wetlands, it is most useful to concentrate attention on the dynamics of the water table instead of soil moisture, which is always more or less equal to one. Here, we are dealing with a water table under saline conditions. The salinity-dependent dynamics of the saturation depth, y, in a homogeneous soil column, can be formulated as :

$$\beta(y)\frac{dy}{dt} = Re(y) + ET(y \mid C) + fl(y) \tag{5.1}$$

where $\beta(y)$ represents the specific yield defined as the ratio between the water volume released from the storage and the corresponding variation in water level.Re(y) is the groundwater recharge rate forced by precipitation, and ET(y—C) is the evapotranspiration rate for a given level of salinization. The function *fl(y)* describes the lateral flow to or from the sea, considered here as the main external water body. Whereas water availability does not limit ET in SWT conditions, the presence of soluble salts in the soil increases the energy plants require to uptake water, thus reducing Transpiration. We have the time series for water level, rainfall, and evapotranspiration. Therefore, the model can be solved for the changes in lateral flows. This application could serve as an important starting point for future works to represent the ecosystem better.

5.2.2 Salty Soil

The *Photo3* model provides several options for simulating soil dynamics. The study of [63] introduces a significant modification by adding a new class, called *Salty Soil*, to account for the effects of saline soil. This modification is relevant for the present study, as both analyzed sites exhibit salinity concentrations, which are higher in the case of the salt marsh site.

The study [63] defines the *Salty Soil* class starting from two initial parameters: soil moisture S_0 and initial salinity concentration C_{s0}. The initial mass of salt in the soil (M_s) is calculated as:

$$M_s = C_{s0} \cdot Z_r \cdot N \cdot S_0$$

where Z_r represents root depth, and N is soil porosity.

In each model iteration, the soil salt concentration is updated assuming that the mass of salt (M_s) remains constant while soil moisture varies. The new concentration is then calculated using a simple dilution equation, which accounts for the amount of water present in the soil.

It could be considered to work on this function by also allowing the mass to vary instead of considering it constant, making the situation more realistic. As previously discussed in this thesis study, salt concentration was introduced as an input due to the availability of data. However, this method could prove useful when such data are not available.

Another possible modification, as an alternative to the previous one, to integrate the effects of soil salinity could involve introducing a reduction function applied to the total biomass (see section 6.2.4). This approach would be analogous to that used to represent the effect of submersion, thus modeling the impact of salinity on the overall productivity of plants.

To analyze these functions, references were made to studies available in the literature to gather sufficient data to evaluate the response of the two plant species under investigation.

Specifically, the reduction levels in total biomass were analyzed as a function of increasing soil salinity concentrations, to define a quantitative relationship that accurately describes the effect of salinity on plant growth.

For *Spartina Patens*, the available data are best described by a Gaussian function, while for *Sagittaria Lancifolia*, a linear function proves more appropriate.

The study [38], used as a reference for *Spartina Patens*, provides specific data for total biomass, obtained by summing aboveground and belowground biomass, which exhibit a linear correlation. The total biomass reduction function, shown in the following figure, indicates that the species' maximum productivity occurs at a salinity level of 5 ppt. Beyond this threshold, productivity progressively decreases with increasing salinity, reflecting the previously analyzed salt tolerance of *Spartina Patens*.

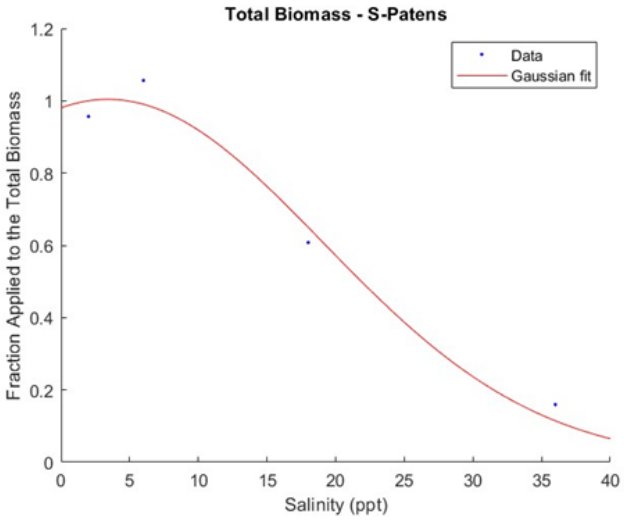

$$y = \exp\left(-\left(\frac{x-3.41}{22.12}\right)^2\right)$$

Figure 5.1: Graphical representation of the reduction function for *Spartina patens* in relation to total biomass. This function describes how biomass is reduced under specific conditions based on the modeled input. The graph illustrates the relationship between salinity and the fraction of biomass applied to the total biomass, using a Gaussian fit to represent the observed data.

In the case of *Sagittaria lancifolia*, the available data were extracted from study [54], which unfortunately reports only three samples corresponding to three different salinity levels: 0, 3, and 6 ppt. Higher salinity levels were not tested, as this species predominantly develops in low-salinity environments and exhibits poor tolerance to more extreme saline conditions.

As shown in the graph below, the trend of the total biomass reduction function follows a linear relationship, consistent with the collected data. This highlights the sensitivity of *Sagittaria lancifolia* to salinity, confirming its limited adaptability to ecosystems with high salt concentrations.

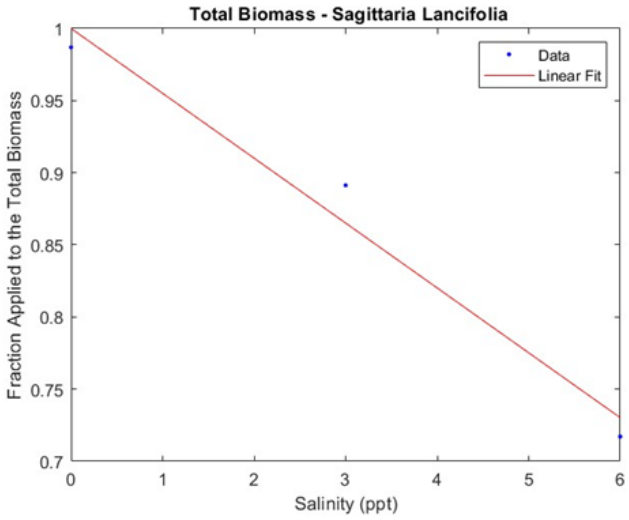

$$y = -0.0450 \cdot x + 1$$

Figure 5.2: Graphical representation of the linear reduction function for *Sagittaria Lancifolia* with the Total Biomass. This function describes how biomass is reduced under specific conditions based on the modeled input. The graph illustrates the relationship between salinity and the fraction of biomass applied to the total biomass, using a Linear fit to represent the observed data

5.2.3 Concentration of the salt in the plant

The work [63] added a critical component to the Photo3 model by incorporating salt concentration into the plant's internal water storage. This adjustment allowed the model to account for salt-tolerant plants that use osmoregulation as a strategy to manage saline environments. By including salt concentration within the storage capacity, the model can simulate how these plants regulate internal solute levels to maintain water uptake and sustain physiological functions in saline conditions. This addition enhances the model's ability to represent the adaptive responses of salt-tolerant species in ecosystems such as wetlands. For this part, the concentration of the salt in the plant C_w was in the storage for the Halophyte with an initial value of C_w The water potential of the water storage tissue now is given by:

$$\psi_w = \left(\frac{vw}{VWT} - D_1\right)^{D_2} - C_W \cdot R \cdot I_V \cdot T_L \cdot 10^{-6} \tag{5.2}$$

Updating the existing hydraulics class HydroCap, The Halophyte class calculates the potential of the storage component as a function of soil salinity.

5.2.4 Biomass accumulation

To model the biomass accumulation, the Photo3 model was also updated, by [37], to include biomass calculations. The changes in total biomass B is given by the net carbon assimilation An (this accounts for leaf respiration) less the root respiration Rr and growth respiration Rg [23].

$$\frac{DB}{dt} = A_n - R_g - R_r \tag{5.3}$$

The biomass accumulated goes to building different parts of the tree. One important ratio, necessary for estimating the root biomass Br, is the below-to-above-ground biomass ratio, or

root ratio r_r. The root biomass accumulation rate is given by a linear relationship between the total biomass accumulation rate and r_r.

$$\frac{DB_r}{dt} = r_r \frac{DB}{dt} \tag{5.4}$$

Growth respiration is assumed to be a constant fraction of the net carbon assimilation as observed in C3 and C4 photosynthetic plants :

$$R_g(A_n) = \eta_g A_n \tag{5.5}$$

Where η_g is a growth respiration constant taken as 0.3 gC g-1 C (Weng et al. 2014). The root maintenance respiration is given following [46], with modifications to account for water stress, as:

$$R_r = \beta_r f_A(T_l) f_T(T_l) f_{\psi l}(\psi_l) B_r \tag{5.6}$$

The β_r root respiration coefficient is equal to 1.25 per year [45]. The respiration is affected by temperature through a modified Arrhenius function, f_A, following Leuning,

$$f_A(T_l) = \exp\left(k\left(\frac{1}{T_0} - \frac{1}{T_1}\right)\right) \tag{5.7}$$

where k =3,000 and T_0 is a reference temperature of 288K; and by a thermal inhibition function, f_T, given by

$$f_T(T_l) = \frac{(1+\exp(0.4(T_L - T_l)))}{(1+\exp(0.4(T_l - T_H)))} \tag{5.8}$$

where TL and TH are the low and high temperatures below and above which respiration is limited (TL=278 K, TH=318 K).

As highlighted earlier, submergence is a critical factor in determining evapotranspiration and assimilation fluxes. The fact that plants spend much of their life cycle under submerged conditions significantly affects their productivity.

When plants begin to be submerged, growth and productivity are compromised, resulting in a reduction in biomass accumulation. Given the complexity of these interactions,

submergence can be incorporated into the model through a reduction function based on the percentage of time plants remain submerged. This approach enables the application of a reduction coefficient directly to the variation in total biomass, simplifying the analysis of the effects of prolonged submergence.

However, in the absence of site-specific data to analyze variations in the total biomass of the plant species of interest, a literature review was conducted. This analysis identified previous studies correlating plant total biomass with the percentage of time of inundation. In some cases, available data allowed for a more precise model fit, while in others, due to the limited availability of sampling data, the fit was less accurate.

Building on the implementation of the total biomass calculation in the Photo3 model, introduced in [37] as described in the Biomass Accumulation section, the aim is to introduce a further modification to adapt the model to the specific conditions of wetlands. These ecosystems exhibit unique characteristics that require a more detailed and tailored-modeling approach to accurately represent their ecophysiological and biophysical processes.

Below, the reduction functions for the two species of interest, *Spartina patens* and *Sagittaria lancifolia*, are illustrated. For both, experimental data are best approximated by an exponential regression function, although in the case of *Spartina Patens*, the fit is notably more accurate.

For *Spartina Patens*, study [55] shows that both aboveground and belowground biomass decrease with increasing hydroperiod. Specifically, an exponential regression function fits the data almost perfectly, showing that biomass approaches zero when the duration of inundation reaches 100%. Additionally, comparing aboveground and belowground biomass values, it is evident that the latter decreases more rapidly than the former. The study also highlights that, at the analyzed site, *S. patens* exhibits a regression coefficient of greater magnitude than that of *Spartina alterniflora*, studied in the same context.

Studies such as [55] have documented a reduction in aboveground biomass in permanently flooded Breakmarsh sites compared to intermittently flooded riverbank margins. These

findings suggest that soils subjected to prolonged waterlogging can accumulate toxic sulfides, causing plant stress due to the reduction of redox potential below critical thresholds.

Mesocosm experiments [57] have further demonstrated that a 30 cm increase in inundation depth for *S. patens* can lead to a nearly 40% reduction in total biomass. The results of these studies confirm findings from numerous other investigations, underscoring the crucial role of hydrological regimes in determining sediment aeration conditions and, consequently, the physiological performance of wetland plants.

In both cases, to define the reduction function, the functions related to the individual compartments (aboveground and belowground) were initially analyzed. Subsequently, by summing the two compartments, the total biomass values were calculated.

The resulting fit function was then normalized to the maximum value on the y-axis, to obtain a reduction factor between 0 and 1. This approach allows for a consistent and standardized representation of the relative variation in total biomass as a function of inundation time or hydrological regime, facilitating the integration of the function into the model. The y-values thus indicate the reduction factor to be applied to the total biomass for each inundation time x.

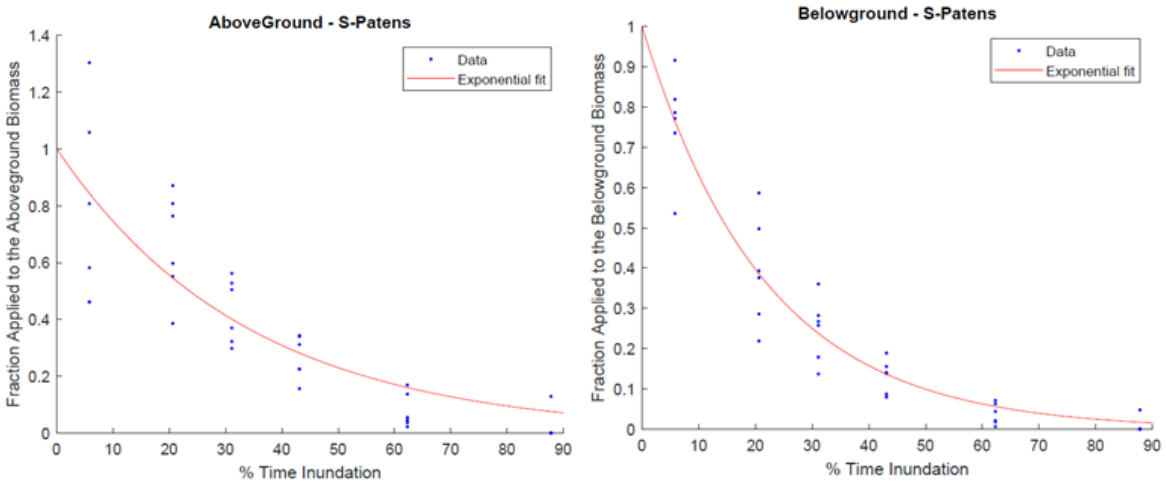

(a) (b)

Figure 5.3: (a) Aboveground Biomass and (b)Belowground Biomass of *Spartina Patens*

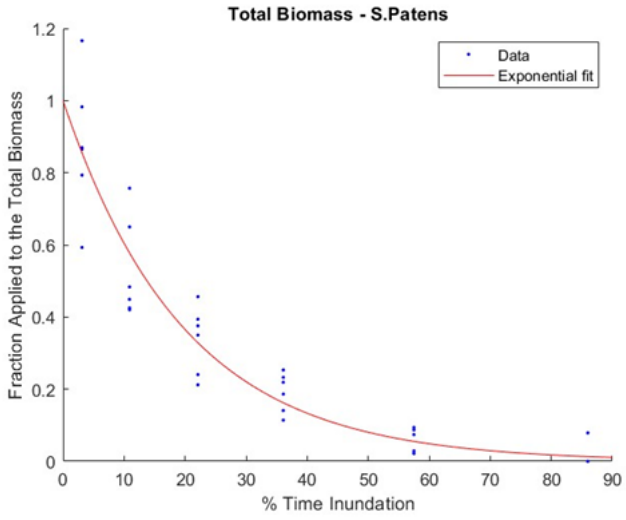

$$y = \exp(-0.05037 \cdot x)$$

Figure 5.4: Graphical representation of the exponential reduction function for *Spartina Patens* in relation to the Total Biomas. The graph illustrates the relationship between % time of inundation and the fraction of biomass applied to the total biomass, using an exponential fit to represent the observed data.

Regarding *Sagittaria lancifolia,* unlike the case of *Spartina Patens*, the only study found in the literature providing data on biomass variation as a function of inundation time unfortunately includes a limited number of sampling points. This constrains the certainty in interpreting the behavior of the species.

From the reported graphs, the aboveground biomass exhibits a non-linear trend: it initially decreases and then shows an increase in a later phase. In contrast, the belowground biomass follows a clear exponential decay pattern.

When considering the total biomass, the resulting fit is represented by an exponential function, but with a significant difference compared to *Spartina patens*: in the case of *Sagittaria lancifolia*, total biomass does not approach zero even when the percentage of inundation time reaches 100%. This behavior suggests a greater adaptability of *S. lancifolia* to prolonged submergence conditions, potentially attributable to specific ecophysiological strategies that allow it to sustain a certain level of productivity even under extreme conditions.

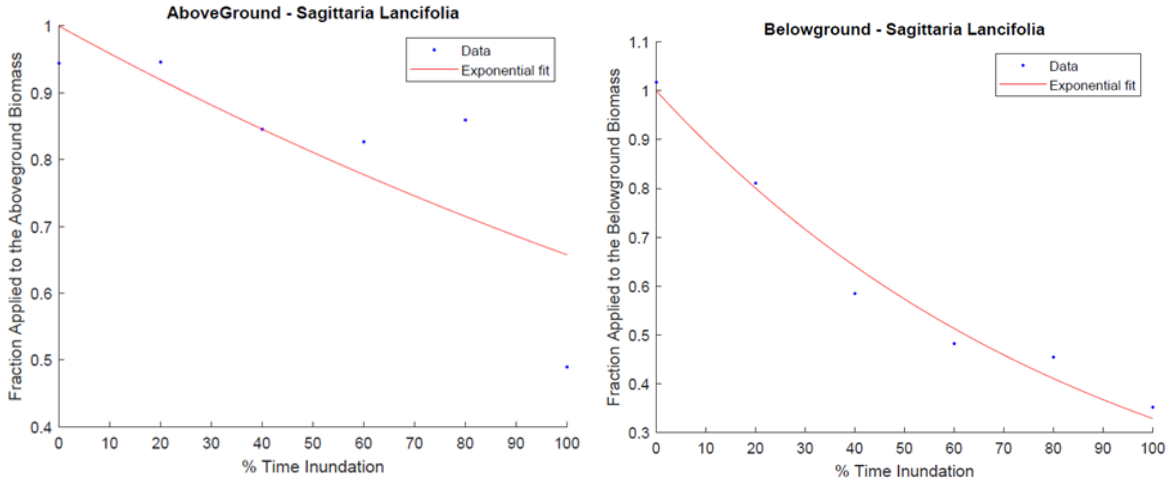

(a) (b)

Figure 5.5: (a) Aboveground Biomass and (b)Belowground Biomass of *Sagittaria Lancifolia*

A further proposed modification, following the introduction of biomass accumulation, involves revising the Root Area Index (RAI), which is used in calculating soil-to-root con-

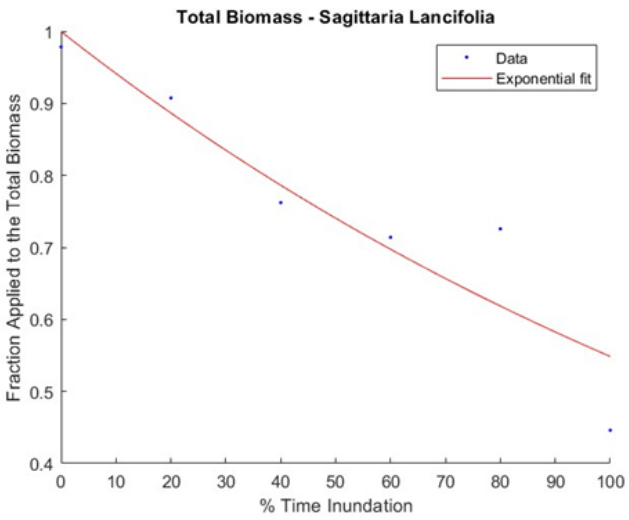

$$y = \exp(-0.006002 \cdot x)$$

Figure 5.6: Graphical representation of the exponential reduction function for *Sagittaria Lancifolia* in relation to the Total Biomas. The graph illustrates the relationship between % time of inundation and the fraction of biomass applied to the total biomass, using an exponential fit to represent the observed data.

ductance, g_{sr}. Currently, in the Photo 3 model, the RAI is defined by the following formula:

$$RAI = RAI_w \cdot s^{-8} \tag{5.9}$$

Where:

- RAI_w represents the index under optimal drainage conditions;
- The exponent describes the response of the root area as a function of soil moisture.

A modification that could be made would be to relate RAI directly to root biomass, calculated as the product of the ratio of below-ground (root) biomass to above-ground biomass and the change in total biomass.

Furthermore, by assigning a percentage to the fraction of biomass occupied by roots, the RAI can be defined as a portion of the below-ground biomass. This approach ensures that

the root area is affected by the reductions that occur when the plant is submerged, as has just been explained.

For a complete understanding of the rationale behind the study of integrating the effects of salinity and submergence on roots, please refer to Appendix B.

Translated with DeepL.com (free version)

6. Conclusions

The Mississippi Delta, one of the most important and complex coastal ecosystems in the world, represents an environment characterized by a delicate balance between natural processes and anthropogenic pressures. Covering an area of approximately 11,000 km², the delta hosts 37% of the estuarine marshes in the United States, serving as a habitat for unique biodiversity and providing natural protection against coastal erosion. In recent decades, the delta has experienced a significant loss of wetlands, estimated at over 3,950 km² since 1930, due to subsidence, sea level rise, and saline intrusion. Freshwater and brackish marshes, key elements for the ecological stability of the delta, are particularly vulnerable to these changes. This thesis focuses specifically on the effects of salt stress.

Salt stress, as illustrated, is one of the primary factors negatively impacting plant growth in the Mississippi Delta wetlands. The effects of salt stress occur in two main phases. The first, the osmotic phase, occurs almost immediately with the increase in soil salinity levels, reducing water potential and compromising the roots' ability to absorb water. This leads to reduced leaf growth, decreased root extension, and lower stomatal conductance, ultimately diminishing productivity. The second, the ionic phase, manifests later with the accumulation of toxic ions in leaf tissues, causing premature senescence in mature leaves. Plants are capable of implementing osmoregulation mechanisms, depending on their tolerance levels, enabling them to survive under such conditions.

The choice of the study site was guided by the need to obtain as much data as possible to support and validate the model. The analysis site, located near the Barataria region, provides both Eddy Covariance (EC) stations for meteorological monitoring and adjacent CRMS stations for hydrological and vegetation-related data collection.

Two types of marshes were identified: a brackish marsh and a freshwater marsh. However, the analysis focused exclusively on the brackish marsh, dominated by *Spartina Patens*,

a species with a salt tolerance level of about 5 ppt, making it vulnerable to high salinity conditions. This marsh, classified as mesohaline, exhibits moderately high salinity levels, making it an ideal context for studying the effects of salt stress.

Additionally, thanks to the CRMS system, detailed salinity data for the study site were obtained. The analysis focused on the year 2022, during which *Spartina Patens* was consistently exposed to salt stress beyond its tolerance levels. This was caused by a severe drought that elevated salinity levels far above the typical values for this brackish marsh, highlighting the significant impact of extreme conditions on the local vegetation.

The objective of this study was to reproduce transpiration and carbon assimilation fluxes, thereby simulating the productivity of the target species under intense salt stress. For this purpose, an open-source plant-scale eco-hydrological model was adapted to the specific case by introducing the saline component into the soil water potential through Van't Hoff's law.

Considering that the studied ecosystem is characterized by the presence of a shallow water table, it was assumed that the soil is close to saturation. To further improve the accuracy and realism of the model, the meteorological data required for its operation were obtained from the EC station, allowing the model to be calibrated in a way that more accurately reflects the real conditions of the study site.

The results obtained from the model were compared with the fluxes measured by the EC station for validation. Yet, it is important to observe that the EC station measures fluxes over a significantly larger footprint than the one simulated by the model (plant-scale). Additionally, while the EC station provides evapotranspiration values, the model can only simulate the transpiration component. To address this discrepancy, transpiration was estimated by subtracting open water evaporation from the observed data. Evaporation was calculated using a combined Aerodynamic and Energy Balance Method.

Despite these limitations, the model results show a good match with experimental data, suggesting that the adopted approach captures many of the key dynamics of the system. However, open questions remain regarding the model's ability to represent more complex pro-

cesses, such as the inclusion of submersion and stochastic variations in the water table essential elements for a more precise description of the studied ecosystem. Future developments should integrate these processes, further enhancing the understanding of plant physiological mechanisms under extreme conditions.

In conclusion, this thesis has laid a preliminary foundation for studying eco-hydrological dynamics in wetlands, highlighting key criticalities and paving the way for new scientific research opportunities.

A. Water flow in the Soil-Plant-Atmosphere Continuum

A.1 Water in the Soil

The soil is the initial element of the SPAC. The water content and movement within soils are determined by the type and structure of the soil, which affect both the pressure gradient and the soil's hydraulic conductivity. Based on the quantity of available water, the water in the soil may form a thin layer clinging to the surfaces of soil particles, occupy smaller channels while leaving larger ones empty, or completely fill the spaces between the particles[59].

The water potential of soils may be dissected into three components [59]:

- The osmotic potential (Ψ_s) of soil water is generally negligible, because except in saline soils, solute concentrations are low.
- The pressure potential (Ψ_p). For wet soils,Ψ_p is very close to zero. As soil dries out, Ψ_p decreases and can become quite negative.
- The gravitational potential Ψ_g. Gravity plays an important role in drainage.

Soil hydraulic conductivity refers to how easily water can move through the soil, and it changes based on the soil type and its moisture levels. As the water content (and consequently the water potential) in the soil decreases, the hydraulic conductivity significantly drops. When more air occupies the soil spaces, water movement is restricted to fewer and narrower channels, leading to a reduction in hydraulic conductivity.

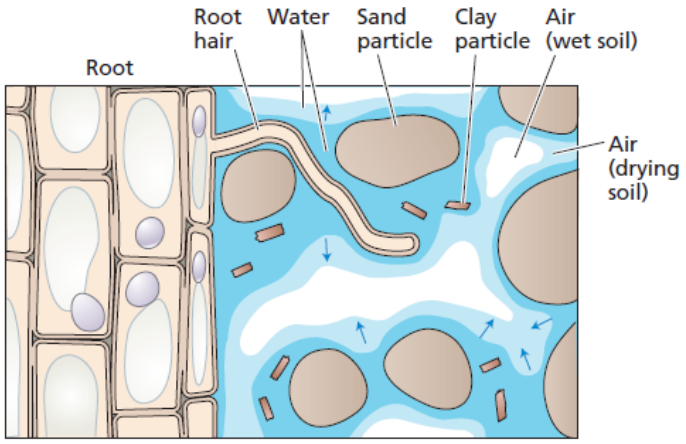

Figure A.1: The intimate contact between root hairs and soil particles greatly increases the surface area for water absorption [59].

A.2 Water Absorption by Roots

For efficient water uptake by the root, close contact between the root surface and the surrounding soil is crucial. This contact increases the surface area available for water absorption and is enhanced by the growth of both the root and root hairs into the soil. Root hairs, which are thin extensions of root epidermal cells, significantly enlarge the root's surface area, thereby improving its ability to absorb water and nutrients from the soil. Water is most easily absorbed near the root tip [59].

Within the soil, water moves between particles. However, once inside the root, from the epidermis to the endodermis, water can follow three different routes: the apoplast, the symplast, or the transmembrane pathway. In the symplast pathway, water travels between cells via the plasmodesmata without crossing the plasma membrane. In the transmembrane pathway, water crosses plasma membranes, briefly passing through the cell wall space before continuing through the root [59].

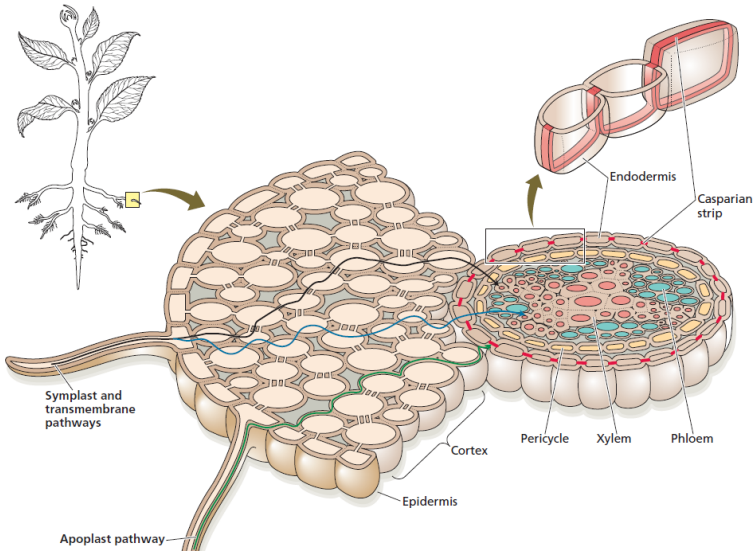

Figure A.2: Pathways for water uptake by the root [59].

The Casparian strip, a structure located in the endodermis, forces water to pass through cell membranes, allowing the plant to regulate which substances enter its vascular system. When transpiration is low or absent, positive hydrostatic pressure accumulates in the xylem as roots continue to absorb ions from the soil and transport them into the xylem. This buildup of solutes decreases the osmotic potential in the xylem sap, consequently reducing the water potential in the xylem. The lowered xylem water potential creates a driving force for water uptake, resulting in positive hydrostatic pressure within the xylem [59].

A.3 Water Transport through the Xylem

In most plants, the xylem forms the longest portion of the water transport pathway. In a plant that is 1 meter tall, over 99.5% of the water's journey occurs within the xylem, and this percentage is even greater in taller trees [59].

The xylem's conducting cells have a specialized structure that allows them to move large volumes of water efficiently with minimal resistance. The two primary types of water-

transporting cells in the xylem are single-celled tracheids and multicellular vessels. Tracheids are elongated, spindle-shaped cells arranged in overlapping vertical rows, while vessel elements are typically shorter and wider than tracheids. Vessel elements have perforated end walls, forming a perforation plate at each end of the cell [59].

Water movement in plants occurs due to a pressure gradient between the base and the top of the plant. In theory, this water movement could be driven either by positive pressure at the plant's base or by negative pressure at the top. Root pressure, generated by the buildup of ions in the xylem, pushes water upwards, but this mechanism would be inefficient because it would require a way to manage the solutes left behind after water evaporates from the leaves [59].

One theory proposes that as water evaporates from the cell walls of leaves, curved air-water interfaces form, creating negative pressure in the remaining water. As more water evaporates, the curvature increases, generating even greater negative pressure. This phenomenon resembles what happens in soil when roots absorb water. Most water lost through transpiration is replaced by water from the soil, which moves through a low-resistance pathway in the xylem. For this to occur, the leaf water potential must be low enough to overcome both soil water potential and the resistance to water flow in the plant. A continuous column of liquid water from the soil to the leaves is essential for effective transport [59].

Cavitation is a damaging process that happens when water columns inside xylem vessels break, forming air bubbles. This disruption typically occurs due to extreme tension on the water in the xylem, often caused by harsh environmental conditions. Cavitation interrupts the water column's continuity, hindering water transport under tension [59].

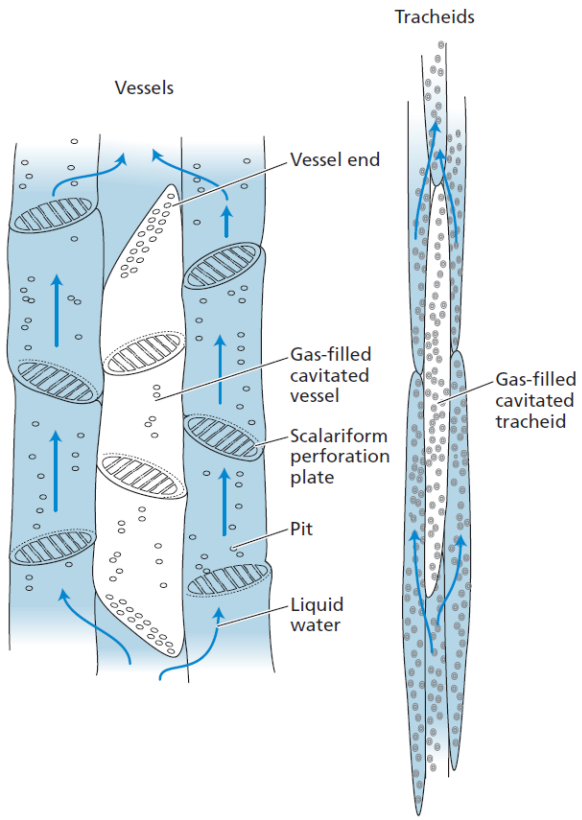

Figure A.3: Vessels (left) and tracheids (right) form a series of parallel, interconnected pathways for water movement. Cavitation blocks water movement because of the formation of gas-filled (embolized) conduits [59].

A.4 Water Movement from the Leaf to the Atmosphere

As water moves from the leaf to the atmosphere, it is drawn from the xylem into the cell walls of the mesophyll, where it evaporates into the leaf's air spaces. Although the distances water travels within the leaf are short compared to the entire soil-to-atmosphere pathway, the leaf significantly contributes to the overall hydraulic resistance [59].

Water enters the leaves and spreads across the leaf lamina through xylem conduits. Before it evaporates, water must pass through the xylem walls and several layers of living cells.

Leaf hydraulic resistance is influenced by the number, distribution, and size of xylem conduits, along with the hydraulic properties of the mesophyll cells. This resistance can change depending on growth conditions and exposure to low leaf water potentials [59].

Transpiration relies on the difference in water vapor concentration between the air spaces inside the leaf and the external air, as well as the diffusional resistance of this pathway. This resistance is determined by both the leaf's stomatal resistance and the boundary layer resistance.

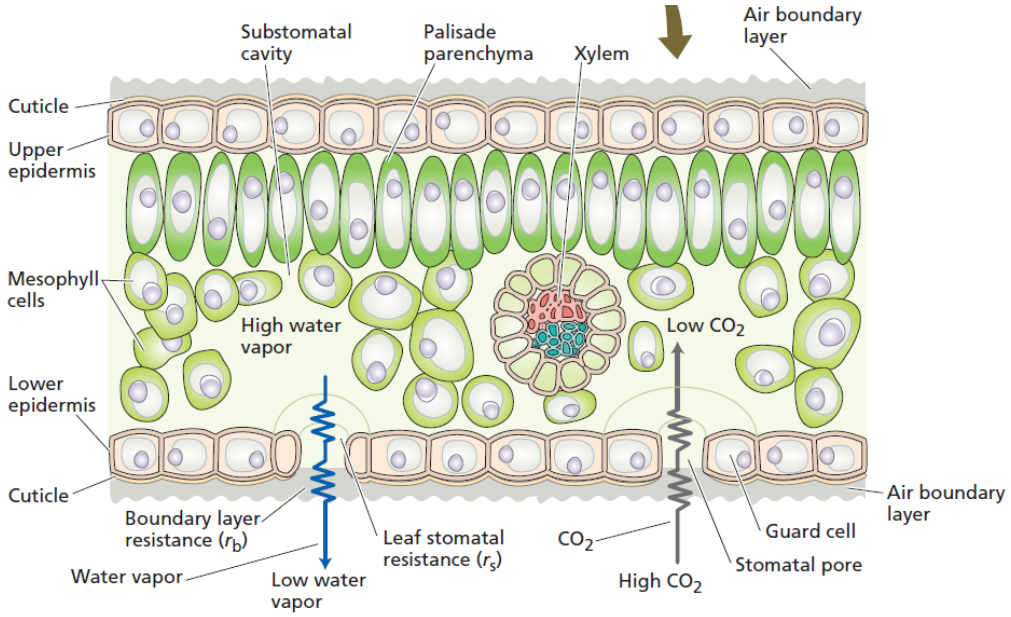

Figure A.4: Water pathway through the leaf [59]

B. Effects of Submersion and Salinity on Roots

A comprehensive literature review was conducted, focusing primarily on *Phragmites australis*, to understand the combined effects of submersion and salinity on roots. This preliminary study enabled the collection of data and information regarding the physiological and morphological responses of this species' roots under environmental stress conditions, with particular emphasis on variations in root density, length, and functional capacity.

In addition to the presence of salt intrusion, coastal wetlands simultaneously face flooding and sulfide stress. These factors interact in complex ways, intensifying each other's effects on wetland vegetation. [36] noted that coastal wetlands are increasingly threatened by climate change, particularly through sea-level rise, which causes both inundation and saltwater intrusion. Another important stressor is the presence of sulfides. Tidal flooding or sea-level rise leads to hypoxic or anoxic conditions in the soil, reducing oxygen availability in the roots. In this oxygen-poor environment, sulfate-reducing bacteria proliferate, decomposing organic matter and producing sulfide as a byproduct. Sulfide is toxic to plants, preventing them from absorbing nutrients, reducing photosynthetic efficiency, and inhibiting root growth [21]. At the same time, salinity exacerbates these effects by increasing osmotic stress, reducing the plant's ability to absorb water. This osmotic stress compromises plant metabolism, making it more challenging to cope with sulfide toxicity. High salinity also alters microbial communities in the soil, potentially increasing the number of sulfate-reducing bacteria and further elevating sulfide concentrations [21]. Plants respond to these stress factors by modifying their root architecture, increasing aerenchyma (air spaces) to enhance oxygen transport, or producing antioxidant compounds to mitigate oxidative damage. However, prolonged exposure can reduce plant growth and mortality, altering wetland ecosystems [33].

Waterlogging poses significant challenges to plant survival, mainly through its effects on root physiology. Waterlogged soils are characterized by an inadequate supply of oxygen,

leading to hypoxic or anoxic conditions for root systems. Oxygen deficiency severely impairs aerobic respiration, crucial for energy production and metabolic function in roots [3]. The lack of oxygen can cause root decay and increase susceptibility to pathogens, ultimately threatening plant viability. The physiological stress induced by prolonged waterlogging leads to root growth inhibition. Many species exhibit stunted root elongation or complete cessation of growth in response to water saturation. This decline is often associated with the death of fine roots, reducing the overall root biomass and negatively impacting the plant's ability to absorb essential resources [13]. In response to oxygen deprivation, many plants develop aerenchyma – specialized tissues containing air-filled spaces facilitating gas exchange between submerged roots and shoots. Aerenchyma formation enhances oxygen diffusion, thereby sustaining metabolic functions even in saturated soils. This adaptation is particularly beneficial for plants in flood-prone environments, allowing them to cope with adverse conditions more effectively [13]. Waterlogging also affects nutrient uptake mechanisms, as damaged root structures and impaired transport systems hinder the absorption of essential nutrients such as nitrogen, phosphorus, and potassium. Moreover, oxygen deficiency can disrupt the microbial communities in the rhizosphere, further complicating nutrient cycling and availability [13]. The hormonal response to waterlogging is complex, involving significant changes in the levels of auxins and ethylene. Increased auxin levels can stimulate the formation of adventitious roots, enhancing the plant's ability to adapt to excess moisture. Conversely, ethylene production, often a response to hypoxia, regulates root growth patterns and overall plant architecture. This interplay between hormones influences a plant's survival and adaptability in waterlogged environments [13].

B.1 Combined Effects of Salinity and Flooding on Biomass and Growth

The study [36] analyzed three main haplogroups of Phragmites australis (Delta, Gulf, and European) in two environments characterized by different salinity levels: the Mississippi Delta, with lower salinity (0-13 ppt), and the Mermentau Basin, with higher levels (6-18 ppt). The plants were exposed to various flooding and salinity conditions for two growing seasons, allowing for the observation of physiological responses and plant survival in relation to these variables. One of the main findings concerns the different tolerances of the haplogroups to salinity and flooding. The Delta haplogroup exhibited greater resilience to higher salinity levels, suggesting a potential capacity for survival in brackish environments. This haplogroup demonstrated a competitive advantage in areas subject to saltwater intrusion, where other plants may be less adapted. In contrast, the Gulf haplogroup proved to be more resistant to flooding stress in freshwater environments, highlighting that different genetic variants of P. australis develop varying adaptation strategies depending on environmental conditions. Salinity significantly negatively impacted plant survival, with a 42% reduction in survival at the brackish site compared to the freshwater site. Prolonged exposure to high salinity and flooding conditions compromised the plant's ability to maintain sustained above-ground biomass. It was observed that increased flooding duration at high salinity sites led to a reduction in biomass, emphasizing how the combination of salinity and flooding intensifies stress on plants. The study by Knight et al. (2020) provides an essential contribution to understanding the effect of salinity on the roots of *Phragmites australis* in the Mississippi Delta, highlighting how this factor, combined with other biotic stresses such as the infestation of the Roseau cane scale (Nipponaclerda biwakoensis), contributes to the phenomenon of "die-back" (vegetation decline). The results indicate that salinity levels between 10 and 15 ppt led to a significant reduction in root biomass, with decreases in root length observed

starting at salinity concentrations of 6 ppt. Controlled experiments showed that prolonged exposure to high salinity conditions caused a reduction in root biomass of up to 50%. These observations connect with previous findings regarding the different responses of *P. australis* haplogroups to salinity and flooding. Knight et al.'s study adds that biomass and root length reduction is accompanied by a general inhibition of growth, with a decline in root length between 20% and 40% under increasing salinity conditions. The Delta haplogroup showed a 12% reduction in height due to the combined stress of salinity and scale infestation. From a physiological standpoint, exposure to salinity levels exceeding 15 ppt induced significant osmotic pressure in the roots, resulting in physiological stress. The plants had to invest more resources in osmotic adjustment to maintain water balance at the expense of root and shoot growth. In extreme cases, chlorosis and necrosis were observed in root tissues, indicating substantial damage caused by salt stress. By combining the results of Knight et al. with the study on the resilience model of *P. australis* haplogroups in wetlands, it becomes clear that salinity represents a crucial factor in plant survival and productivity. The interaction between salinity, flooding, and biotic stress underscores the need to manage these factors to preserve coastal wetlands carefully. The findings provide relevant insights for developing conservation strategies that consider not only the genetic diversity of *P. australis* populations but also the impact of environmental stresses on both local and global scales.

B.2 Effects of Sulfides and Organic Acids on the Root Structure

A key factor in the decline of P. australis is the accumulation of sulfides and organic acids (such as acetic acid) in water-saturated soils. The study by [3] demonstrated that exposure to concentrations of acetic acid at 1.67 mM and sulfides at 1.4 mM resulted in significant root and bud mortality. Acetic acid halted root growth in just five days, causing necrosis of the root tips and a 50% reduction in the length of adventitious roots.

It is possible to compare the findings of [3] study with those obtained in the Mississippi River Delta (MRD) by [36], in which a concentration of 1.50 mM of acetic acid (similar to values reported in Armstrong's study) resulted in a sharp decrease in survival probability. Furthermore, it was observed that under 100% flooding conditions, acetic acid concentrations increased significantly. The study also demonstrated that belowground biomass decreased as the concentration of sulfide in the pore water increased. Aeration of the rhizosphere, promoted by exposing sediments to oxygen, may alleviate sulfide toxicity by oxidizing it into non-toxic sulfate. However, the presence of marsh reeds may have hindered rhizosphere aeration, contributing to the high sulfide levels observed. A critical sulfide concentration threshold was identified, beyond which none of the experimental plants survived (approximately 3800 µmol/L), while most plants did not survive concentrations above 1000 µmol/L. Lower concentrations of sulfide in the pore water were associated with reduced growth, resulting in shorter Phragmites shoots.

Exposure to toxic levels of organic acids and sulfides has devastating effects on Phragmites australis, with evident manifestations of abnormal lignification and obstructions in the vascular systems. Lignification, which represents the hardening of cell walls, particularly affects the epidermal and cortical cells of the roots, preventing the emergence of lateral roots and trapping them within the cortical tissue. This phenomenon is accompanied by the formation of calluses, occurring at the junction between the root and rhizome, completely blocking the cortical aerenchyma. This structure is essential for root aeration, and its obstruction significantly contributes to reduced gas exchange within the plant [3]. In addition to the direct effects on growth, gas flow experiments demonstrated that 60-70% of the nodes in the rhizomes of treated plants exhibited infinite resistance, preventing air passage due to obstructions caused by callus formation. This resistance to gas flow further compromises root aeration, increasing the risk of anoxia and contributing to the overall deterioration of the plant [3], [4]. Furthermore, acetic acid and sulfide treatments induce obstructions in the vascular system, particularly in the xylem, compromising the plant's ability to absorb water and nu-

trients. Obstructions in the xylem and phloem, occurring at the bases of shoots, in rhizomes, and at root-rhizome junctions, are as significant as those affecting the aeration system. The presence of lignified materials in the intercellular spaces of roots and rhizomes may further reduce oxygenation in the rhizosphere, making the tips of adventitious roots, lateral roots, and underground buds more vulnerable to damage from phytotoxins [3], [4]. The physiological responses of *P. australis* roots to these toxic conditions also include the thickening of the cell walls of adventitious roots. This defense mechanism, while limiting the entry of harmful substances, also reduces the absorption of water and nutrients and hinders the growth of lateral roots. The epidermal and hypodermal zones, which are normally non-lignified, become compromised, further increasing the plant's stress [3], [4].

Figure B.1: Effects of Lignification and Vascular Obstructions of the Roots [4]

B.3 Root Cortex Structure and Metabolic Responses to Soil Redox Conditions

The study conducted by ù[5] analyzes the anatomical and metabolic responses of *S. Patens* roots, which belong to the same family as Phragmites, following hypoxia induced by flooding. The investigation highlights the adverse effects of low redox conditions on soil and roots and the plant's adaptive strategies to cope with the unfavorable environment. Prolonged flooding causes a significant reduction in soil redox potential (Eh), with values ranging from -250 mV to -300 mV in strongly reduced soils, compared to +400 mV and +700 mV present in well-aerated soils. This reduction leads to the transformation of ferric iron to ferrous iron and sulfate to sulfide, elements that tend to accumulate in the soil, creating a toxic environment for the roots and compromising the plant's ability to maintain an oxygenated rhizosphere [5]. In response to these adverse conditions, the roots of Spartina patens show significant anatomical modifications. Large areas of aerenchyma are developed and reduce the need for respiratory tissue. The cortical cells, typically isodiametric, substantially increase in size, forming large intercellular spaces not found in the vascular cylinder. This adaptation suggests a decrease in cell division, compensated by increased cell size, indicative of a stress response mechanism [5]. Low Eh conditions negatively impact root elongation. Measurements taken over 22 days reveal that roots exposed to well-oxygenated soils show notable elongation and healthier development, while those grown in reduced environments exhibit limited growth. Just a few days after the start of the experiment, root elongation in reduced soils shows a drastic inhibition compared to the control [5]. Under anaerobic conditions, the activity of alcohol dehydrogenase (ADH), a key enzyme in anaerobic fermentation, increases significantly, reaching about three times the level observed in well-aerated conditions. This increase highlights a greater reliance on fermentation for the survival of roots in environments with low oxygen availability. The measured ADH activity in stressed roots is 230 ± 32 µmol

of NADH oxidized per gram of fresh weight per hour, compared to 78 ± 38 μmol/g/h in the control sample [5].

Bibliography

[1] Ignacio Rodriguez-Iturbe Amilcare Porporato. “Ecohydrology of Water-Controlled Ecosystems, Soil Moisture and Plant Dynamics”. In: *Cambridge University Press* (2005).

[2] Jun Yin Amilcare Porporato. *Ecohydrology: dynamics of life and water in the critical zone*. Cambridge University Press, 2022.

[3] J. Armstrong, F. Afreen-Zobayed, and W. Armstrong. “Phragmites die-back: sulphide and acetic acid-induced bud and root death, lignifications, and blockages within aeration and vascular systems”. In: *Annals of Botany* (1996). Received 18 March 1996; accepted 16 August 1996.

[4] Jean Armstrong and William Armstrong. “An overview of the effects of phytotoxins on *Phragmites australis* in relation to die-back”. In: *Aquatic Botany* 69.2–4 (2001), pp. 251–268.

[5] Jean Armstrong and William Armstrong. “An overview of the effects of phytotoxins on *Phragmites australis* in relation to die-back”. In: *Aquatic Botany* 69.2–4 (2001), pp. 251–268.

[6] Birdfoot Festival. *About Birdfoot Festival*. Accesso il: 2023-09-21. 2023. URL: https://birdfootfestival.org/about/.

[7] George Burba. *Eddy Covariance Method for Scientific, Regulatory, and Commercial Applications*. Lincoln, Nebraska, USA: LI-COR Biosciences, 2013.

[8] Donald R Cahoon, Karen L Mckee, and James T Morris. “How Plants Influence Resilience of Salt Marsh and Mangrove Wetlands to Sea-Level Rise”. In: (2020). DOI: 10.1007/s12237-020-00834-w/Published. URL: https://doi.org/10.1007/s12237-020-00834-w.

[9] Ven Te Chow, David R. Maidment, and Larry W. Mays. *Applied Hydrology*. New York: McGraw-Hill, 1988. ISBN: 978-0070108103.

[10] B.R. Couvillion et al. “Land Area Change in Coastal Louisiana: 1932 to 2016”. In: Scientific Investigations Map 3381 (2017). URL: https://doi.org/10.3133/sim3381.

[11] CSIRO. “Max Carboxylation Rate and Electron Transport Rate in C4 Plants”. In: *Functional Plant Biology* (1992). Accessed: January 3, 2025. URL: https://www.publish.csiro.au/fp/pp9920519.

[12] Edoardo Daly, Amilcare Porporato, and Ignacio Rodriguez-Iturbe. “Coupled Dynamics of Photosynthesis, Transpiration, and Soil Water Balance. Part I: Upscaling from Hourly to Daily Level”. In: *Journal of Hydrometeorology* 5.3 (2004), pp. 546–558. DOI: 10.1175/1525-7541(2004)005<0546:CDOPTA>2.0.CO;2. URL: https://journals.ametsoc.org/view/journals/hydr/5/3/1525-7541_2004_005_0546_cdopta_2_0_co_2.xml.

[13] Kevin Daniel and Sjon Hartman. “How plant roots respond to waterlogging”. In: *Journal of Experimental Botany* 75.2 (Jan. 2024), pp. 511–525.

[14] F. M. DuPont. “Salt-Induced Changes in Ion Transport: Regulation of Primary Pumps and Secondary Transporters”. In: *Transport and Receptor Proteins of Plant Membranes: Molecular Structure and Function*. Springer US, 1992, pp. 91–100.

[15] Earth.org. “The Saltwater Crisis in the Mississippi River, Explained”. In: *Earth.org* (Sept. 2023). URL: https://earth.org/the-saltwater-crisis-in-the-mississippi-river-explained/.

[16] L. Elango and B. Karthikeyan. “Hydrochemical modelling of the impact of irrigation return flow on groundwater quality in a coastal aquifer”. In: *Applied Water Science* 3.4 (2013), pp. 763–775. URL: https://link.springer.com/article/10.1007/s13201-013-0142-x.

[17] Tracy Elsey-Quirk et al. “Vegetation dieback in the Mississippi River Delta triggered by acute drought and chronic relative sea-level rise”. In: *Nature Communications* (Apr. 2024).

[18] Wieland Fricke et al. “Rapid and tissue-specific changes in ABA and in growth rate in response to salinity in barley leaves”. In: *Journal of Experimental Botany* 55.399 (May 2004), pp. 1115–1123.

[19] Wieland Fricke et al. “The short-term growth response to salt of the developing barley leaf”. In: *Journal of Experimental Botany* 57.5 (Mar. 2006), pp. 1079–1095.

[20] Edgar W. Garbisch. “Biology and Management of Sagittaria latifolia Willd (Broad-leaf Arrow-head) for Wetland Restoration and Creation”. In: *Wetlands Ecology and Management* 10.3 (2002), pp. 381–394. URL: https://link.springer.com/article/10.1023/A:1020356408563.

[21] A. Hanson, R. Johnson, C. Wigand, et al. “Responses of *Spartina alterniflora* to Multiple Stressors: Changing Precipitation Patterns, Accelerated Sea Level Rise, and Nutrient Enrichment”. In: *Estuaries and Coasts* 39 (2016), pp. 1376–1385.

[22] Samantha Hartzell, Mark S. Bartlett, and Amilcare Porporato. “Unified representation of the C3, C4, and CAM photosynthetic pathways with the Photo3 model”. In: *Ecological Modelling* 384 (2018), pp. 173–187.

[23] Samantha Hartzell et al. “Modelling nonlinear dynamics of Crassulacean acid metabolism productivity and water use for global predictions”. In: *Plant, Cell & Environment* 44.1 (2021), pp. 34–48.

[24] G. O. Holm, B. C. Perez, D. E. McWhorter, et al. “Ecosystem Level Methane Fluxes from Tidal Freshwater and Brackish Marshes of the Mississippi River Delta: Implications for Coastal Wetland Carbon Projects”. In: *Wetlands* 36 (2016), pp. 401–413. DOI: 10.1007/s13157-016-0746-7.

[25] Harry H. Roberts James M. Coleman and Gregory W. Stone. “Mississippi River Delta: An Overview”. In: *Journal of Coastal Research* (1998).

[26] Hamlyn G. Jones. *Plants and Microclimate: A Quantitative Approach to Environmental Plant Physiology*. Cambridge, UK: Cambridge University Press, 1992.

[27] Richard M. Mizelle Jr. *Record low water levels on the Mississippi River in 2022 show how climate change is altering large rivers*. Accessed: 2024-09-23. 2022. URL: https://theconversation.com/record-low-water-levels-on-the-mississippi-river-in-2022-show-how-climate-change-is-altering-large-rivers-193920.

[28] M. Keisham, S. Mukherjee, and S. C. Bhatla. “Mechanisms of Sodium Transport in Plants: Progresses and Challenges”. In: *Physiologia Plantarum* 170 (2020), pp. 233–245. DOI: 10.1111/ppl.13111.

[29] A. C. Kemp, J. M. Rybczyk, et al. “Dynamic Changes and Processes in the Mississippi River Delta”. In: *Geological Society of America Special Papers* 508 (2011), pp. 1–28. URL: https://doi.org/10.1130/2011.2508(01).

[30] Mikołaj Kordowiecki and Adam Modzelewski. “The Importance of Biological and Ecological Properties of Phragmites Australis (Cav.) Trin. Ex Steud., in Phytoremediation of Aquatic Ecosystems—A Review”. In: *Water* 12.6 (2020), p. 1774. URL: https://www.mdpi.com/2073-4441/12/6/1774.

[31] Ken W. Krauss et al. “Component greenhouse gas fluxes and radiative balance from two deltaic marshes in Louisiana: Pairing chamber techniques and eddy covariance”. In: *Journal of Geophysical Research: Biogeosciences* 126.10 (2021), e2021JG006235.

[32] Guandong Li, Torbjörn E. Törnqvist, and Sönke Dangendorf. “Real-world time-travel experiment shows ecosystem collapse due to anthropogenic climate change”. In: *Nature Communications* 15 (Dec. 2024).

[33] Y. Li, J. Hua, C. He, et al. “*Spartina alterniflora* raised sediment sulfide in a tidal environment and buffered it with iron in the Jiuduansha Wetland”. In: *Journal of Soils and Sediments* 24 (2024), pp. 657–669.

[34] Wiley Online Library. “Global Change Biology Article on Leaf Area Index”. In: *Global Change Biology* (2015). Accessed: January 3, 2025. URL: https://onlinelibrary.wiley.com/doi/full/10.1111/gcb.12631.

[35] Léa Lorrain-Soligon et al. “Long-term trends of salinity in coastal wetlands: Effects of climate, extreme weather events, and sea water level”. In: *Environmental Research* 237 (2023), p. 116937. ISSN: 0013-9351. DOI: https://doi.org/10.1016/j.envres.2023.116937. URL: https://www.sciencedirect.com/science/article/pii/S0013935123017413.

[36] A. Lynn and T. Elsey-Quirk. “Salt Water Exposure Exacerbates the Negative Response of *Phragmites australis* Haplotypes to Sea-Level Rise”. In: *Plants* 13.6 (Mar. 2024), p. 906.

[37] Maya McHugh. “Synergies of Restoring Red Mangroves: Flood Mitigation, Carbon Sequestration, and Coastal Adaptation”. Unpublished doctoral dissertation. PhD thesis. University of [Nome dell’Università], 2024.

[38] J.H. Merino, D. Huval, and A.J. Nyman. “Implication of nutrient and salinity interaction on the productivity of Spartina patens”. In: *Wetlands Ecology and Management* 18 (2010), pp. 111–117. DOI: 10.1007/s11273-008-9124-4.

[39] William J. Mitsch and James G. Gosselink. *Wetlands*. 5th. Hoboken, NJ: John Wiley & Sons, 2015.

[40] Rana Munns. “Comparative physiology of salt and water stress”. In: *Plant, Cell and Environment* 25 (2 2002), pp. 239–250. ISSN: 01407791. DOI: 10.1046/j.0016-8025.2001.00808.x.

[41] Rana Munns and Mark Tester. *Mechanisms of salinity tolerance*. 2008. DOI: 10.1146/annurev.arplant.59.032607.092911.

[42] Scott O'Brien and Denise J. Reed. "Life Cycle of Oil and Gas Fields in the Mississippi River Delta: A Review". In: *Environmental Reviews* 28.4 (2020), pp. 431–451. URL: https://cdnsciencepub.com/doi/10.1139/er-2019-0045.

[43] Alexandre Bosco de Oliveira, Nara Lídia Mendes Alencar, and Enéas Gomes-Filho. "Comparison Between the Water and Salt Stress Effects on Plant Growth and Development". In: *Responses of Organisms to Water Stress*. Ed. by Sener Akıncı. Rijeka: IntechOpen, 2013. Chap. 4. DOI: 10.5772/54223. URL: https://doi.org/10.5772/54223.

[44] Kenneth R. Olson and Cory D. Suski. "Mississippi River Delta: Land Subsidence and Coastal Erosion". In: *Open Journal of Soil Science* 11 (2021), pp. 139–163.

[45] Saverio Perri, Dara Entekhabi, and Annalisa Molini. "Plant Osmoregulation as an Emergent Water-Saving Adaptation". In: *Water Resources Research* 54 (Apr. 2018), pp. 2781–2798. URL: https://agupubs.onlinelibrary.wiley.com/doi/10.1002/2017WR022319.

[46] Saverio Perri, Gabriel G. Katul, and Annalisa Molini. "Xylem–phloem hydraulic coupling explains multiple osmoregulatory responses to salt stress". In: *New Phytologist* 224 (2 Oct. 2019), pp. 644–662. ISSN: 0028-646X. DOI: 10.1111/nph.16072. URL: https://nph.onlinelibrary.wiley.com/doi/10.1111/nph.16072.

[47] Saverio Perri et al. "Salinity and periodic inundation controls on the soil-plant-atmosphere continuum of gray mangroves". In: *Hydrological Processes* 31 (6 Mar. 2017), pp. 1271–1282. ISSN: 08856087. DOI: 10.1002/hyp.11095. URL: https://onlinelibrary.wiley.com/doi/10.1002/hyp.11095.

[48] Saverio Perri et al. “Salinity-induced limits to mangrove canopy height”. In: *Global Ecology and Biogeography* 32.9 (2023), pp. 1561–1574. DOI: 10.1111/geb.13720. URL: https://onlinelibrary.wiley.com/doi/10.1111/geb.13720.

[49] Coastal Protection and Restoration Authority of Louisiana. *Louisiana’s Comprehensive Master Plan for a Sustainable Coast*. Accessed: 2024-10-03. 2023. URL: https://cims.coastal.louisiana.gov/masterplan/.

[50] Louisiana Coastal Protection and Restoration Authority. *Coastwide Reference Monitoring System (CRMS)*. Accessed: 2024-09-21. 2024. URL: https://www.lacpra.org/.

[51] Dario Pumo et al. “Modeling belowground water table fluctuations in the Everglades”. In: *Water Resources Research* 46 (2010).

[52] ResearchGate. “Water Relations of an Invasive Halophyte Spartina patens: Osmotic and Hydrostatic Adjustments”. In: *ResearchGate* (2015). Accessed: January 3, 2025. URL: https://www.researchgate.net/publication/277683397_Water_relations_of_an_invasive_halophyte_Spartina_patens_Osmotic_and_Hydrostatic_Adjustments.

[53] ScienceDirect. “Point of Maximum and Onset of Plant Water Stress in Salt Marsh Vegetation”. In: *Environmental and Experimental Botany* (2007). Accessed: January 3, 2025. URL: https://www.sciencedirect.com/science/article/pii/S0098847207000299.

[54] G. Shaffer. “Sagittaria Biomass Partitioning Relative to Salinity, Hydrologic Regime, and Substrate Type: Implications for Plant Distribution Patterns in Coastal Louisiana, United States”. In: *Journal of Coastal Research* (2005).

[55] Gregg A. Snedden, Kari Cretini, and Brett Patton. “Inundation and salinity impacts to above- and belowground productivity in Spartina patens and Spartina alterniflora in

the Mississippi River deltaic plain: Implications for using river diversions as restoration tools". In: *Ecological Engineering* 81 (2015), pp. 133–139.

[56] National Geographic Society. *Mississippi Delta Formation*. Accessed: 2024-09-21. 2023. URL: https://education.nationalgeographic.org/resource/miss-delta-formation/.

[57] EA Spalding and MW Hester. "Interactive effects of hydrology and salinity on oligohaline plant species productivity: implications of relative sea-level rise". In: *Estuaries and Coasts* 30 (2007), pp. 214–225.

[58] U.S. Geological Survey. *Land Area Change in Coastal Louisiana (1932 to 2016)*. U.S. Geological Survey, 2016. URL: https://pubs.usgs.gov/ha/ha733/.

[59] Lincoln Taiz et al. *Plant Physiology and Development*. 6th. Sunderland, MA: Oxford University Press, 2021.

[60] J. Tracy. "Salt Water Exposure Exacerbates the Negative Response of Phragmites australis Haplotypes to Sea-Level Rise". In: *Wetlands* 43.2 (2023), pp. 307–319. DOI: 10.1007/s13157-022-00534-4.

[61] U.S. Geological Survey. *Open-File Report 99-218*. Accessed: 2025-01-04. 1999. URL: https://pubs.usgs.gov/of/1999/0218/report.pdf.

[62] John T. Wells and James M. Coleman. "Wetland loss and the subdelta life cycle". In: *Estuarine, Coastal and Shelf Science* 25.1 (1987), pp. 111–125.

[63] E. S. Weng et al. "Scaling from individuals to ecosystems in an Earth System Model using a mathematically tractable model of height-structured competition for light". In: *Biogeosciences* 12.9 (2015), pp. 2655–2694.

[64] Wikipedia contributors. *Eddy covariance*. [Online; accessed 11-November-2024]. n.d. URL: https://en.wikipedia.org/wiki/Eddy_covariance.

[65] Jian-Kang Zhu. “Plant salt tolerance”. In: *TRENDS in Plant Science* 6 (2001), p. 66. URL: http://plants.trends.com.

C. Acknowledgements

A conclusione di questo elaborato, desidero dedicare qualche riga a tutti coloro che mi sono stati vicini in questo percorso di crescita personale e professionale.

Un sentito grazie al mio relatore, Pierluigi Claps, che mi ha dato la disponibilità di poter realizzare questa esperienza indimenticabile. Un grazie anche alla mia correlatrice, Annalisa Molini, per la sua grande disponibilità e dedizione nel suo lavoro, che ha saputo guidarmi, con suggerimenti pratici, nelle ricerche e nella stesura dell'elaborato.

Dal profondo del mio cuore, ringrazio tutta la mia famiglia, che mi è sempre stata vicina anche se fisicamente distante. Il loro amore è stato la forza che mi ha permesso di realizzare ogni cosa. Mi hanno sostenuto in ogni momento di questo percorso, condividendo gioie e difficoltà, e continuando a essere fieri di me. Mamma, Papà, Cristiana, Nonni e Zii questo traguardo lo dedico a voi. Lo dedico anche a te, Zio Ale, sapendo che da lassù ci osservi e continui a vegliare su di noi.

Un ringraziamento speciale va alla mia famiglia americana, che per cinque intensi mesi è stata una vera casa lontano da casa. Il loro amore e la loro accoglienza mi hanno fatto sentire parte di qualcosa di grande, rendendo tale esperienza unica e indimenticabile.

Ringrazio tutti gli amici con cui ho condiviso l'avventura dell'Erasmus a Valencia, un periodo che resterà sempre nel mio cuore. Un grazie particolare ad Alessio, con cui ho vissuto un viaggio indimenticabile, e a Pietro, coinquilino di mille avventure e risate.

Grazie di cuore anche alle mie coinquiline, che sono state un pilastro in questo percorso.

Avete illuminato i momenti bui, regalandomi risate indimenticabili e serate all'insegna della spensieratezza e delle magnifiche cene condivise. Avete reso questo viaggio più bello, più leggero e più autentico.

Un grazie sincero va anche ai miei amici e compagni di corso: le persone con cui ho condiviso centinaia di ore al Poli, tra studio, risate e momenti indimenticabili. Senza di voi, raggiungere la laurea non avrebbe avuto lo stesso significato. Avete reso tutto meno faticoso, più divertente e soprattutto più umano.

Un ringraziamento speciale alla mia famiglia di Torino, Alessia e Francesco.

Alessia, tu sei diventata molto più di un'amica: sei il mio punto di riferimento, una confidente, una sorella, una spalla su cui appoggiarmi nei momenti difficili. Durante questi due anni, la tua vicinanza e il tuo supporto sono stati fondamentali per me. Sei stata sempre presente, anche da lontano, venendomi a trovare a Valencia e a New Orleans, e regalandoci momenti di pura complicità. Grazie per avermi fatto conoscere la te più vera che pochi ne hanno la possibilità.

Francesco, all'inizio della magistrale non sembravo starti molto simpatica, ma pian piano abbiamo iniziato a conoscerci e siamo arrivati a condividere un legame speciale. Sei diventato più di un amico: sei una parte importante della mia vita. Grazie per la tua allegria, che ha saputo darmi energia anche nei momenti più difficili. Ma non è solo la tua gioia a colpirmi: quando fai il serio, sei una delle persone con cui mi sento più a mio agio a confidarmi. E ogni volta che sono triste, basta un tuo "mozzico" sulla guancia per strapparmi un sorriso e farmi stare meglio.

Un ringraziamento importante va anche alle mie due amiche di una vita, le due persone che hanno fatto parte di ogni momento della mia vita, Luna e Martina. Voi ci siete sempre

state e spero ci sarete per sempre. Ogni volta che ritorno a Roma, la prima cosa che desidero fare è vederci per poter parlare di tutto, e vedere la piccola Giulia che cresce. So che noi tre ci saremo sempre l'una per l'altra.

Ringrazio anche i miei amici di Roma, quelli dei tempi del liceo, con voi ho condiviso tantissimi bei momenti e spero di portavi sempre con me.

Un ringraziamento finale va a Edoardo. Tu mi sei stato vicino sempre, sia nei momenti bui sia nei belli. La serenità che trasmetti mi ha permesso di vivere questo percorso in maniera differente. Averti vicino mi fa essere la donna che sono diventata, e spero di continuare ad avere questa fortuna per il resto della mia vita,